[1983]

(12)

FINAL REPORT

LIGHTNING PHYSICS: A THREE YEAR PROGRAM

ONR contract N0014-81-K-0177

by

Martin A. Uman
Department of Electrical Engineering
University of Florida
Gainesville, FL 32611

The work ~~done on ONR contract N0014-81-K-0177 has been~~ was reported in five publications:

"Calculations of Lightning Return Stroke Electric and Magnetic Fields above Ground," J. Geophys. Res., 86, 12127-12132 (1981), M.J. Master, M.A. Uman, Y.T. Lin, and R.B. Standler.

"Electric Fields Preceding Cloud-to-Ground Lightning Flashes," J. Geophys. Res., 87, 4883-4902 (1982), W.H. Beasley, M.A. Uman, and P.L. Rustan.

"A Comparison of Lightning Electromagnetic Fields with the Nuclear Electromagnetic Pulse in the Frequency Range 10^4 - 10^7 Hz," IEEE Trans. EMC, EMC-24, 410-416 (1982), M.A. Uman, M.J. Master, E.P. Krider. (10000 to 10000000)

"Transient Electric and Magnetic Fields Associated with Establishing a Finite Electrostatic Dipole," Am. J. Phys., 51, 118-126 (1983), M.J. Master and M.A. Uman.

"Variation in Light Intensity with Height and Time from Subsequent Lightning Return Strokes," J. Geophys. Res., 88, 6555-6562 (1983), D.M. Jordan and M.A. Uman.

These five journal articles are reproduced in Appendices 1 through 5.

In Appendix 1 the first detailed calculations of lightning return stroke electric and magnetic fields above ground are presented. Waveforms are given for altitudes from 0 to 10 km and ranges from 20 m to 10 km. These waveforms are computed using the model of Lin et al. (1980) and a modification of that model in which the initial current peak decays with height above ground. Both the original and the modified models result in accurate prediction of measured ground-based fields. Return stroke field measurements above ground close to the stroke, with which the calculations could be compared, have not yet been made. Salient aspects of the calculated fields are discussed, including their use in calibrating airborne field measurements from simultaneous ground and airborne data.

In Appendix 2 we analyzed in detail the electric field variations preceding the first return strokes of 80 cloud-to-ground lightning flashes in nine different storms observed at the NASA Kennedy Space Center during the summers of 1976 and 1977. The electric field variations are best characterized as having two sections: preliminary variations and stepped leader.

The stepped-leader electric-field change begins during a transition period of a few milliseconds duration marked by characteristic bipolar pulses. The durations of stepped leaders lie most frequently in the range 6-20 milliseconds. We infer from our measurements and critical review of the previous literature that there is only one type of stepped leader, not the two types, α and β, often referred to in the literature.

In Appendix 3 the electromagnetic fields produced by both direct lightning strikes and nearby lightning are compared with the nuclear electromagnetic pulse (NEMP) from an exoatmospheric burst. Model calculations indicate that, in the frequency range from 10^4 to near 10^7 Hz, the Fourier amplitude spectra of the return stroke magnetic fields near ground 1 m from an average lightning strike will exceed that of the NEMP. Nearby first return strokes at a range of about 50 m, if they are severe, produce electric-field spectra near ground which exceed that of the NEMP below about 10^6 Hz, while the spectra of average nearby first return strokes exceed that of the NEMP below about 3×10^5 Hz. Implications of these results for aircraft in flight are discussed.

In Appendix 4 we obtain analytical solutions in the time domain for the electric and magnetic fields associated with establishing a finite electrostatic dipole. We assume that a simple source current distribution, a square pulse of current, produces the dipole, and solve for the fields produced by that source current distribution using Maxwell's equations. Salient features of the fields are discussed from a physical point of view. We outline a technique to determine in the time domain the electric and magnetic fields produced by any arbitrary time-varying current propagating along a straight antenna, given the calculated fields due to a short square pulse of current.

In Appendix 5 we present relative light intensity measured photographically as a function of height and time for seven subsequent return strokes in two lightning flashes at ranges of 7.8 and 8.7 km. The film used was Kodak 5474 Shellburst, which has a roughly constant spectral response between 300 and 670 nm. The time resolution was about 1.0 μs, and the spatial resolution was about 4 m. The observed light signals consisted of a fast rise to peak, followed by a slower decrease to a relatively constant value. The amplitude of the initial light peak decreases exponentially with height with a decay constant of about 0.6 to 0.8 km. The 20% to 80% rise time of the initial light signal is between 1 and 4 μs near ground and increases by an additional 1 to 2 μs by the time the return stroke reaches the cloud base, a height between 1 and 2 km. The light intensity 30 μs after the initial peak is relatively constant with height and has an amplitude that is 15% to 30% of the initial peak near the ground and 50% to 100% of the initial peak at cloud base. The logarithm of the peak light intensity near the ground is roughly proportional to the initial peak electric field intensity, and this in turn implies that the current decrease with height may be much slower than the light decrease. The absolute light intensity has been estimated by integrating the photographic signals from individual channel segments to simulate the calibrated all-sky photoelectric data of Guo and Krider (1982). Using this method, we find that the mean peak radiance near the ground is 8.3×10^5 W/m, with a total range from 1.4×10^5 to 3.8×10^6 W/m.

APPENDIX 1

Calculations of Lightning Return Stroke Electric and Magnetic Fields Above Ground

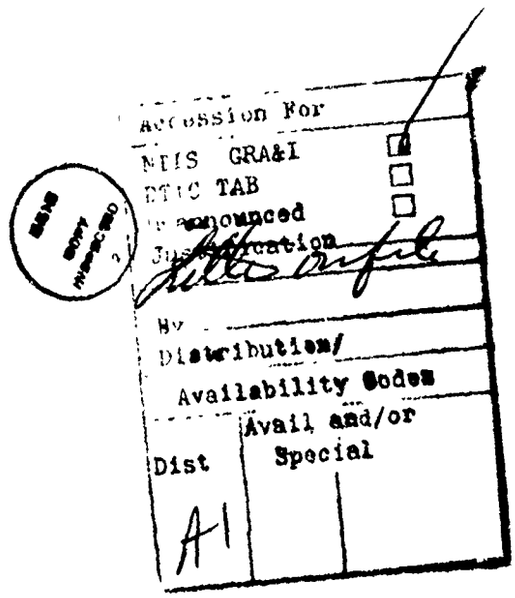

JOURNAL OF GEOPHYSICAL RESEARCH, VOL. 86, NO. C12, PAGES 12,127–12,132, DECEMBER 20, 1981

Calculations of Lightning Return Stroke Electric and Magnetic Fields Above Ground

M. J. MASTER, M. A. UMAN, Y. T. LIN[1] AND R. B. STANDLER[2]

Department of Electrical Engineering, University of Florida, Gainesville, Florida 32611

The first detailed calculations of lightning return stroke electric and magnetic fields above ground are presented. Waveforms are given for altitudes from 0 to 10 km and ranges from 20 m to 10 km. These waveforms are computed using the model of Lin et al. (1980) and a modification of that model in which the initial current peak decays with height above ground. Both the original and the modified models result in accurate prediction of measured ground-based fields. Return stroke field measurements above ground close to the stroke, with which the calculations could be compared, have not yet been made. Salient aspects of the calculated fields are discussed, including their use in calibrating airborne field measurements from simultaneous ground and airborne data.

INTRODUCTION

Lin et al. [1980] have recently introduced a lightning return stroke model with which return stroke electric and magnetic fields measured at ground level [*Lin et al.*, 1979] can be reproduced. Here we use that model and a modification of it to compute electric and magnetic fields at altitudes up to 10 km and at ranges from 20 m to 10 km. These calculations provide the first detailed estimates of the return stroke fields that exist above ground and that are encountered by aircraft in flight. The most recent generation of aircraft may be particularly susceptible to lightning electric and magnetic fields because these aircraft are controlled with low-voltage digital electronics and are in part constructed of advanced composite materials which provide a reduced level of electromagnetic shielding [*Corbin*, 1979]. Hence, in the context of aircraft safety, calculations of the magnitude and waveshape of airborne electric and magnetic fields are of considerable practical interest. Furthermore, from a scientific point of view, since airborne electric and magnetic fields are presently being measured [*Pitts et al.*, 1979; *Pitts and Thomas*, 1981; *Baum*, 1980], a comparison of the calculations given in this paper with appropriate experimental data, when they are available, will constitute a test of the return stroke model.

THEORY

The lightning return stroke current is assumed to flow in a thin, straight, vertical channel of height H above a perfectly conducting ground plane, as shown in Figure 1. The electric and magnetic fields at altitude z and range r from a vertical dipole of length dz' at height z' and arbitrary current $i(z', t)$ are

$$d\mathbf{E}(r, \phi, z, t) = \frac{dz'}{4\pi\varepsilon_0}\left[\left\{\frac{3r(z-z')}{R^5}\int_0^t i(z', \tau - R/c)\,d\tau + \frac{3r(z-z')}{cR^4}\,i(z', t-R/c) + \frac{r(z-z')}{c^2R^3}\,\frac{\partial i(z', t-R/c)}{\partial t}\right\}\mathbf{a}_r + \left\{\frac{2(z-z')^2 - r^2}{R^5}\int_0^t i(z', \tau - R/c)\,d\tau + \frac{2(z-z')^2 - r^2}{cR^4}\,i(z', t-R/c) - \frac{r^2}{c^2R^3}\,\frac{\partial i(z', t-R/c)}{\partial t}\right\}\mathbf{a}_z\right] \quad (1)$$

$$d\mathbf{B}(r, \phi, z, t) = \frac{\mu_0 dz'}{4\pi}\left\{\frac{r}{R^3}\,i(z', t-R/c) + \frac{r}{cR^2}\,\frac{\partial i(z', t-R/c)}{\partial t}\right\}\mathbf{a}_\phi \quad (2)$$

where (1) and (2) are expressed in cylindrical coordinates, ε_0 is the permittivity and μ_0 the permeability of vacuum, and all geometrical factors are illustrated in Figure 1. Equations (1) and (2) are obtained in a straightforward manner using an approach similar to that of *Uman et al.* [1975]. In (1) the first and fourth terms are generally called the electrostatic field, the second and fifth the induction or intermediate field, and the remaining two terms the radiation field. In (2) the first term is the induction field and the second, the radiation field. The effects of the perfectly conducting ground plane on the electric and magnetic fields due to the source dipole are included by replacing the ground plane by an image current dipole at distance $-z'$ beneath the plane, as shown in Figure 1 [*Stratton*, 1941]. The electric and magnetic fields due to the image dipole may be obtained by substituting R_i for R and $-z'$ for z' in (1) and (2) above.

In this paper we examine only the fields of a typical subsequent return stroke because it is subsequent strokes with which *Lin et al.* [1980] have tested their model. Subsequent strokes are more easily modeled than first strokes because in contrast to firsts, subsequents have few if any branches, have relatively constant return stroke velocities, and are probably initiated at ground level rather than by upward-going leaders [*Schonland*, 1956].

The model of *Lin et al.* [1980] postulates that the return stroke current is composed of three components: (1) a short-duration upward-propagating pulse of current of constant magnitude and waveshape associated with the electrical breakdown at the return stroke wavefront and responsible

[1] Now with Texas Instruments, Dallas, Texas 75234.
[2] Now at the Rochester Institute of Technology, Rochester, New York 14523.

Paper number 1C1479.
0148-0227/81/001C-1479$01.00

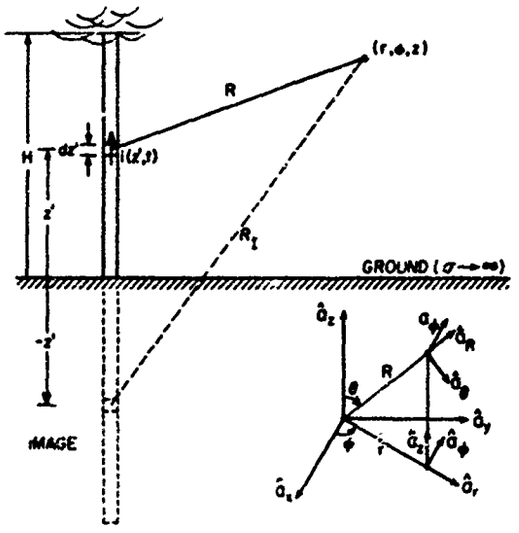

Fig. 1. Geometry for field computations.

for the return stroke peak current; the pulse is assumed to propagate at a constant velocity; (2) a uniform current which may already be flowing (leader current), an assumption we use in this paper, or it may start to flow soon after the commencement of the return stroke; and (3) a 'corona' current caused by the downward movement of the charge initially stored in the corona sheath around the leader channel and discharged by the passage of the return stroke wavefront. These three current components are illustrated in Figure 2.

Two observations form the basis for a modification of the model of *Lin et al.* [1980]:

1. At the time that the research of *Lin et al.* [1980] was done, subsequent strokes were thought to have both luminosities (hence, by implication, currents) and return stroke velocities that were invariant with height [*Schonland*, 1956]. However, *Jordan and Uman* [1980] have since shown that subsequent stroke initial peak luminosity varies markedly with height, decreasing to half-value in less than 1 km above ground. The implication of this result is that the breakdown pulse current (component (1) in the model) must also decrease with height.

2. When the breakdown pulse reaches the top of the channel, the model of *Lin et al.* [1980] predicts a field change of opposite polarity to that of the initial field, the waveshape of the field change being a 'mirror image' of the initial field change. A detailed discussion of the mirror image effect is given by *Uman et al.* [1975]. It is observed occasionally in the fields from first return strokes but almost never in the fields from subsequent return strokes [*Lin et al.*, 1979]. If the breakdown pulse current is allowed to decay with height so that it has a negligible value when it reaches the end of the channel, the mirror image should no longer be manifest in the calculated fields.

In view of observations 1 and 2 above, we propose the following modification to the model of *Lin et al.* [1980]: the breakdown pulse current is allowed to decrease with height above the ground; all other features of the original model remain unchanged. As we shall see, the fields at ground level produced by the modified model are essentially the same as those due to the original model except for the absence of the mirror image. However, the fields in the air, especially at close ranges, differ considerably.

We first consider the calculation of the electric and magnetic fields of a typical subsequent stroke using the original model of *Lin et al.* [1980]. We then repeat the calculation for the modified version of the model. The subsequent stroke used in this study is that for which the following data are given in Figure 11 of *Lin et al.* [1980]: both measured and calculated fields at ranges of 2 km and 200 km at ground level and calculated current at ground level. This calculated current and the three components which constitute it are shown in Figure 3. The rise-to-peak of the breakdown pulse component has been altered from that given by *Lin et al.* [1980] so as to be consistent with the measurements of *Weidman and Krider* [1978]. The salient parameters of the current used in the field calculations for the case of a constant breakdown pulse current are (1) breakdown pulse current: increase from 0 to 3 kA in 1.0 μs, followed by a fast transition to a peak value of 14.9 kA at 1.1 μs, half value at 3.8 μs, and zero at 40 μs; the breakdown

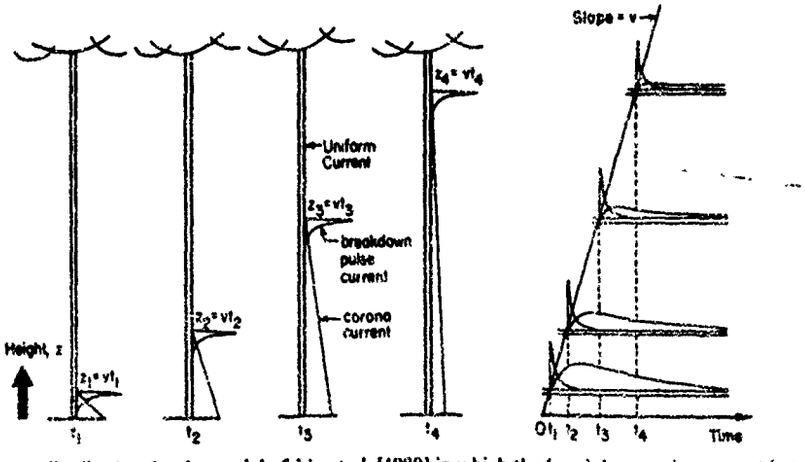

Fig. 2. Current distribution for the model of *Lin et al.* [1980] in which the breakdown pulse current is constant with height. The constant velocity of the breakdown pulse current is v. Current profiles are shown at four different times, t_1 through t_4, when the return stroke wavefront and the breakdown pulse current are at four different heights z_1 through z_4, respectively.

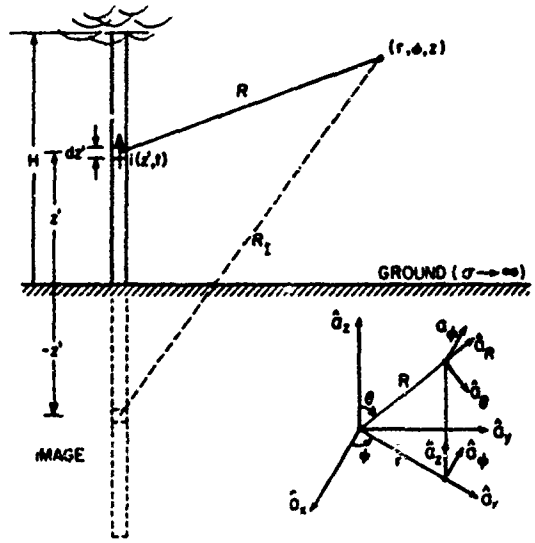

Fig. 1. Geometry for field computations.

for the return stroke peak current; the pulse is assumed to propagate at a constant velocity; (2) a uniform current which may already be flowing (leader current), an assumption we use in this paper, or it may start to flow soon after the commencement of the return stroke; and (3) a 'corona' current caused by the downward movement of the charge initially stored in the corona sheath around the leader channel and discharged by the passage of the return stroke wavefront. These three current components are illustrated in Figure 2.

Two observations form the basis for a modification of the model of *Lin et al.* [1980]:

1. At the time that the research of *Lin et al.* [1980] was done, subsequent strokes were thought to have both luminosities (hence, by implication, currents) and return stroke velocities that were invariant with height [*Schonland*, 1956]. However, *Jordan and Uman* [1980] have since shown that subsequent stroke initial peak luminosity varies markedly with height, decreasing to half-value in less than 1 km above ground. The implication of this result is that the breakdown pulse current (component (1) in the model) must also decrease with height.

2. When the breakdown pulse reaches the top of the channel, the model of *Lin et al.* [1980] predicts a field change of opposite polarity to that of the initial field, the waveshape of the field change being a 'mirror image' of the initial field change. A detailed discussion of the mirror image effect is given by *Uman et al.* [1975]. It is observed occasionally in the fields from first return strokes but almost never in the fields from subsequent return strokes [*Lin et al.*, 1979]. If the breakdown pulse current is allowed to decay with height so that it has a negligible value when it reaches the end of the channel, the mirror image should no longer be manifest in the calculated fields.

In view of observations 1 and 2 above, we propose the following modification to the model of *Lin et al.* [1980]: the breakdown pulse current is allowed to decrease with height above the ground; all other features of the original model remain unchanged. As we shall see, the fields at ground level produced by the modified model are essentially the same as those due to the original model except for the absence of the mirror image. However, the fields in the air, especially at close ranges, differ considerably.

We first consider the calculation of the electric and magnetic fields of a typical subsequent stroke using the original model of *Lin et al.* [1980]. We then repeat the calculation for the modified version of the model. The subsequent stroke used in this study is that for which the following data are given in Figure 11 of *Lin et al.* [1980]: both measured and calculated fields at ranges of 2 km and 200 km at ground level and calculated current at ground level. This calculated current and the three components which constitute it are shown in Figure 3. The rise-to-peak of the breakdown pulse component has been altered from that given by *Lin et al.* [1980] so as to be consistent with the measurements of *Weidman and Krider* [1978]. The salient parameters of the current used in the field calculations for the case of a constant breakdown pulse current are (1) breakdown pulse current: increase from 0 to 3 kA in 1.0 μs, followed by a fast transition to a peak value of 14.9 kA at 1.1 μs, half value at 3.8 μs, and zero at 40 μs; the breakdown

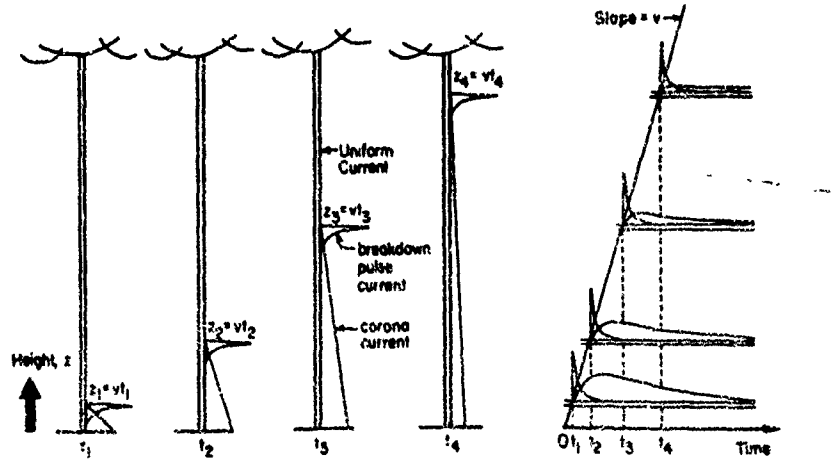

Fig. 2. Current distribution for the model of *Lin et al.* [1980] in which the breakdown pulse current is constant with height. The constant velocity of the breakdown pulse current is v. Current profiles are shown at four different times, t_1 through t_4, when the return stroke wavefront and the breakdown pulse current are at four different heights z_1 through z_4, respectively.

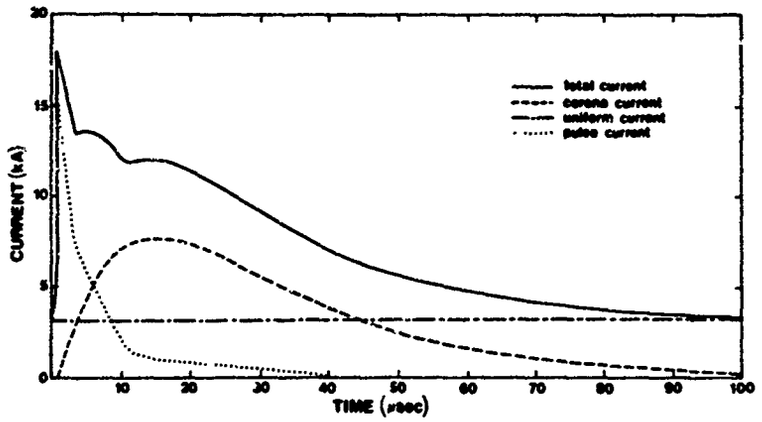

Fig. 3. Return stroke current components at ground calculated from measured electric and magnetic fields for a typical subsequent stroke.

pulse current propagates upward with an assumed constant velocity of 1×10^8 m/s, (2) uniform current: 3100 A, and (3) corona current injected per meter of channel: $I_0 e^{-z'/\lambda}(e^{-\alpha t} - e^{-\beta t})$, with $I_0 = 21$ A/m, $\lambda = 1500$ m, $\alpha = 10^5$ s^{-1}, and $b = 3 \times 10^6$ s^{-1}. The initial charge stored on the leader and lowered by the return stroke is 0.3 C. The channel length is 7.5 km. In the modified version of the model we use a breakdown pulse current whose amplitude decreases with height as $e^{-z'/\lambda}$, with $\lambda = 1500$ m; that is, the breakdown pulse current decreases with height in exactly the same way as does the corona current. All other parameters for the modified model are the same as those for the original model.

Since both first and subsequent strokes probably have initial currents which decrease with height [*Schonland*, 1956; *Jordan and Uman*, 1980], and since the measured waveshapes of first and subsequent stroke fields at ground level are qualitatively similar [*Lin et al.*, 1979], one would also expect the airborne subsequent stroke fields calculated using the modified model to be qualitatively similar to airborne first stroke fields.

RESULTS

Calculated vertical and horizontal electric fields are shown in Figures 4*a* and 4*b*, respectively, and calculated magnetic fields in Figure 4*c*. Solid lines represent the original model of *Lin et al.* [1980] and dashed lines the modified version of the model in which the breakdown pulse current decreases with height. All zero times on the figures indicate the time at which the return stroke current originates at ground level. The waveforms at the field points begin after the appropriate propagation time delay. The intersections of the slanted solid lines with the horizontal dotted lines at various heights indicate the times at which the return stroke wavefront passes those heights. A number of features of the calculated waveforms are worthy of note:

1. With the exception of the absence of the abrupt field changes associated with the end of the channel, the fields on the ground at all distances and the fields on the ground and in the air beyond about 10 km are not much influenced by the breakdown current pulse decrease with height. This is the case because the initial parts of these field waveforms are radiated by the breakdown current pulse while it is very close to the ground and near its maximum amplitude, while later portions of the field waveform are primarily due to the uniform and corona currents which are the same in the original and modified models. Hence it follows that ground-based or distant airborne measurements cannot be used to test the validity of the model modification introduced here.

2. The abrupt field changes associated with the unattenuated breakdown pulse current reaching the idealized ends of the real and image channels [*Uman et al.*, 1975] do not occur when that pulse current is attenuated with height so that it does not have an appreciable magnitude when it reaches the channel end. As noted earlier, the fact that these abrupt changes do not often occur in the experimental data [*Lin et al.*, 1979] was one of the reasons for the proposed modification to the original model of *Lin et al.* [1980].

3. At ranges less than about 200 m the horizontal electric and the magnetic field components above ground attain initial peak values at about the time at which the return stroke breakdown pulse current is at the same altitude as the field point. The vertical electric field component undergoes a sharp decrease at this point. The maximum electric and magnetic fields are due to the charge and current, respectively, associated with the breakdown pulse component at about the time of its closest approach to the field point. The peak electric field is essentially electrostatic, the peak magnetic field essentially induction. The initial peak field present in measurements made beyond a few kilometers and associated with the radiation field component of the breakdown pulse current is present in the close electric and magnetic fields but is small compared with the electrostatic and induction fields, respectively. The effect of the decrease of the breakdown pulse current with height is primarily to decrease the magnitude of the initial electrostatic and induction peaks.

4. At ranges less than about 200 m the vertical electric field above ground is bipolar for the unattenuated pulse current due to the passage from below to above of the charge associated with the breakdown pulse current. As one moves farther away from the channel, is near the ground, or considers a pulse which decays with height, this bipolar effect is reduced. On the ground near the channel the electric field is always unipolar and of opposite polarity as compared to the initial bipolar field, since the charge motion is always at a height above that of the field point.

5. At ranges less than about 1 km the peak value of the horizontal electric field above ground is larger than the associated vertical electric field. The horizontal and vertical

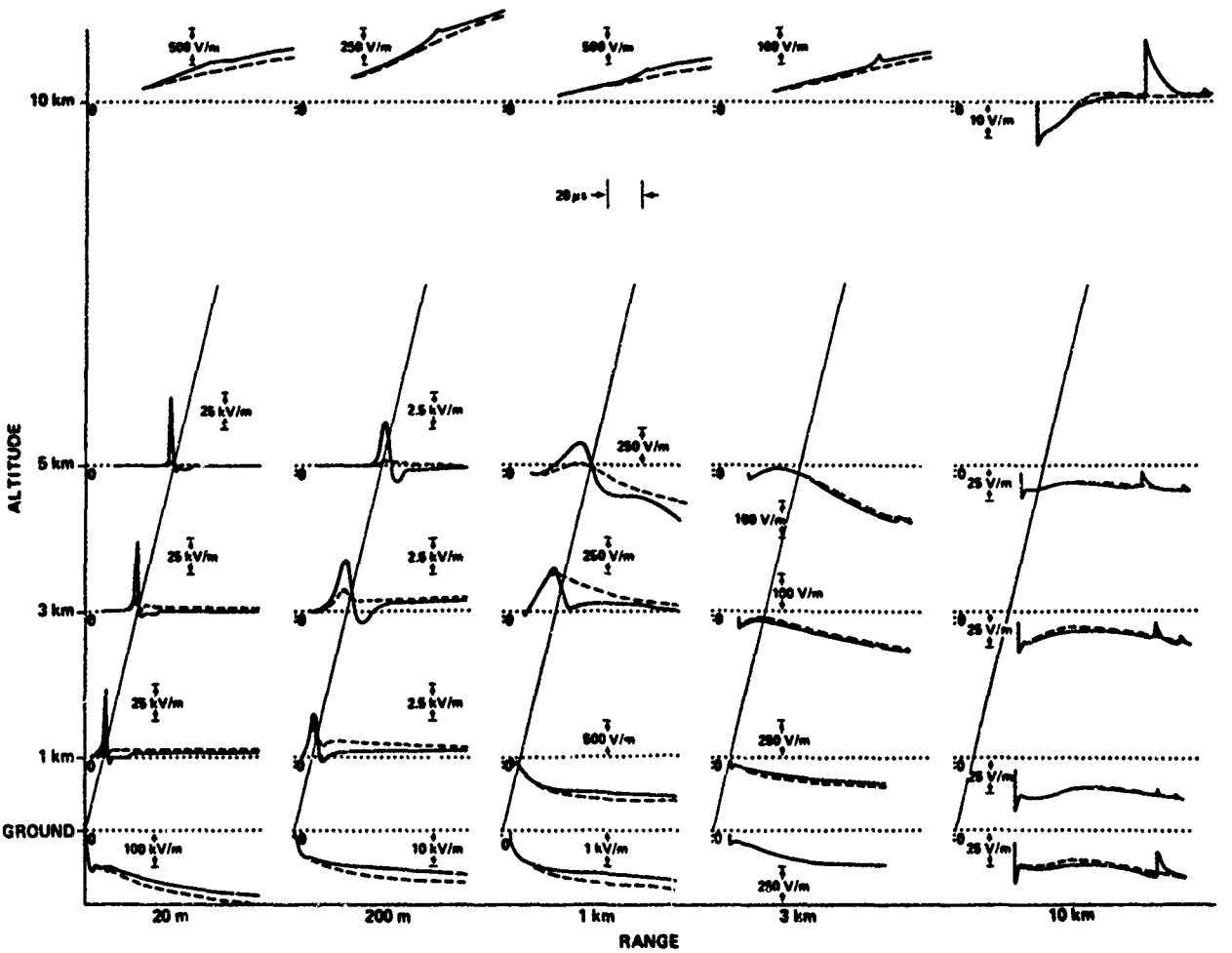

Fig. 4*a*. Calculated vertical electric fields for a typical subsequent return stroke. The solid lines represent the original model in which the breakdown pulse current is constant with height; the dashed lines the modified model in which it decreases with height.

fields above ground are roughly equal in peak magnitude in the 3 km range, and the vertical field is larger beyond about 10 km.

6. At ranges greater than 10 km the magnetic field and the vertical electric field are relatively weak functions of altitude, whereas the horizontal electric field increases roughly linearly with altitude. The magnetic field and the vertical electric field are height independent as long as the difference between the propagation paths from the source dipole and its image is much less than the wavelength of the highest significant frequency component of the electromagnetic radiation from the source, a condition which is met to a reasonable approximation at a range of about 10 km at altitudes below about 3 km for the current waveshapes used in the model. Hence measurements of distant magnetic and vertical electric fields made simultaneously on the ground and in the air provide a simple means of calibrating the airborne measurements.

7. The initial nonzero value associated with the waveforms, which can be clearly seen in Figures 4*a*, 4*b*, and 4*c* at, for example, 10 km, is due to the induction field from the uniform current component (component 2 in the model) assumed to exist at the time at which the breakdown pulse current is initiated at ground level. We associate the uniform current with the dart leader which preceeds the return stroke. The electrostatic field value at the time of the initiation of the return stroke at ground due to the current flow prior to that time is unknown and hence is not included in the calculated fields. In the work by *Lin et al.* [1980] the initial field value was plotted as zero, since the actual value could not in general be determined from the type of measurements made by *Lin et al* [1979].

Discussion

In this paper we have presented the first detailed estimates of airborne electric and magnetic fields due to lightning. We have used the original model of *Lin et al.* [1980] and also a modified version based on observations of *Lin et al.* [1979] and of *Jordan and Uman* [1980]. The new version of the model (1) results in fields which do not exhibit abrupt changes associated with the breakdown pulse current reaching the top of the channel and (2) can be expected to produce an initial luminosity which decreases with height above the ground. Though the individual currents which define the modified model are not unique (see discussion by *Lin et al.* [1980]), it is likely that the total current, which results in accurate prediction of ground-based fields and is consistent with (1) and (2) above, predicts airborne fields which are at least qualitatively correct.

We have modeled the return stroke channel as a straight vertical antenna. An actual return stroke channel is charac-

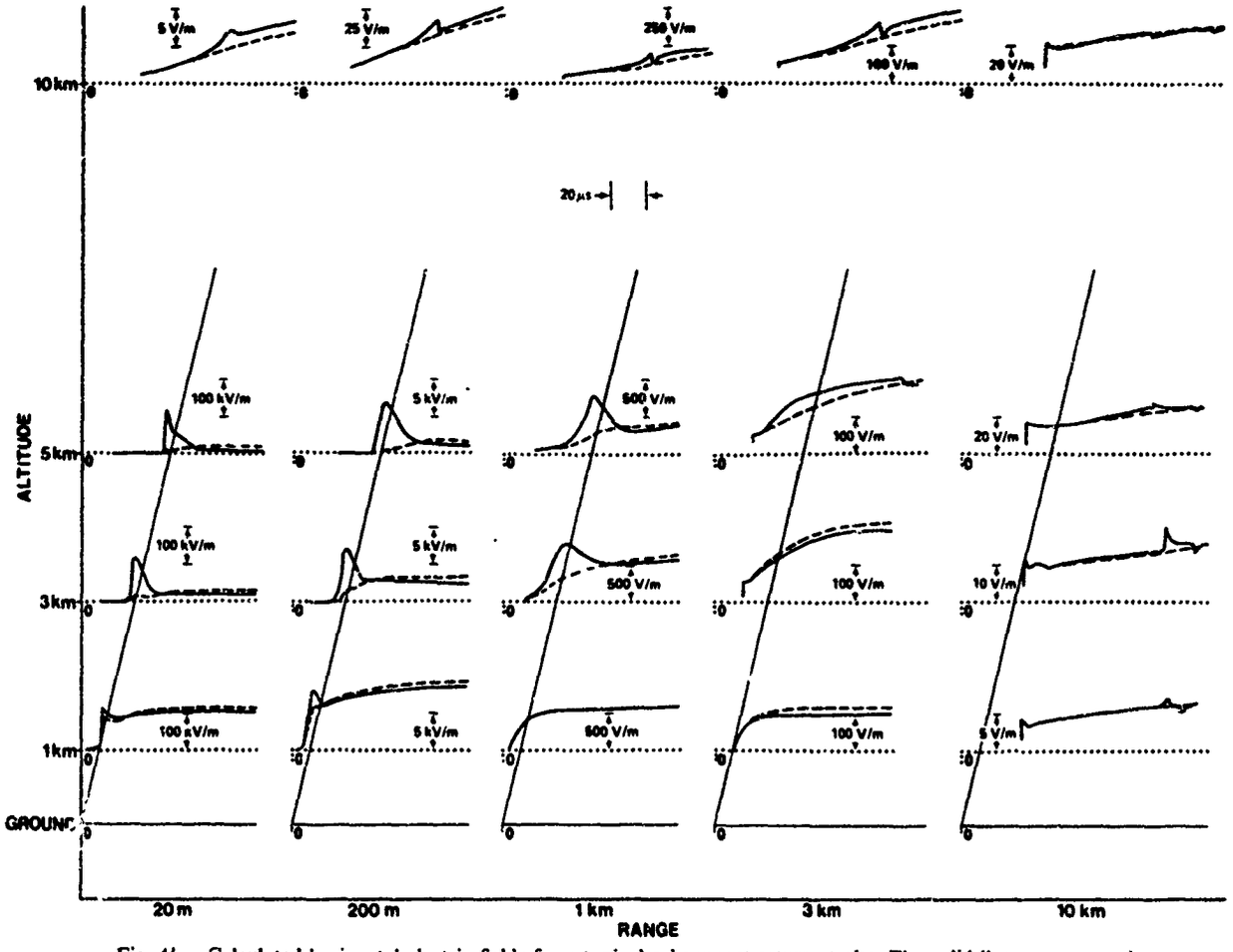

Fig. 4*b*. Calculated horizontal electric fields for a typical subsequent return stroke. The solid lines represent the original model in which the breakdown pulse current is constant with height; the dashed lines the modified model in which it decreases with height.

terized by tortuosity on a scale from less than 1 m to over 1 km [e.g., *Evans and Walker*, 1963; *Hill*, 1968]. *Hill* [1969] and *LeVine and Meneghini* [1978], using simple models, have investigated the effects of channel tortuosity on distant radiation fields. LeVine and Meneghini find that the waveforms computed for the case of a tortuous channel have finer structure than those for a straight channel, resulting in a frequency spectrum for the tortuous channel that has larger amplitude at frequencies above about 100 kHz. Hill shows that horizontal channel sections radiate significantly for frequencies above 20–30 kHz but does not compare the radiation from horizontal channel sections with that from vertical sections. The effect of using a tortuous channel to model the lightning return stroke fields at close range has been investigated by *Pearlman* [1979], again using a simple model. His results indicate that channel tortuosity has little effect on the close fields. Since the peaks in the close electric and magnetic fields are due to the charge and current, respectively, associated with the breakdown pulse current (as discussed in (3) of the previous section), we suggest on physical grounds that the general shapes of the close fields should not be greatly different from those shown. However, the peak fields at close range should occur at the time the breakdown pulse reaches the point of closest approach to the field point, and thus the distance of closest approach replaces the range in Figures 4*a*, 4*b*, and 4*c*.

Available data on airborne field measurements are limited to the observations of *Pitts and Thomas* [1980] and of *Baum* [1980]. Pitts and Thomas do not appear to have any data on return stroke fields. Baum presents airborne measurements made on first and subsequent return stroke electric and magnetic fields. He gives one typical first and one typical subsequent return stroke electric field waveform. He does not, however, make an independent measurement of the distance to the lightning flashes he records. Rather, he uses the values of the observed airborne initial peak fields and the average observed values on the ground as a function of distance obtained by *Lin et al.* [1979] to estimate the range. We have shown in this paper that the peak radiation fields for distances beyond about 10 km are about the same in the air and on the ground. However, the comparison with average values of the fields on the ground as a function of distance can lead to range errors of two or three, since individual field values may differ from the average by this factor [*Lin et al.*, 1979]. If we do use Baum's ranging technique, the subsequent stroke waveform he gives is at a range of about 20 km. The aircraft was at an altitude between 3 km and 5 km. The measured airborne electric field is very similar to typical measured fields on the ground at that range, as expected from the theory presented in this paper. A test of the validity of the predicted fields and hence the model awaits measurement at close range of simultaneous

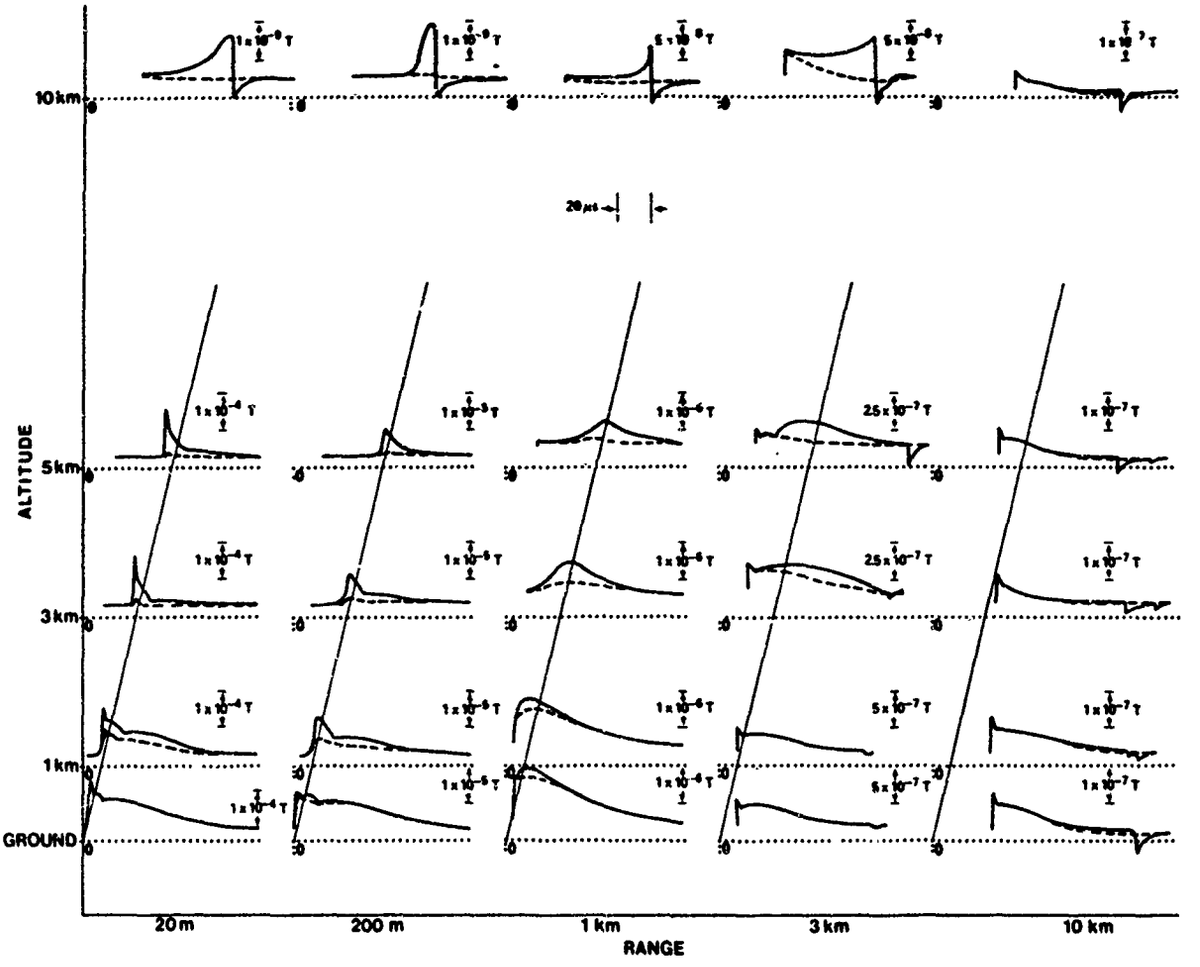

Fig. 4c. Calculated magnetic fields for a typical subsequent return stroke. The solid lines represent the original model in which the breakdown pulse current is constant with height; the dashed lines the modified model in which it decreases with height.

ground-based and airborne return stroke electric and magnetic fields.

Acknowledgments. The research reported here was primarily funded by the National Science Foundation (ATM-79-02627), the National Aeronautics and Space Administration, Kennedy Space Center (NGR-10-005-169), and the Office of Naval Research (N00014-81-K-0177). Additional funding was provided by Wright Aeronautical Laboratories, Wright Patterson Air Force Base, under contract F33615-79-C-3412, through Lightning Location and Protection, Inc., Tucson, Arizona.

REFERENCES

Baum, R. K., Airborne lightning characterization, Lightning Technology, suppl., *NASA Conf. Publ. 2128*, 1–19, 1980.

Corbin, J. C., Protection/Hardening of aircraft electronic systems against the indirect effects of lightning, *Rep FAA-RD-79-6*, 97–103, Fed. Aviat. Admin., Washington, D. C., 1979.

Evans, W. H., and R. L Walker, High speed photographs of lightning at close range, *J. Geophys. Res.*, *68* 4455–4461, 1963.

Hill, R. D., Analysis of irregular paths of lightning channels, *J. Geophys. Res.*, *73*, 1897–1906 1968.

Hill, R. D., Electromagnetic radiation from erratic paths of lightning strokes, *J. Geophys. Res.*, *74*, 1922–1929, 1969.

Jordan, D. J., and M. A. Uman, Variations of light intensity with height and time from subsequent return strokes, *Eos Trans. AGU*, *61*, 977, 1980.

LeVine, D. M., and R. Meneghini, Simulation of radiation from lightning return strokes, *Radio Sci.*, *13*, 801–809, 1978.

Lin, Y. T., M. A. Uman, J. A. Tiller, R. D. Brantley, W. H. Beasley, E. P. Krider, and C. D. Weidman, Characterization of lightning return stroke electric and magnetic fields from simultaneous two-station measurements, *J. Geophys. Res.*, *84*, 6307–6314, 1979.

Lin, Y. T., M. A. Uman, and R. B. Standler, Lightning return stroke models, *J. Geophys. Res.*, *85*, 1571–1583, 1980.

Pearlman, R. A., Lightning near fields generated by return stroke current, International Symposium on Electromagnetic Compatibility, Inst. Electr. Electron. Eng., San Diego, Calif., 1979.

Pitts, F. L., and M. E. Thomas, 1980 direct strike lightning data, *NASA Tech. Memo.*, *81946*, 1981.

Pitts, F. L., M. E. Thomas, R. E. Campbell, R. M. Thomas, and K. P. Zaepfel, Inflight lightning characteristics measurement system, *Rep. FAA-RD-79-6*, 105–111, Fed. Aviat. Admin., Washington, D. C., 1979.

Schonland, B. F. J., The lightning discharge, in *Handbuch der Physik*, vol. 22, pp. 576–628, Springer-Verlag, Berlin, 1956.

Stratton, J. A., *Electromagnetic Theory*, pp. 582–583, McGraw-Hill, New York, 1941.

Uman, M. A., D. K. McLain, and E. P. Krider, the electromagnetic radiation from a finite antenna, *Am. J. Phys.*, *43*, 33–38, 1975.

Weidman, C. D., and E. P. Krider, The fine structure of lightning return stroke waveforms, *J. Geophys. Res.*, *83*, 6239–6247, 1978.

(Received July 20, 1981;
revised September 21, 1981;
accepted September 21, 1981.)

APPENDIX 2

Electric Fields Preceding Cloud-to-ground Lightning Flashes

Electric Fields Preceding Cloud-to-Ground Lightning Flashes

WILLIAM BEASLEY, MARTIN A. UMAN, AND P. L. RUSTAN JR.[1]

Journal of Geophysical Research, vol. 87, no. C6, June 20, 1982

JOURNAL OF GEOPHYSICAL RESEARCH, VOL. 87, NO. C7, PAGES 4883–4902, JUNE 20, 1982

Electric Fields Preceding Cloud-to-Ground Lightning Flashes

WILLIAM BEASLEY, MARTIN A. UMAN, AND P. L. RUSTAN JR.[1]

Department of Electrical Engineering, University of Florida, Gainesville, Florida 32611

We analyzed in detail the electric field variations preceding the first return strokes of 80 cloud-to-ground lightning flashes in nine different storms observed at the NASA Kennedy Space Center during the summers of 1976 and 1977. The electric field variations are best characterized as having two sections: preliminary variations and stepped leader. The stepped-leader electric-field change begins during a transition period of a few milliseconds duration marked by characteristic bipolar pulses. The durations of stepped leaders lie most frequently in the range 6–20 milliseconds. We infer from our measurements and critical review of the previous literature that there is only one type of stepped leader, not the two types, α and β, often referred to in the literature.

INTRODUCTION

Electric field variations preceding cloud-to-ground lightning flashes have been the subject of numerous studies dating from the earliest days of lightning research to the present. Some of the more important results are reported in papers by *Appleton and Chapman* [1937], *Schonland et al.* [1938*a*], *Chapman* [1939], *Malan and Schonland* [1951], *Pierce* [1955], *Kitagawa* [1957], *Clarence and Malan* [1957], *Kitagawa and Brook* [1960], *Krehbiel et al.* [1979], and *Thomson* [1980]. Unfortunately, there is considerable confusion in the literature in the terminology used to describe the observations and in the physical interpretations of the data. In an attempt to improve matters, we analyzed in detail the electric fields preceding first-return strokes of 80 cloud-to-ground lightning flashes from nine Florida thunderstorms to address the questions that follow.

1. In the continually varying electric fields that occur during local thunderstorms are there ever, sometimes, or always, characteristic preliminary variations that occur significantly in advance of stepped-leader field changes and which are related to, or even causative precursors of, the eventual first return strokes of cloud-to-ground flashes?
2. If so, what are the durations of the preliminary variations, and how does one distinguish those which may be related to the succeeding cloud-to-ground flash from the other variations in electric fields which may occur continuously during thunderstorms?
3. How does one identify the beginning of a stepped-leader electric field change?
4. What shapes do stepped-leader electric fields have at various nominal distances from lightning flashes?
5. What are the durations of stepped-leader field changes, and do they vary with distance or storm?
6. Can we construct a coherent, inclusive description of the phenomenology of electric fields preceding first return strokes to help reconcile the disparate inferences of previous studies?

One of our primary concerns has been to separate, as much as possible, the description of electric field variations from speculation or presumptions about the processes giving rise to the fields.

In the paragraphs to follow, we describe the instrumentation and procedures we used to record, reduce, and analyze the electric field data for this study. Then we present examples of waveforms at various distances along with discussions of definitions, subjective judgements, and possible biases, concluding with the results compiled from the measurements of 80 flashes. Next, we compare our results with those of previous studies, making, in the process, a first attempt at a synthesis that comprises previous disparate views of the field changes preceding first-return strokes and that answers the questions raised in the paragraphs above.

ACQUISITION AND REDUCTION OF DATA

The systems we used to record the lightning electric fields and supporting data are shown in Figure 1. These were employed by us at the Kennedy Space Center of the United States National Aeronautics and Space Administration during the Thunderstorm Research International Program (TRIP) (1976–1978). For a description of TRIP, see *Pierce* [1976].

In 1976 the system consisted of a flat-plate electric field antenna of area 0.2 m^2 and an analog integrator (symbol $\int_s$, *s* for slow decay) with 3 dB bandwidth of about 0.03 Hz to 2 MHz. The sensitivity was switchable for close, intermediate, or distant lightning (C, I, D). The signals were recorded on an instrumentation tape recorder on two channels: one FM channel with 3 dB bandwidth from 0 Hz to 20 kHz and one direct channel with 3 dB bandwidth from 300 Hz to 300 kHz. The electric field signals were ac-coupled to the direct channel through a preamplifier with switchable gain.

In 1977 we used a similar system but with improved recorder bandwidth and dynamic range. There were two flat-plate antennas having areas 0.2 m^2 and 0.05 m^2, each followed by integrators and amplifiers to provide four channels of electric field signals with approximate 3 dB bandwidth of 0.03 Hz to 1 MHz with 80 dB dynamic range set to cover the range 4 V/m to 40,000 V/m. These signals were recorded in FM mode with record-reproduce bandwidth from 0 Hz to 500 kHz (−6 dB). Also, we recorded the signals from another electric field antenna (integrator symbol $\int_f$, *f* for fast decay) on direct channels (3 dB bandwidth 400 Hz to 1.5 MHz) for the triggered oscilloscope recording system used for other studies as described by *Lin et al.* [1979].

In both years we recorded thunder, time code, and electric

[1] Now at Air Force Institute of Technology, Wright-Patterson Air Force Base, Ohio 45433

Paper number 2C0389.
0148-0227/82/002C-0389$5.00

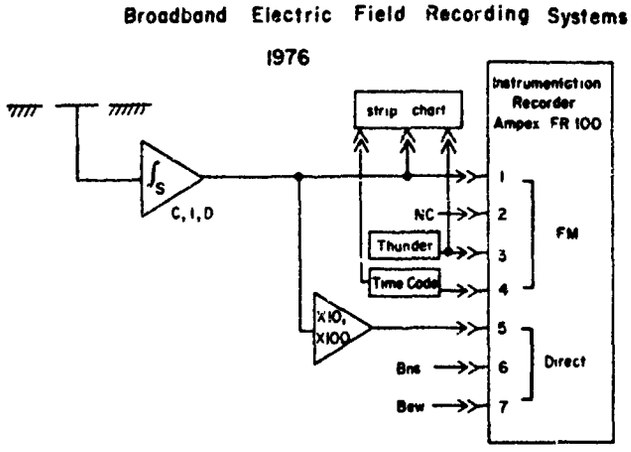

Fig. 1a. Electric field recording system, 1976.

field on strip charts, on which observers' comments were written. We searched these strip charts for cloud-to-ground flashes for which time to thunder could be determined with little or no ambiguity to within about ±1 s or less. This uncertainty in time corresponds to an uncertainty in distance of about ±30% at 1 km and ±3% at 10 km. The result was a list of several hundred flashes of which 80 survived the reduction and analysis procedures to be described next.

To render the electric field signals recorded on magnetic tape in a form suitable for analysis, we played back the tapes into Biomation 805 digital waveform recorders. We set the waveform recorders to trigger on the first return stroke of each flash. We sometimes set the recorder to trigger on pulses preceding the first return stroke, and sometimes played the tape in reverse, triggering on the first return stroke, to obtain details of all significant portions of the field variations. We used both pretrigger and delayed-trigger modes and a variety of sample rates. We made permanent records of the field variations on polaroid prints and/or strip charts.

The uniqueness of our data derives from its combination of wide bandwidth, great dynamic range, and high time resolution. These features allowed us to eliminate some of the ambiguities hindering past studies because we were able to study a wide range of pulses and small-scale variations, in more detail, for longer intervals in data records, than ever before possible.

In the course of this work we studied several cases for which we had available to us the locations of VHF radiation sources active during the stepped leader and a few milliseconds before. The principal purpose of the case studies was to try to find a reasonably precise way to determine the beginning of the electric field change attributable to stepped leaders; that is, to differentiate between preliminary processes occurring within the cloud and the beginning of the motion toward earth of significant quantities of charge. The locations of VHF radiation sources were obtained by the technique of *Rustan* [1979] and *Rustan et al.* [1980], a computer-implemented time-series analysis for determination of differences in time of arrival of VHF radiation pulses at four ground stations, coupled with a hyperbolic position-fixing program that calculated the source locations from the differences in time of arrival.

Analysis of Electric Field Data

Procedure

On the waveforms of electric field for each flash, we chose the following measuring points according to criteria described later: (1) the beginning of the preliminary variations; (2) the beginning of the stepped leader (and end of the preliminary variations); (3) the return-stroke radiation field peak; (4) the end of the most rapidly changing portion of the electric field change of the first return stoke; and (5) the 1, 2, and 3 ms points of the return-stroke field change following the radiation field peak. The points 1, 2, 4, 5 were measured with respect to the time of occurrence of the radiation field peak of the return stroke, (point 3), which is the most obvious, least ambiguous portion of electric field change records of cloud-to-ground lightning flashes when recorded with enough bandwidth to preserve significant variations that occur on a scale of microseconds. Since the preliminary variations, stepped leaders, and the rapidly changing portion of the return-stroke field changes have durations of hundreds of milliseconds, tens of milliseconds, and hundreds of microseconds, respectively, the time of occurrence of the return-stroke radiation field peak, measured with an uncertainty of a few microseconds, is an excellent reference point. For this study we were concerned only with the field variations up to and including the first return stroke of each flash. Subsequent strokes, even if preceded by a so-called dart-stepped leader, were not included.

Preliminary Variations

In the simplest cases there were no significant variations in electric field before the stepped leader, but often there was a

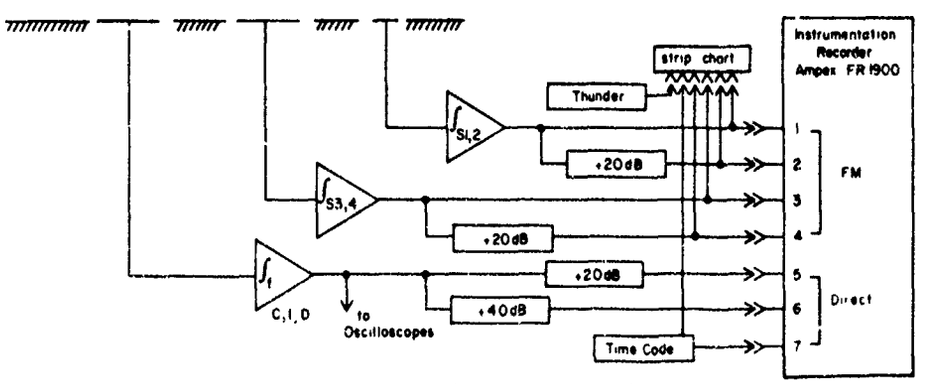

Fig 1b. Electric field recording system, 1977.

step, an abrupt change in slope, or a pulse a few to a few hundred milliseconds before the beginning of the stepped leader. If the electric field record had been quiet up to that point, then it was relatively easy to label it as the beginning of the preliminary variations.

There were, however, numerous cases in which the decision was not easy. At one extreme were cases in which the field record was relatively quiet, but never for long enough between noisy sections to allow much certainty as to which was the best choice of point to call the beginning of the preliminary variations. At the other extreme were a few cases in which there were almost continuously occurring, relatively large-scale, electric field changes (comparable in magnitude with cloud-to-ground flashes) of both positive and negative polarity, punctuated every few seconds by cloud-to-ground flashes. In these cases, an arbitrary, intuitive, intrinsically subjective decision was made as to which point on the record to call the beginning. This subjectivity must be taken into consideration if any attempt is made to draw too broad conclusions about discharge processes from the data on preliminary variations.

Stepped Leaders

Though still not always without ambiguity, the decisions as to where in the field variations stepped leaders began and preliminary variations ended were usually less difficult than the decisions as to where preliminary variations began. In some cases, there was no doubt. In more complex cases we chose among alternatives by using either, directly or indirectly, some or all of the following: (1) the occurrence of characteristic pulses in the broadband electric field record at about the same time that the last electrostatic field change comparable in size with the return stroke began; (2) the occurrence of similar characteristic pulses in the envelope of VHF radiation at the same time and the behavior of the VHF radiation sources at that time; (3) limits on shape and duration of field changes indicated by a simple physical model consisting of a point source at height H, from which a uniform line charge extends vertically downward at constant velocity toward a conducting earth [*Malan and Schonland*, 1947; *Uman*, 1969]; and (4) limits, indicated by the simple physical model, on the ratio of stepped-leader electric field change to return-stroke electric field change at various distances.

The guidance of the first and second, above, was derived from our study of six cases for which there were reasonably good records of characteristic pulses in the electric-field waveform at about the time of the beginning of the last significant electrostatic field-change interval. We examined the field records for these cases with high time resolution for durations of 5–20 ms. In the case illustrated in Figure 2, significant VHF radiation, called preliminary breakdown by *Rustan* [1979], began at about the same time as the preliminary variations in electric field. The last millisecond of the preliminary variations is marked PV in Figure 2*a*. The characteristic pulses, examples of which are marked CP in Figure 2*a*, are typically bipolar, with initial excursion in the same direction as the succeeding return-stroke field change, marked RS. Total widths are between about 20 and 100 μs in different cases, and they occur at intervals of 30–200 μs. We believe it reasonable to assume that these pulses are probably the same as seen by *Appleton and Chapman* [1937] as the fine structure of the initial part of a lightning flash electric field variation (see discussion later). They are also possibly those called 'beta' leader pulses by *Schonland et al.* [1938*a*], and many others [for example, *Kitagawa*, 1957; and *Kitagawa and Brook*, 1960]. They are probably also the same as those seen to occur before first strokes by *Weidman and Krider* [1979].

The example shown in Figure 2 was especially interesting because the envelope of VHF radiation showed clearly the same pulses as in the broadband electric field records, as shown in Figure 2*b*. The sources radiating the pulses, located by the technique cited earlier, were in the thunderstorm cloud at heights between about 4 and about 6 km; that is, approximately between the 0°C and −10°C ambient air temperatures. The occurrence of these pulses apparently marks a transition in character of the VHF noise records and a shift in the average locations of active source regions from above to below the region between 4 and 6 km. Although a more extensive study of the significance of these characteristic pulses is necessary before we can draw firm conclusions, we believe it is reasonable to say that these pulses probably signify a period of transition between preliminary discharge activity involving little net motion of charge (PV) and the onset of the stepped leader (SL). It is important to note that the 'preliminary breakdown' of *Rustan* [1979] and *Rustan et al.* [1980] is identified on the basis of the character of the VHF radiation and is not presumed to be identical with the discharge processes that give rise to what we have labeled 'preliminary variations' in the electric field records, although there may be at least some portions of both that are manifestations of the same processes. The characteristic pulses such as those shown in Figure 2 appear, at least some of the time, to mark the beginning of a period in the electric field record during which there is no further major discontinuity other than narrow pulses in the field change up to the return stroke. We used this observation to provide general insight as to how to determine where the stepped leader began, so that, lacking other evidence, we take the beginning of the stepped leader at the earliest point after which there is no discontinuity or abrupt change in slope except in a few special cases in which that choice leads to violation of the third and fourth requirements above.

A simple model for a leader can be constructed by postulating a spherically symmetric charge source distribution centered at height H, from which a uniform line charge extends

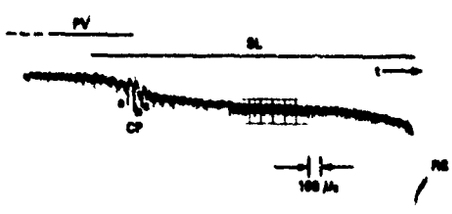

Fig. 2*a*. Preliminary variation (PV) and stepped-leader electric fields (SL) preceding a cloud-to-ground flash at 11 km distance. Characteristic pulses are labeled 'CP.'

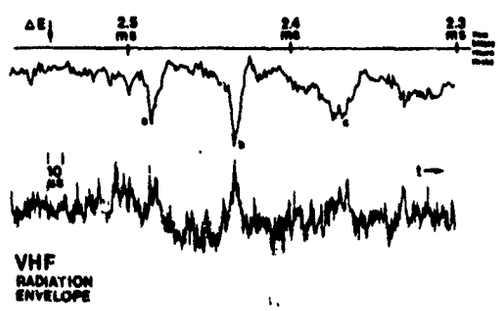

Fig. 2*b*. Comparison of VHF radiation envelope and broadband electric field records of 'characteristic' pulses.

vertically downward at constant velocity v toward a conducting ground plane. This model accounts for the effects of the line charge (leader) as well as the decrease in charge at height H. Details may be found in *Malan* and *Schonland* [1947] and *Uman* [1969]. The electric field change at the ground at any instant t at distance D from the channel is

$$\Delta E = \frac{-2p}{4\pi\varepsilon_0 D}\left[\frac{1}{(1+x^2/D^2)^{1/2}} - \frac{1}{(1+H^2/D^2)^{1/2}} - \frac{(H-x)}{D}\frac{H}{D}\frac{1}{(1+H^2/D^2)^{3/2}}\right]$$

where $x = H - vt$ is the height of the bottom of the line charge. We expect this model to be a better approximation for distant flashes, where branches and channel tortuosity have less effect and local point discharge should not affect the measured fields. The extent of the effects of branching or of charge distributions other than the uniform one postulated can be judged at least qualitatively by the ratio of leader field change to return-stroke field change at distances greater than about 30 km. The simple model predicts the ratio will approach unity if we assume that the charge deposited on the channel by the leader, no more, no less, is removed by the return stroke.

Because of both physical variations and uncertainties in data analysis the observed ratio of leader and return-stroke field changes could differ from unity for distant flashes. For example, failure of the return stroke to remove all the charge deposited uniformly on the leader would result in a ratio greater than unity. Even if all the charge were removed, a nonuniform distribution on the leader could lead to a ratio greater or less than unity, if the distribution were weighted toward the bottom or top. If, in addition to removing the charge deposited on the channel by the leader, the return stroke were to lower charge from its source within the cloud as well, the ratio could be less than unity. Choice of a 'wrong' starting point in field-change records for a leader could lead to an incorrect field-change value. Choice of the 'wrong' point for the cessation of the return stroke could lead to an incorrect return-stroke field-change value, although this can be avoided in most cases by taking the return-stroke field-change value after the field has stopped changing appreciably, usually by 2 or 3 ms after the return stroke starts, as our results will show. Furthermore, a measured ratio of unity for distant flashes might occur sometimes as a result of a combination of the effects described above even if the assumption regarding the model were not satisfied. All of these possibilities imply that we should exercise caution in our drawing conclusions from the occurrence or lack of occurrence of a unity ratio. Nonetheless, we felt compelled to examine the ratio of leader and return-stroke electric field changes for a large number of distant flashes if for no other reason than to compare with previous results.

The model predicts particular shapes of leader field changes and ratios of leader and return-stroke field changes as a function of distance and also provides some estimates of limits on durations, based on assumption of leader velocities. In the case of shapes and ratios, the extent to which the model appears to fit is dependent especially on the choices of starting points for stepped leaders and the end value of return-stroke field changes. But, since we have in mind the shapes and ratios predicted by the model, we cannot avoid at least a subconscious influence by our expectations on the choices we make. It therefore seemed better, and more direct, consciously to use the predicted shapes and ratios as arbiters in otherwise ambiguous cases than to pretend complete objectivity and independence from influence by the model predictions. We estimate that we used our expectations as to shape or ratio of leader and return-stroke field changes overtly to decide between two alternative choices for the starting point of a stepped leader in approximately 25–50% of the cases presented herein. For example, the model predicts that stepped leaders having their origins at 5 km height should have electric field changes that start in the negative direction when observed at distances up to about 7 km. For 10 km height, the field change would start in the negative direction at distances up to about 14 km. So in all cases we expect the leader of flashes at greater distances to start out nonnegative. If the field variations preceding the first return stroke of a distant flash had an early negative-going portion and a later positive one, this result caused us usually to choose the latter of the two alternative points as the beginning of the stepped leader. The model predicts that the net field change at the end of the leader should be zero when $H/D = 1.27$. For heights between 5 and 10 km, we expect the net leader field change to be near zero for distances between about 6 and 13 km. This expectation caused us sometimes to pick the earlier of two alternative starting points, if it were negative-going, for flashes in this range. The result, shown later, that leader duration is not apparently dependent on distance, serves as a measure of evidence that our occasional use of model predictions did not cause undue bias in the data. Also, if there were significant horizontal extent of the leader channel, as discussed by *Krehbiel et al.* [1979] and *Thomson* [1980], the use of this simple model would be questionable. We believe that there were few, if any, such occasions in our data because the storms were mainly afternoon convective thunderstorms. We cannot completely rule out the possibility, though. We deal with it briefly in conjunction with the discussion of a few anomalous results.

To make estimates of limits on leader durations, we assumed the height of the leader-charge source could be between 6 and 10 km as found in *Jacobson and Krider* [1976]. If we take a leader velocity between 1×10^5 m s^{-1} and 3×10^6 m s^{-1} [*Uman*, 1969] and assume a straight vertical channel, we obtain estimates of stepped-leader durations from 2 to 100 ms. If we asume that the first-stroke charge source height falls toward the lower end of the range, say 6 km, and a typical velocity of 1.5×10^5 m s^{-1} [*Uman*, 1969], then we would expect the most frequent value of duration to be about 40 ms. This compares favorably with the results in Table 3.

Return Strokes

After the initial radiation field peak, the electric field changes of return strokes in the range of distances we are considering, 0–20 km, exibit a relatively steep slope that gradually decreases for, say, 50–400 μs, then usually exhibits a more abrupt decrease in slope, a sort of 'knee,' after which the field increases only relatively gradually for an additional millisecond or so. In most cases the field does not increase by more than a few percent after 2 or 3 ms. For use in calculations of the ratio of the electric fields of the leader and return stroke, we measured the time of occurrence of the 'knee' and the value of the return-stroke field change at the 'knee' and at 1, 2, and 3 ms.

RESULTS

Preliminary Variations

We were unable to discern any particular significance in the variety of shapes, sizes, and durations of preliminary variations

TABLE 1. Start Times of Preliminary Variations

Storm Year Day	Earliest, ms	Latest, ms	Mean, ms	Standard Deviation, ms	Median, ms	Number of Events	Mode, ms
76181	290	28	98	108	60	5	
76195	400	11.5	75	102	60	13	
76201	58	14	40	16	40	5	
76203	100	11.5	42	37	29	4	
77203	150	120	135	21	—	2	
77211	270	22	92	64	65	26	
77212a	500	130	369	141	430	7	
77212b	270	56	148	76	135	12	
77220	60	11	21	19	14	6	
Overall	500	11	118	66	65	80	60–70

Milliseconds before first return stroke.

as they appeared in our measurements other than that there is very frequently some discharge activity in thunderstorm clouds as much as a few hundred milliseconds before a cloud-to-ground flash. Sometimes there is almost continuous discharge activity for long periods of time, minutes up to many tens of minutes, with a cloud-to-ground flash every few seconds. Any pattern that might exist has eluded us.

We assigned a start time (that is, a number of milliseconds before the return stroke) to each preliminary variation. These are summarized in Table 1, and plotted in Figure 3. In Figure 3 and all succeeding plots, we use a separate symbol for each storm. In the table and figures to follow, the five-digit numbers such as 76181 are the year and Julian day. After the start time for the preliminary variation had been chosen, we chose the start time for the stepped leader. The difference in the two times was the duration of the preliminary variation, summarized in Table 2. In Figure 4 we have plotted these durations versus distance. The apparent start times and durations show some tendency to be dependent on the particular storm in which the flashes occurred. Note that all but one of the events from storm 77212a were assigned start times and durations greater than about 200 ms and that all but one event assigned a start time or duration greater than 300 ms was in that storm. Also, note that all the preliminary variations on storm day 77220 had relatively short, sometimes zero, duration. Whether the apparent dependence on storm day is evidence for some physical mechanism or is a result of unknown biases in data analysis is not clear. It is clear from Table 1 that the preliminary variations most frequently began approximately 60–70 ms before the return stroke. About as many started more than 65 ms before the return stroke as started less than 65 ms before it. Most frequently the preliminary variations lasted between 0 and 20 ms before the return stroke. The median duration was about 42 ms. We assigned start times to 80 preliminary variations, but durations to only 79 because we could not determine with confidence the start time of one stepped leader.

Stepped Leaders

It appears that the preliminary variations end and stepped leaders begin during a transition period of a few millisecond during which certain characteristic bipolar pulses appear in the broadband electric field record and also in the envelope of 30–50 MHz radiation. Though we have examined only six cases in sufficient detail, we believe that these pulses are probably

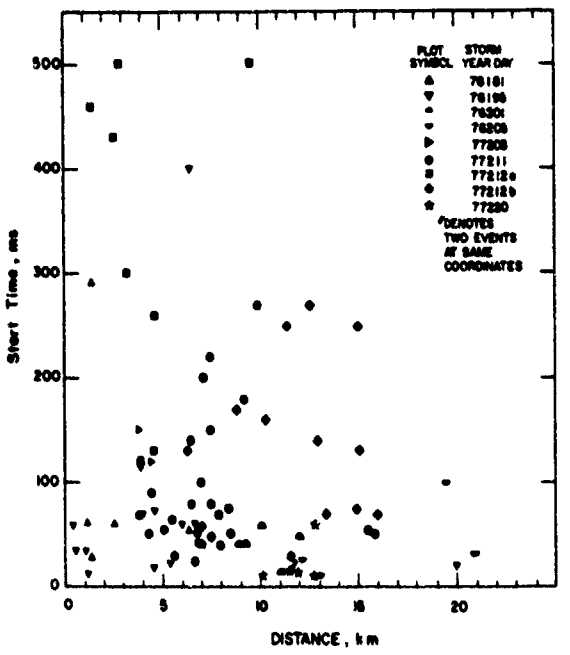

Fig. 3. Start time, before return stroke, of preliminary variations in electric field, as function of distance and by storm.

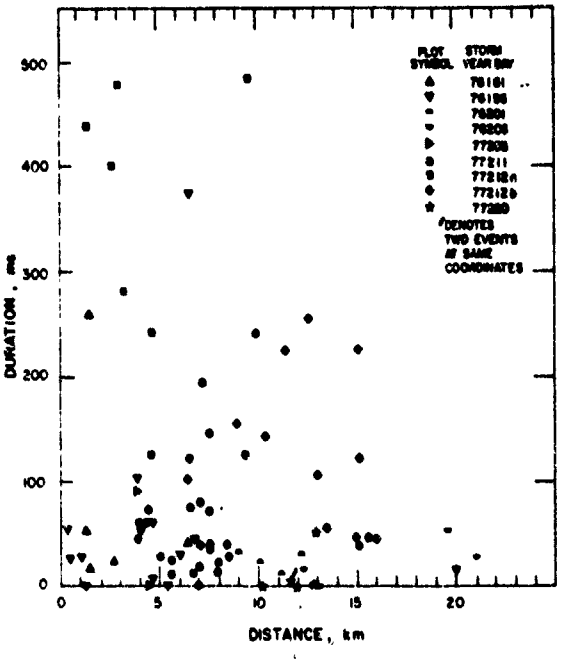

Fig. 4. Duration of preliminary variations in electric field preceding stepped leader, as function of distance, by storm.

TABLE 2. Durations of Preliminary Variations

Storm Year Day	Longest, ms	Shortest, ms	Mean, ms	Standard Deviation, ms	Median, ms	Number of Events	Mode, ms
76181	258	18	79	101	42	5	
76195	373	0	61	98	30	13	
76201	34	11	24	10	~26	4	
76203	52	0	24	22	~22	4	
77203	90	0	45	64	—	2	
77211	240	0	61	59	39.5	26	
77212a	484	123	349	137	400	7	
77212b	254	38	126	77	114	12	
77220	53	0	12	20	~5	6	
Overall	484	0	90	115	42	79	0–20

present in all cases. They may sometimes be small and difficult to observe because of a high noise level, or insufficient sensitivity, for example. However, until a thorough study of the occurrence of the pulses and of the VHF radiation source locations during their occurrence has been completed, we hesitate to state categorically that they are always present or to speculate too much as to their physical significance. Although it is not yet completely clear whether they should be considered part of the stepped leader or of the preliminary variations, and since the matter is perhaps primarily one of definition, we have decided to be consistent with earlier definitions, from the time of *Appleton and Chapman* [1937] onward, which have the stepped leader begin with the onset of pulses. Another reason for this is that although the pulses sometimes start to occur before the slow field change, they also tend to continue into the early part of it, so that it is reasonable to believe that they have something to do with the beginning of earthward transfer of significant amounts of charge.

The 79 stepped leaders we analyzed in detail fall into either of two categories: about 70–80%, which could be matched reasonably well in shape, duration, and size, by the simple model discussed earlier; and about 20–30%, which could not. Those that fall roughly within bounds set by the model and that form groups of similar shapes within ranges of distance we will call 'representative' and will illustrate with examples of real waveforms in Figures 5–15. We will discuss special cases separately. In each figure the asterisk marks the time chosen as the beginning of the stepped-leader electric field change. The reason for the choice may not always be evident from the data in the figure. The direction and scale of electric field change are shown to the left. The time scale is shown at lower right. The Julian day, time (UT) and distance to the ground strike point are shown along the top.

The two closest stepped-leader electric field changes studied are presented in Figures 5 and 6. They are similar in all respects to those of *Livingston and Krider* [1978, Figure 11]. The closer one was at 300 m, had a duration of 6 ms, and a net electric field change of −41,500 V/m. The ratio of field changes of the leader and return stroke 3 ms after the beginning of the return stroke was −0.91. The other flash was at 500 m, had duration of 9 ms, net electric field change of −39,000 V/m, and leader to return-stroke ratio of −1.05. We note that these field-change values are about 10 times as great as the threshold for point discharge at the ground. We are assuming that any resulting space charge will have negligible effect on the measured field-change values on these time scales. We have chosen to call stepped leaders having this general shape 'close.' The slope of the electric field is always increasing up to the time of the return stroke. The most distant example of a field change having this shape in our data set, other than a special case (discussed later and illustrated in Figure 17) is shown in Figure 7. The flash was at 3.9 km. The field change had a duration of 26 ms, a net value of −540 V/m, and a leader to return-stroke ratio of −0.41.

The next most distant, clearly identifiable, group of waveforms we have chosen to call 'near intermediate.' The electric field changes start like those in the previous group, but then have decreasing slope up to the time of the return stroke. The field change may level off or even begin to go in the positive direction, but the net change for this group is always at least slightly negative. The closest example of such a shape is shown in Figure 8. The flash occurred at 1.2 km, had field change duration of 11.5 ms, field change of −6600 V/m, and ratio −0.46. The most distant example of a stepped leader with a shape in this class was at 7 km, shown in Figure 9. The duration was 40 ms, the field change −820 V/m, and the ratio −1.1. There is some question as to whether this example should be treated as a special case because of the large negative ratio of leader and return-stroke field changes, but none of the 'objective' criteria cited above could be invoked to interpret the data otherwise. It is definitely a borderline case. A more nearly

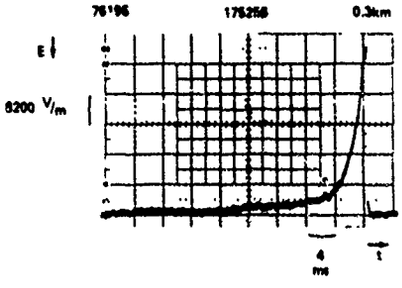

Fig. 5. Stepped-leader electric field change of a flash at 300 m ('close') distance. Arrow indicates 'positive' field according to convention of atmospheric electricity [*Uman*, 1969]. Asterisk marks beginning of stepped leader.

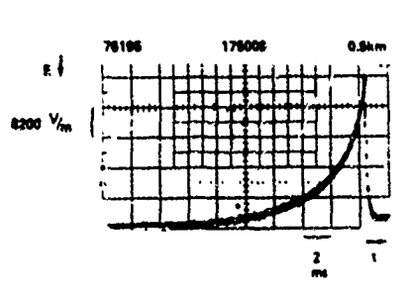

Fig. 6. Stepped-leader electric field change of a flash at 500 m ('close') distance. Arrow indicates 'positive' field according to convention of atmospheric electricity [*Uman*, 1969]. Asterisk marks beginning of stepped leader.

Fig. 7. ('close') di tion of at of stepp

Fig. 8. ('near inte to conven beginning

Fig. 9 ('near int to conve beginnin

Fig. 10 ('near int to conve beginnin

Fig. 1 intermed conventi beginnin

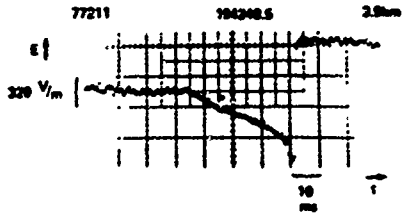

Fig. 7. Stepped-leader electric field change of a flash at 3.9 km ('close') distance. Arrow indicates 'positive' field according to convention of atmospheric electricity [*Uman*, 1969]. Asterisk marks beginning of stepped leader.

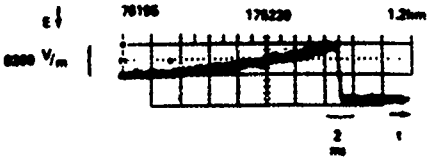

Fig. 8. Stepped-leader electric field change of a flash at 1.2 km ('near intermediate') distance. Arrow indicates 'positive' field according to convention of atmospheric electricity [*Uman*, 1969]. Asterisk marks beginning of stepped leader.

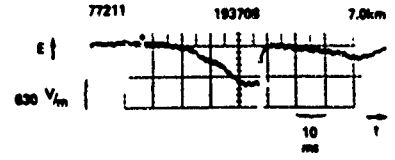

Fig. 9. Stepped-leader electric field change of a flash at 7.0 km ('near intermediate') distance. Arrow indicates 'positive' field according to convention of atmospheric electricity [*Uman*, 1969]. Asterisk marks beginning of stepped leader.

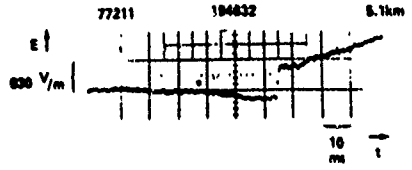

Fig. 10. Stepped-leader electric field change of a flash at 5.1 km ('near intermediate') distance. Arrow indicates 'positive' field according to convention of atmospheric electricity [*Uman*, 1969]. Asterisk marks beginning of stepped leader.

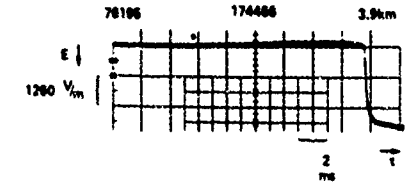

Fig. 11. Stepped-leader electric field change of a flash at 3.9 km ('far intermediate') distance. Arrow indicates 'positive' field according to convention of atmospheric electricity [*Uman*, 1969]. Asterisk marks beginning of stepped leader.

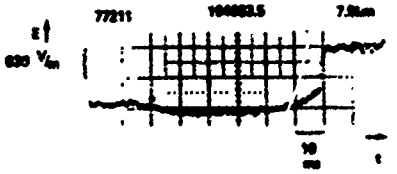

Fig. 12. Stepped-leader electric field change of a flash at 7.9 km ('far intermediate') distance. Arrow indicates 'positive' field according to convention of atmospheric electricity [*Uman*, 1969]. Asterisk marks beginning of stepped leader.

typical example of field change in this group is shown in Figure 10, which is for a flash at 5.1 km, with leader duration of 26 ms, net electric field change of about −160 V/m, and ratio −0.25.

The next group of field changes we call 'far intermediate.' They have relatively small net change, which may be either slightly negative, zero, or slightly positive. The starting point of these is more difficult to determine because the change in slope is very gradual and the initial field change may be either positive or negative though the magnitude of the net change is small, the magnitude of maximum field change may be up to about one half that of the return stroke, and will likely be negative if the initial slope is negative. If not negative, then the maximum magnitude will likely be the same as the net field change at the end of the leader. The closest example of this category is shown in Figure 11, a flash that occurred at 3.9 km. The duration was 12 ms, the net electric field change was about +100 V/m, and the ratio was +0.03. The most distant example of these was at about 8 km with duration of 58 ms, net field change of about +160 V/m, and ratio +0.36. It is shown in Figure 12. It would not have been included in this class except that it clearly started in the negative direction and had a negative maximum. Perhaps a better example of this class is in Figure 13, at 6.5 km, with 19 ms duration, net field change of about −440 V/m, and ratio −0.02.

The last group of field changes we call 'distant.' In these cases the electric field change starts in the positive direction, as far as can be determined within the limits of the noise level, and ends with a net positive value. In general the slope is always increasing, as in very close cases, the difference being that the field change is always in the same direction as the return stroke. The closest example of this class is shown in Figure 14. It occurred at 5.3 km, had duration of 23 ms, net field change of +280 V/m, and leader-to-return-stroke ratio of +0.24. The example in Figure 15 is a nearly ideal one in the 'distant' class. The flash was at 11.4 km, the duration of the stepped leader was 25 ms, the net field change was +170 V/m, and the ratio was +0.51.

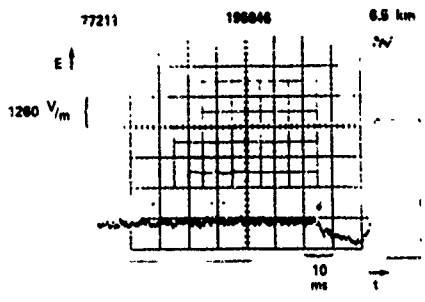

Fig. 13. Stepped-leader electric field change of a flash at 6.5 km ('far intermediate') distance. Arrow indicates 'positive' field according to convention of atmospheric electricity [*Uman*, 1969]. Asterisk marks beginning of stepped leader.

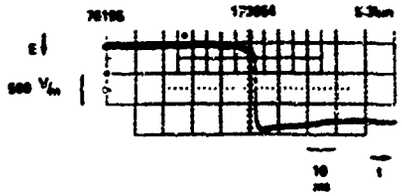

Fig. 14. Stepped-leader electric field change of a flash at 5.3 km ('distant') distance. Arrow indicates 'positive' field according to convention of atmospheric electricity [*Uman*, 1969]. Asterisk marks beginning of stepped leader.

This example also illustrates a case in which the decision processes discussed previously were used to choose the starting point for the stepped leader as shown and not at the point in the preliminary variations 10–15 ms earlier. Examination of the field record on a larger scale showed that there were significant variations as much as 250 ms before the return stroke. Approximately 75% of the cases at distances greater than 5.3 km and 100% of the cases at distances greater than 9.5 km fit in the 'distant' class. That there are no sharp boundaries in distance range between classes as we have defined them here is not surprising. That real waveforms, from lightning at distances that are uncertain because of uncertainties in thunder range, with tortuous tilted channels, possibly variable velocities, and possibly nonuniform change distributions should be susceptible of even this much classification is perhaps the surprising result.

To summarize our findings with regard to leader shapes at various distances, we have drawn, in Figure 16, a set of 'representative' leader field changes, normalized with respect to duration and return-stroke field-change size. The shapes shown for the close and distant categories were attained more often to better approximation than those in the intermediate ranges.

As mentioned previously, about 25% of the waveforms did not fit well the patterns to be expected from the simple model. One such case is shown in Figure 17. The distance, 4.4 km, is very well known because in addition to thunder range, there was a closed-circuit television image available. The channel appeared to be fairly straight, with no apparent branches in the direction of the measurement location. The net field change of −2360 V/m is 2–20 times larger than that of other flashes at similar distances. The duration, 120 ms, is quite long, in fact, the longest in the data set. The ratio of leader to return-stroke field changes is −1.1, as the shape shows, normally attributable only to very close flashes. It is easy to see that a flash striking ground at a distance greater than the height from the measuring station to a horizontal portion of the channel could give a thunder range that is less than the true distance to the ground strike point. It is more difficult, but not impossible, to conjecture that effects of temperature gradients or wind gradients

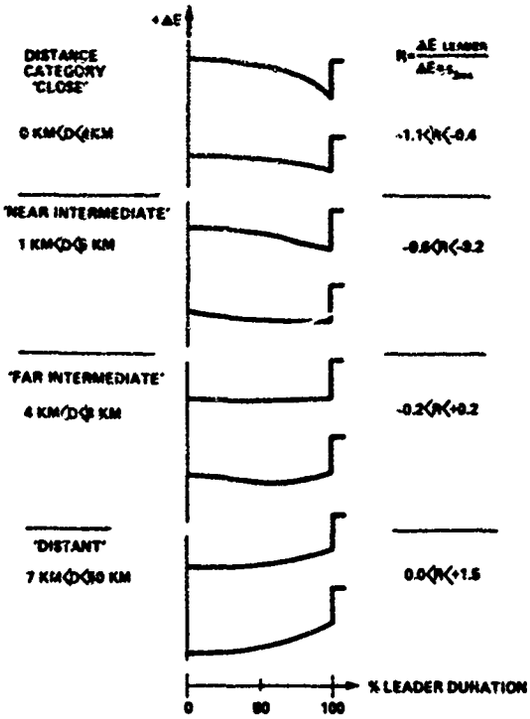

Fig. 16. Representative shapes of stepped-leader electric field changes in four distance categories. Note that categories overlap.

could cause thunder range to over-estimate the distance. This example and a few others like it remain enigmatic.

In Figure 18 we show the most unusual and difficult to interpret case included in our study. The flash occurred at 9.5 km and had a stepped-leader electric field change lasting 16 ms. The net field change of the leader was zero. As a result, its ratio to return-stroke field change was zero. This example accounts for the one case of zero net field change and ratio at distance greater than 7.5 km to be seen in Figures 22 and 23.

We have plotted the durations of 79 stepped-leader field changes versus distance in Figure 19 with a different symbol for each storm. We define duration as the time interval between the start time of a leader and the beginning of the return stroke. We believe this plot shows that the measurements were not distance dependent, as might have been the case if our measurements had been limited by low signal-to-noise ratio or if our use of model predictions had biased the data. The plot also shows that although there is, as might be expected, a tendency for a number of events from one storm to occur at about the same distance, the stepped-leader field-change durations for these events are spread over a fairly wide range. We believe, therefore, that, in contrast with preliminary variations, the

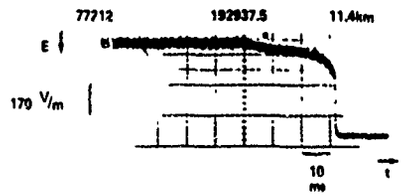

Fig. 15. Stepped-leader electric field change of a flash at 11.4 km ('distant') distance. Arrow indicates 'positive' field according to convention of atmospheric electricity [*Uman*, 1969]. Asterisk marks beginning of stepped leader.

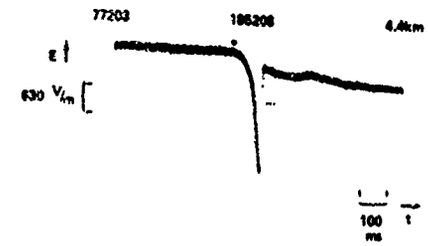

Fig. 17. Stepped-leader electric field change of a flash at 4.4 km distance (special case).

Fig. 18. S

durations
or charac
study.
The le
with dur
we see th
22.5 ms.
another
vided in
that 50%
duration
The n
ted agai
The larg
V m^{-1}
measure
figure ar

Fig.
functio
greater

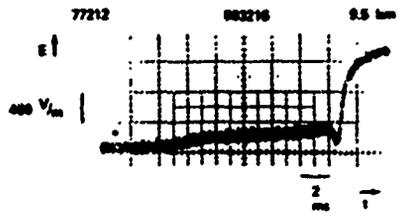

Fig. 18. Stepped-leader field change of a flash at 9.5 km distance (special case).

durations of stepped leaders are not dependent on storm type or character, at least not strongly enough to be observed in this study.

The leader durations in Figure 20 and Table 3 show none with duration less than 2.8 ms. From the histogram in Fig. 20 we see that the most frequent values lay between 2.5 ms. and 22.5 ms. The durations are tabulated, by storm, in Table 3. Still another view of stepped-leader field-change durations is provided in Figure 21, showing the cumulative distribution. Note that 50% had duration greater than 18 ms and only 25% had duration greater than 30 ms.

The net electric field changes of 78 stepped leaders are plotted against distance (thunder range), by storm, in Figure 22. The largest net negative field change we measured was $-41{,}500$ V m^{-1} at 0.3 km. The largest net positive field change we measured was $+1250$ V m^{-1} at 7.5 km. Also shown in the figure are the distances covered by the classes of shapes dis-

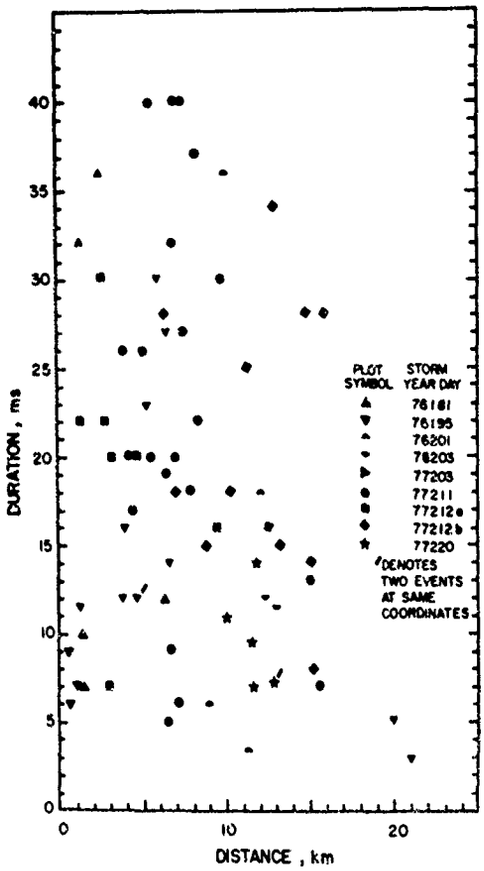

Fig. 19. Durations of stepped-leader electric field changes, as a function of distance, by storm, 0–40 ms. Nine cases, with duration greater than 40 ms, are not shown.

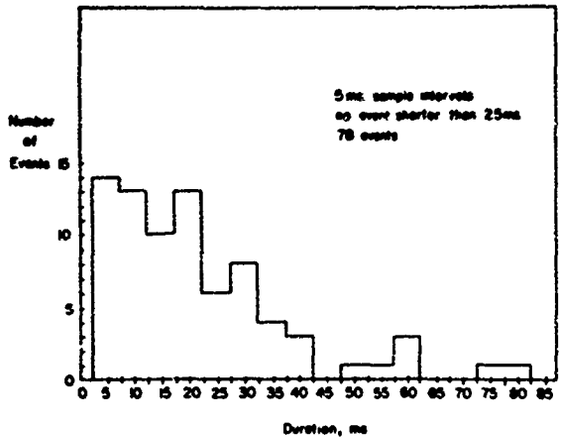

Fig. 20. Frequency-of-occurrence distribution for stepped-leader durations.

cussed previously. From this figure it is clear that the net field change was never positive at distances less than about 3.5 km, never negative at distances greater than 7.5 km, and either negative, positive, or zero between about 3.5 km and 7.5 km. Note again the one case in which the net field change was zero at a distance greater than 7.5 km, which appears at 9.5 km and results from the example of Figure 18.

We have prepared Table 4 to compare various estimates of stepped-leader duration. Our results are in reasonably good agreement with the others for the shortest and most frequent durations. There is a greater disparity among results for maximum duration. Our results fall toward the shorter values. We believe the greater disparity may represent both possible physical differences in lightning at various locations and times and likely differences in definitions, measurement techniques, and subjective decisions in data analysis. Others may have included more of what we have called 'preliminary variations' in the measurements of stepped leaders.

Return Strokes

In Table 5 we have summarized the measured duration of return-stroke field changes at the end of the most rapidly changing portion, or 'knee.' We used the values of field change at these points and at 1, 2, and 3 ms after the fast rise to initial peak to calculate the ratio of the stepped-leader field change and the return-stroke field change in each case. These ratios are plotted in Figures 23*a*, 23*b*, 23*c*, and 23*d* against distance and by storm. In addition, the ratios of stepped-leader field change and return-stroke field change measured at approximately 3 ms for 97 flashes in the range 20–50 km plotted in a histogram at the right of Figure 23*d*. They are shown on that figure because they correspond most closely with the data for return-stroke measurement at 3 ms. In 68 cases for which the measured ratio of leader to return-stroke field change at 1, 2, and 3 ms was available, 19% had the same ratio at all three times, 37% had the same ratio at 2 and 3 ms, and 44% had a change of a few percent between 2 and 3 ms. Also shown in the figures are curves of the leader to return-stroke ratio predicted by the simple physical model, for $H = 5$ km and $H = 10$ km. That more of the observed ratios fit between the two curves at 2 and 3 ms and that there is little change between 2 and 3 ms, both in the ratios and in the number of them that fall between the curves, we believe to be a good indication that within 2–3 ms after the beginning of the return stroke practically all of the

TABLE 3. Durations of Stepped Leaders

Storm Year Day	Longest, ms	Shortest, ms	Mean, ms	Standard Deviation, ms	Median, ms	Number of Events	Mode, ms
76181	36	10	21	12	13	5	
76195	30	5	14	8	12	13	
76201	36	3.4	16	15	12	4	
76203	48	2.8	19	20	12	4	
77203	120	60	90	42	—	2	
77211	78	5	31	20	26	26	
77212a	30	7	20	7	20	7	
77212b	34	8	21	8	18	12	
77220	14	7	9	3	9	6	
Overall	120	2.8	27	15	18	79	6–20

charge that is going to be removed from the channel has been removed. Occasionally, in cases with continuing currents, the electric field value would continue to increase significantly after 2 or 3 ms, but the charge source in these cases is probably within the cloud and not from the charge deposited on the channel by the leader. Many of the cases for which the ratio fell outside the model limits were for distances closer than about 5 km distance, with the observed ratio more negative than the theoretical and often of greater than unity magnitude, a condtion not allowed by the model. Apparently similar results have been reported in *Jacobson and Krider* [1976] and *Livingston and Krider* [1978].

The precision of measurements of starting and stopping times of various portions of the discharge has a direct bearing on the hypotheses we can entertain about physical processes of breakdown and the stepped leader. However, for distant flashes the ratio of stepped-leader and return-stroke field changes is not strongly dependent on the precision with which we choose the start time of the leader and end time of the return stroke, since for them there is not much change in the field before the beginning of the stepped leader (usually) or after about 3 ms after the return stroke. Therefore, we could measure a large number of leader/return-stroke ratios without the high time resolution required in the painstaking analysis previously described. To do this, we played the instrumentation tape into an oscilloscope with horizontal sweep off, and exposed moving film to give equivalent time resolution of about 40 ms/mm. This was sufficient for us to make measurements, with approximately 1–2 ms resolution, of the leader/return-stroke ratio for a large number of distant flashes in a short time. We did this for 97 flashes from storms on Julian days 193, 196, 203, and 209 of 1977 at ranges of approximately 20–50 km, as determined from the real-time display of lightning sources of VHF radiation on LDAR [*Lennon*, 1975], the WSR-72x radar at Kennedy Space Center, the AFETR weather radar at Cape Kennedy AFS, and visual observation. The results are plotted on the right side of Figure 23*d*. The mean value for ratio of leader and return-stroke field changes at distances greater than about 20 km was 0.8 ± 0.3, not far from the ideal value of unity for the simple physical model discussed earlier. These results also agree with those of *Schonland et al.* [1938*a*] for 26 first leaders of α type and 46 subsequent leaders altogether giving a most frequent ratio of one, with 85% between 0.3 and 3. Though not in any sense a proof that leaders are, on the average, uniformly

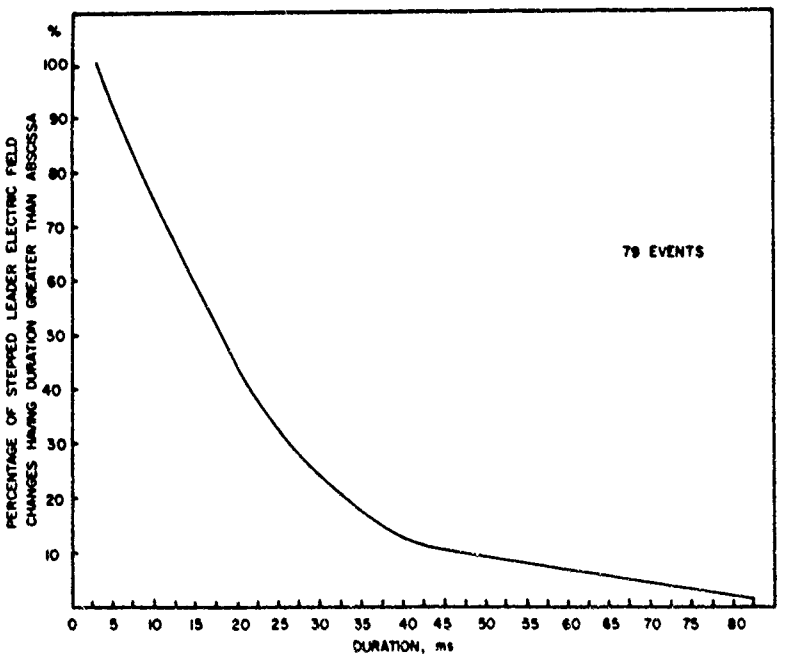

Fig. 21. Cumulative frequency-of-occurrence distribution (percent) for stepped-leader durations

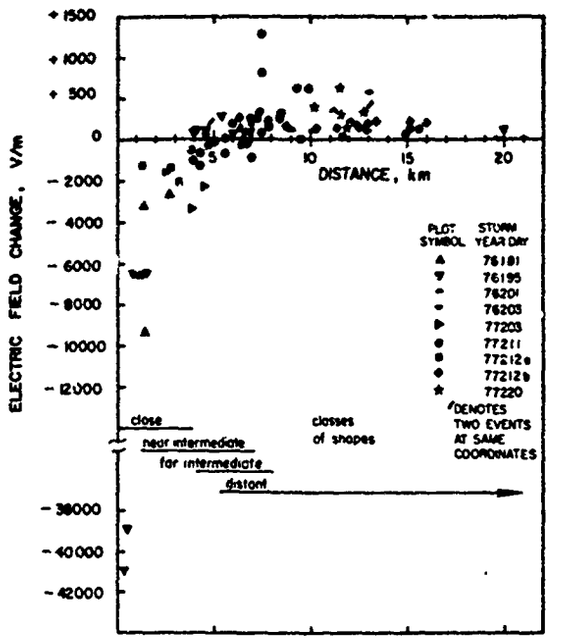

Fig. 22. Net stepped-leader electric field change (difference between end value and starting value of electric field) as a function of distance, by storm. Polarity according to convention of atmospheric electricity.

charged, for the many reasons cited earlier, at least the result is not inconsistent with that possibility or with results of previous studies.

SUMMARY, DISCUSSION, AND LITERATURE REVIEW

Our study of electric field records preceding cloud-to-ground lightning flashes has led us to conclude that the record is best characterized as having two major divisions, the preliminary variations and the stepped leader. The division between the two is marked by a period of a few milliseconds during which characteristic bipolar pulses appear in the record of electric fields variations. These pulses are probably the same ones reported by previous investigators at the beginning of 'β type' stepped leaders. Furthermore, our results and a review of the literature lead us to believe that there is only one type of stepped leader, not two, α and β, as widely believed. We suspect that the two types are really just extreme cases of the variability in one phenomenon.

We now review the variety of disparate views, theories, and conjectures to be found in the published literature pertaining to electric fields preceding first return strokes. We believe this review supports our unifying hypothesis that the observed variety can be explained within a single consistent framework.

As far as we can tell, the first observations relevant to our work were reported in a paper by *Appleton and Chapman* [1937]. Their measurement systems had frequency response from about 0.5 Hz to about 100 kHz. The main observation of interest to us are reproduced here in Figures 24 and 25. Figure 24 shows a typical variation of electric field during a single cloud to ground lightning flash, thought to be at a distance of about 3 km. The 'a' portion of the variation was attributed to the stepped leader. The pulses in the fine structure illustrated in Figure 25 appear to be the same as we see and have discussed previously. We called them 'characteristic pulses.' Appleton and Chapman believed these pulses were the result of branching and the discontinuous nature of the first (stepped) leader as shown in photographs in the paper by *Schonland et al.* [1935]. Reproduced here in Figure 26 is part of a table in which Appleton and Chapman gave typical shapes of field variation at various distances. We believe there must have been a systematic error in their distance estimates for the close cases. The lack of a negative-going excursion at the beginning suggests the flashes must have been more likely at 10 km than at 3–5 km. Perhaps the distances were estimated by time to thunder, which we noted earlier to be especially susceptible of under-estimation. It is also possible, but improbable because of lack of later similar findings, that the negative charge centers from which the leaders emanated were very much lower, say at 1 or 2 km above ground, than has been found normally in work subsequent to theirs, including our own. Nonetheless, their figures serve to show that some 45 years ago the main features of the leader field change preceding first strokes had been observed, including the pulses we call 'characteristic' at the beginning of the field change.

A closely related paper by *Schonland* [1938], the fourth part of a series on 'progressive lightning,' is apparently the first to make distinction between two classes of stepped leader. On the basis of photographic records, the most frequently occurring type (70%), labeled type α, was that for which the observed velocity (of luminosity) was fairly regular. Schonland stated that the α leaders were associated with the type of field-change records described by Appleton and Chapman. The second type of leader appearing in the photographs, labeled type β, occurred in about 30% of the cases discussed, and had fast, bright, initial stages, followed by a slow final stage essentially like the α type. Schonland noted that their field-change records showed effects similar to the luminous behavior. The field changes he attributed to type β leaders began with a large, rapid field change, with 'abnormally large' superimposed pulses (presumed by him to be due to steps) and ending with a small, slow field change showing no observable pulses. If he thought the pulses 'abnormally large,' he must have seen smaller ones in other cases, including, we presume, the cases of type α stepped lead-

TABLE 4. Durations of Electric Field Change of Stepped Leaders

Reference	Number of Flashes	Distance Range, km	Duration, ms			System Frequency Response
			Minimum	Maximum	Mode	
Schonland et al. [1938a]	69	0–24	0–3	66	9–12	30 Hz to 20 kHz
Pierce [1955]	~340	40–100	0–20	525–550	20–40	~1 Hz to 4 kHz
Clarence and Malan [1957]	234	0–80	6	442	—	0 Hz to 300 kHz
Kitagawa [1957]	41	0–15	8	89	20–30	0 Hz to 100 kHz or 300 kHz
Kitagawa and Brook [1960]	290	—	0–10	210	10–30	1 Hz to 1 MHz
Thomson [1980]	53	6–40	~4	~36	—	0.1 Hz to 7.2 kHz
This study	79	0–20	2.8	120	6–20	0.03 Hz to 300 kHz or 1.5 MHz

TABLE 5. Durations of Return-Stroke Electric Field Change (To End of Most Rapidly Changing Portion)

Storm Year Day	Longest, μs	Shortest, μs	Mean, μs	Standard Deviation, μs	Median, μs	Number of Events	Modes, μs
76181	160	60	112	46	100	5	
76195	400	50	219	128	210	12	
76[illegible]	400	120	260	200	—	2	
76[illegible]	400	400	400	—	—	1	
77[illegible]	—	—	—	—	—	0	
77211	800	135	462	333	~250	3	
77212a	600	200	313	136	260	7	
77212b	1000	200	408	236	350	12	
77220	250	150	195	34	200	6	
Overall	1000	50	238	203	240	48	200, 400

ers. Citations of this paper have tended, we believe, to overlook this implicit observation and instead make an unwarranted leap to the assumption that α type leaders had no pulses at the beginning.

The next important treatment of the stepped-leader problem was the fifth in the series on 'progressive lightning' by *Schonland et al.* [1938*a*]. It was concerned with combined photographic and electric field observations. We have reproduced here in Figures 27 and 28, their Figures 2 and 4. It is clear from Figure 2 of the preceding paper by *Schonland* [1938] that the line along the top of the B part of Figure 28 is intended to represent the cloud base. It is also clearly implicit in the figure that the field change begins with the emergence beneath the cloud of the visible stepped leader. This picture, we believe, may have led to confusion in the literature regarding the correlation in time between visible leader phenomena and electric field records. Figure 28, ostensibly of the β type leader field change, also contains the implicit assumption that the beginning of the electric field change of the leader and the emergence of luminosity beneath the cloud occur at the same time. Yet careful reading of the text shows that the drawings reproduced here as Figures 27 and 28 were based not on correlated electric field and luminosity observations but, rather, on similarity of durations of field changes and photographically observed luminous phenomena. For reasons similar to those cited in our own data analysis, principally because of the influence of noise thresholds on the electric field records and height of cloud base on the photographs, such indirect comparisons can lead to erroneous conclusions. There were no direct correlations between electric field and streak photographs for first strokes and only two claimed but not shown for subsequent strokes.

The sixth in the series on 'progressive lightning,' a paper by *Schonland et al.* [1938*b*], contains a few observations with some bearing on our study. Details of the extremes of variations in behavior of β type leaders as observed on streak photographs are discussed in terms of two subclasses, β_1 and β_2. There was no mention of electric field observations. The authors cite the 'not infrequent occurrence of leaders which actually cease after executing their first and heavily branched portions....' Since there were no electric field records, it is not possible to determine whether or not the same characteristic pulses as occur at the beginning of leaders, or if similar but oppositely polarized pulses of either one, accompanied the beginning of these 'air discharges.'

Extension and refinement of the work by *Appleton and Chapman* [1937] was reported by *Chapman* [1939]. His Figure 5, reproduced here as Figure 29, illustrates the general nature of field change for a single ground stroke at a distance of 10-20 km. Chapman cites the photographic results of Schonland, Malan, and Collens in support of the identification of the 'a' portion of the field change with the stepped leader. It is not clear whether he believed that the assertion of correspondence was based on a direct comparison or not, but in any case, it is easy, almost inevitable for the reader to infer that they were. He again notes the occurrence of the characteristic pulses at the beginning of the field change and infers, we believe erroneously, that they are due to radiation from the successive steps of the stepped leader. Our interpretation is that the characteristic pulses occur for a couple of milliseconds at the beginning of leader field changes and therefore will likely have stopped by the time the leader becomes visible below cloud base. Chapman further remarks that the nature of the field variations leading up to the first return stroke is diverse, noting that the pulsations were quite often very feeble or absent. Perhaps they were below the noise level of the system, or were masked by noise from other discharges in the cloud. It is interesting that he describes a mechanism for the pulses that accounts for variations in relative size of pulses with respect to the electrostatic change, as a function of distance, but did not invoke the mechanism to explain, at least to some degree, the fact of feebleness or absence of pulses in some cases. Almost certainly such an argument could be constructed, based on distance dependence and a range of variation in pulse amplitude. Chapman reiterated the attribution of the characteristic pulses at the beginning of the slow, steady, leader field change to the step process and gave the interval between pulses as 30 μs to 100 μs.

Malan and Schonland [1947] presented the results of direct correlation between luminous processes and electric field changes in 37 ground flashes, most of which were within 6 km range. Unfortunately, the camera shutter was activated by the first leader, so that there was little chance for them to obtain new information regarding the correlation between pulses at the beginning of stepped leaders and any luminous behavior. However, there are several interesting comments in the paper worthy of note. For example, Figure 1 of the paper, reproduced here as Figure 30, was said to be based on the work reported in the paper by *Schonland et al.* [1938*a*] yet the figure and accompanying discussion show slightly greater circumspection with regard to the correlations between electric field change and luminous behavior of the stepped leader. In particular, they note specifically that the durations of field changes are greater than those of the corresponding luminous phenomena. They presumed that the cloud obscures the latter during part of the time. The figure also shows the differences in shape of the electric field change of the same flash at distances of 3 km (middle waveforms) and 15 km (bottom waveforms). The lack

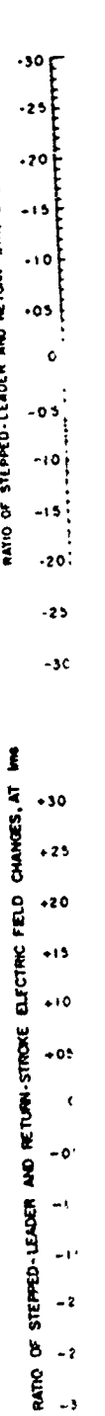

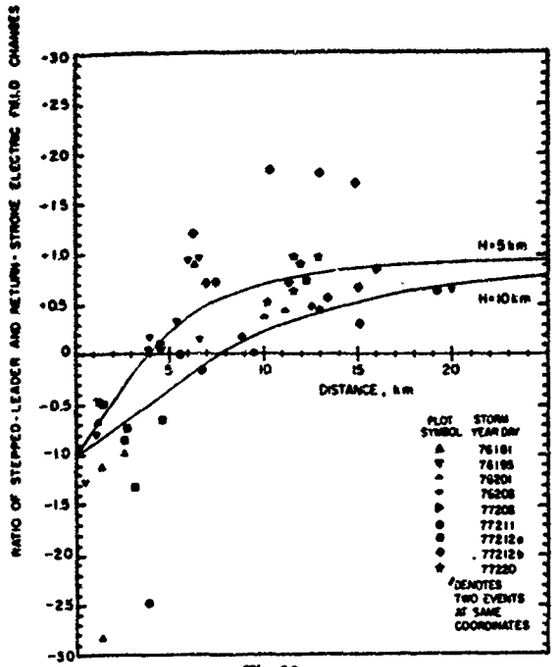

Fig. 23*a*

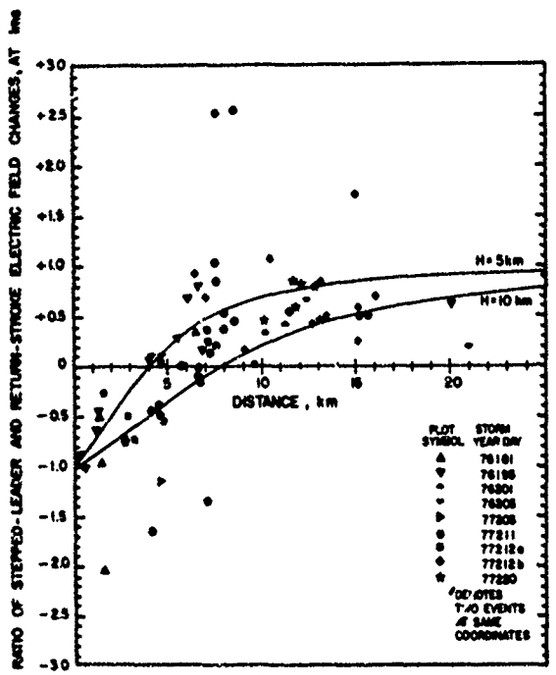

Fig. 23*b*

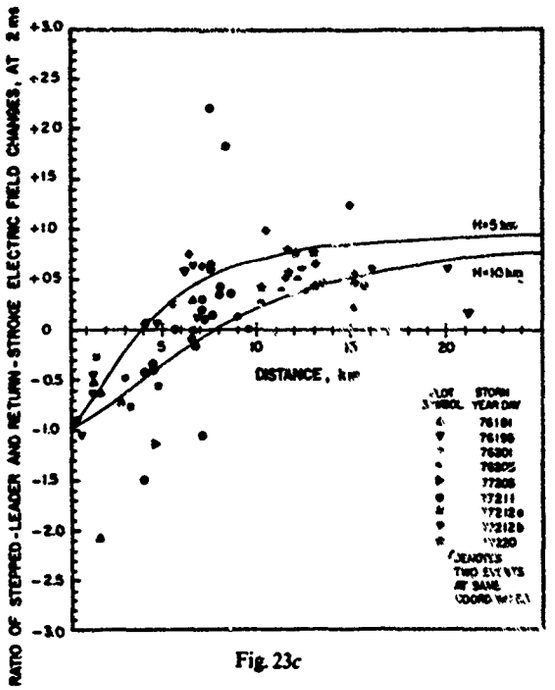

Fig. 23*c*

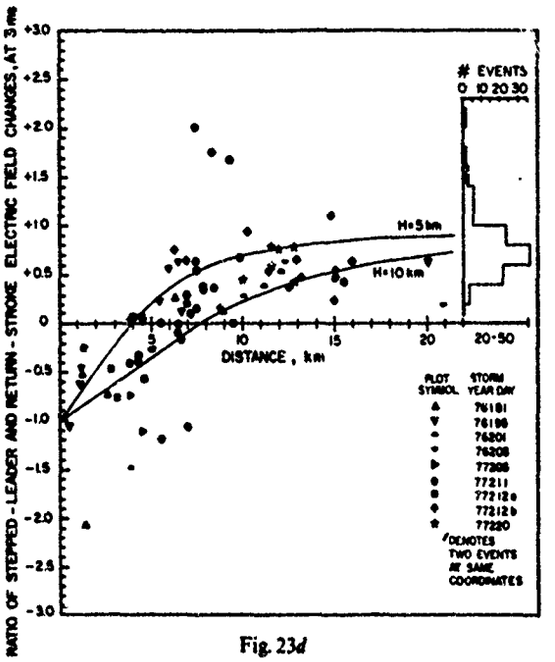

Fig. 23*d*

Fig. 23. Ratio of stepped-leader and return-stroke electric field changes, with return-stroke change measured at (*a*) end of rapidly changing portion of return-stroke field change, (*b*) 1 ms after return stroke, (*c*) 2 ms after return stroke, (*d*) 3 ms after return stroke. In (*d*), histogram shows ratios at approximate 3 ms for nearly 100 flashes at 20–50 km distances.

of pulses on the near observation is probably a result of the need for much-reduced amplification to keep the electrostatic field change on scale. Finally, they say that the duration of the whole leader process, based on the electric field change, is about twice that of the luminous phenomena observable below cloud base. They do not state specifically how they knew where the beginning of the field change attributable to the leader was, but, presumably, they may have used the appearance of pulses.

In a later paper, *Malan and Schonland* [1951] remark that it is known that the β leader process generally takes place in two stages, the first being within the cloud and much more rapid than the second, which follows in the air below the base of the cloud. This appears to be a reinterpretation or at least a shift in emphasis without reference, since earlier papers, which were not clear about the visibility of early stages of first leaders. Indeed, in the next paragraph in the paper, Malan and Schonland say that the two stages are clearly shown by records of electric field changes and that sometimes both stages are visible

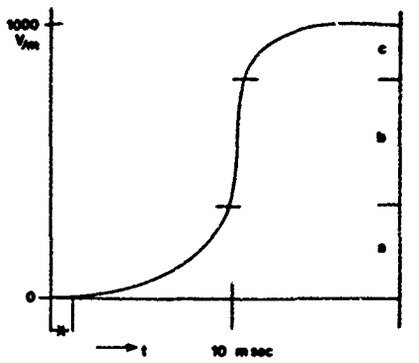

Fig. 24. 'Typical' variation of electric field during lightning flash at a 'short' distance. From *Appleton and Chapman* [1937].

below the cloud base. In a later paragraph they say that the second stage of a β type leader is just an α type leader. They then provide a table of the duration of the two stages, labeled t_β and t_α. The mean values were 1.3 ms for the β portion and 8.9 ms for the α portion. This is well within the range of our results as shown in Figures 20 and 21 and Table 3. Finally, they note that the original estimation by *Schonland et al.* [1938*a*] that 35% of both photographic and electric field records were of type β was in error and that actually at least 65% of first-leader electric field change records are of β type. The crucial comment from our viewpoint is their explanation of the reason for the earlier result. They say that at distances greater than 12 km, with the equipment they had used, many type β leader field changes could not be distinguished from those of type α.

In a later paper dealing with the mechanism of the step process, *Schonland* [1953] noted the absence of appreciable steps in the electrostatic field change of stepped leaders.

Further discussion of the evidence for the unified point of view we have been developing is to be found in a note by *Hodges* [1954]. In it he discusses the data cited in *Schonland* [1953] showing that β type leaders are characterized by an initial stage of about 1 ms duration with large pulses, and a final stage of about 9 ms duration, of the α type, but with barely observable pulses. It seems reasonable to us to speculate that the difference could have been due, at least in part, to differences in amplification. When the system gain happened to be right for the observation of the large early pulses without saturation, the later small pulses may have been relatively close to the noise level. No mention was made of pulse shapes.

In discussion of the 'leader' field change, *Pierce* [1955] used the label '*L*' for the portion of the record leading up to the return stroke (the same portion as labeled 'a' by *Appleton and Chapman* [1937]) and distinguished two types. In the first type, of which there were 284, the increase in field was uninterrupted from the beginning, which showed in his illustrations as a gradual change in slope with no discontinuity, to the end, marked by the onset of the return-stroke field change ('b' of Appleton and Chapman's notation). The other type, of which there were 48, he described as having an initial slow change, succeeded by a 'quiet' part up to the return stroke, with a short slow rise sometimes just prior to the return-stroke field change. The two sketches shown as examples of the latter type do not show the latter final slow rise. Instead, they show a feature not mentioned in the discussion, a discontinuity in slope at the beginning, followed by a field change with decreasing slope, much like that of a continuing current or nearby cloud discharge. We must be cautious not to read too much into the data. Since the decay time constant of the system was apparently a little less than 200 ms, the curvature may be misleading in cases of long duration. Noticing the observation of similar effects in *Schonland et al.* [1938*a*], Pierce adopted the nomenclature '$L(\alpha)$' and '$L(\beta)$' for the two classes of '*L*' field change described above. He found that the mean and median durations of $L(\alpha)$ field changes were 50 and 35 ms. For $L(\beta)$ field changes, the mean was 175 ms and the median 140 ms. A further interesting observation was that for the first type the mean and median values of ratio of leader and return-stroke field change (return-stroke value at about 5 ms) were 1.2 and 0.95. For the second type the mean and median were 2.4 and 2.2. There was no mention of variations between the extremes. In essence, Pierce's use of the α, β designation is based on duration, rather than behavior of field pulsations or luminous phenomena.

A review article on lightning by *Schonland* [1956] seems to illustrate his best thinking on the subject as of that date and presents a more or less consolidated view of the phenomena. Type α leaders were said to have a low, fairly uniform value of velocity, about 10^5 m/s during their passage between cloud base and ground. They occurred in 55% (sic) of the photo-

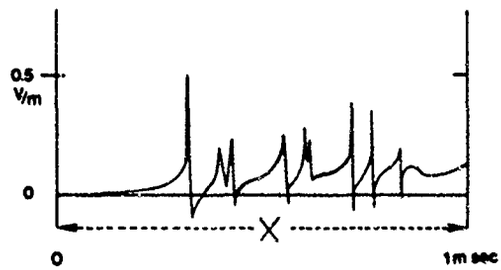

Fig. 25. 'Fine structure' at beginning of field variation in Figure 25. From Appleton and Chapman [1937].

Distance in km.	E_s in v./m.	E_r in v./m.	Typical wave-form
3-5	1300	Not observed	
10	700	Not observed	
20-30	45	Not observed	
45-50	12	5	
60	3	3	

Fig. 26. Table of 'typical' waveforms at various distances. From *Appleton and Chapman* [1937]. The column headed 'E_s' is 'electrostatic' field changes The column headed 'E_r' is 'radiation' field changes.

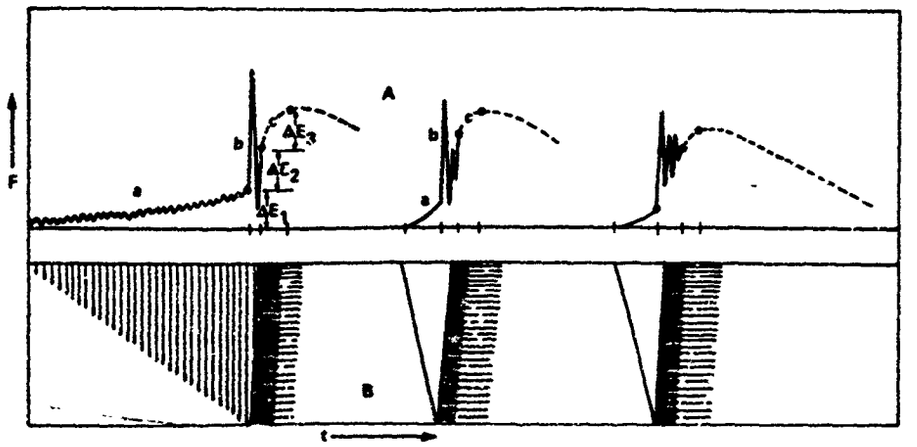

Fig. 27. Diagrammatic illustration, not to scale, of electric field variation in A and streak photograph in B of a 'type α' stepped leader. From *Schonland et al.* [1938a].

graphed flashes in South Africa. The steps were said to be short, almost uniform in length and brightness, but weakly luminous and difficult to photograph. The type β leaders were extensively branched and had high velocity, between 1×10^6 m/s and 2×10^6 m/s at the top of the channel, with long and fairly bright steps. In later stages the velocity decreased to a value characteristic of type β leaders. The branching and higher velocity of the early stages of type β leaders were attributed to accumulations of positive space charge below cloud base.

Figure 31 illustrates the general correlations made by *Schonland* [1956] (coincidentally, this figure was Figure 31 in his paper also) between luminous phenomena and electric field variations. In the accompanying discussion, the lack of steps in the electric field records is cited as evidence that charge must be lowered more or less continuously, though accompanied by a secondary mechanism involving rapid current variations that result in radiation pulses. In Figure 32 we reproduce Schonland's Figure 32, which illustrates two distinct types of first leader field records, with L_1' corresponding to type α and L_1'' to type β photographs. Type α leaders had electric field variations having radiation pulses of fairly regular amplitude over the entire duration. The mean amplitude of pulses was about 8% of the return-stroke field change. It is not clear whether the return-stroke field changes were measured at the initial radiation peak or a few milliseconds later to obtain the 8% value. The second type of field record, labeled L_1'' said to correspond with β photographs, had a large change at the beginning, with radiation pulses of mean amplitude about 30% of the return-stroke field change. The early stage is succeeded by a slower change with smaller pulses. In reference to papers previously cited herein, Schonland suggests that since 65% of first leader field changes are of the β type, but only 35% of the photographs are of β type, a considerable number of leaders designated type α on the basis of photography may have had an initial β portion hidden in the cloud. It is not much of an extension from this point to postulate that all first leaders have similar behavior, that is, large pulses at the beginning of a rapid field change, followed by a period of slower field change with smaller pulses, and that for various reasons, both real ones and artifacts, some portions of the sequence of events sometimes might not be evident in field records.

The paper by *Clarence and Malan* [1957] is often cited as authority in regard to the processes leading up to first strokes of ground flashes. See, for example, *Uman* [1969]. The paper reported that the typical pattern of electric field changes preceding cloud-to-ground lightning flashes had three main identifiable sections, which they labeled 'B,' 'I,' and 'L' for breakdown, intermediate, and leader, as shown in their Figure 1,

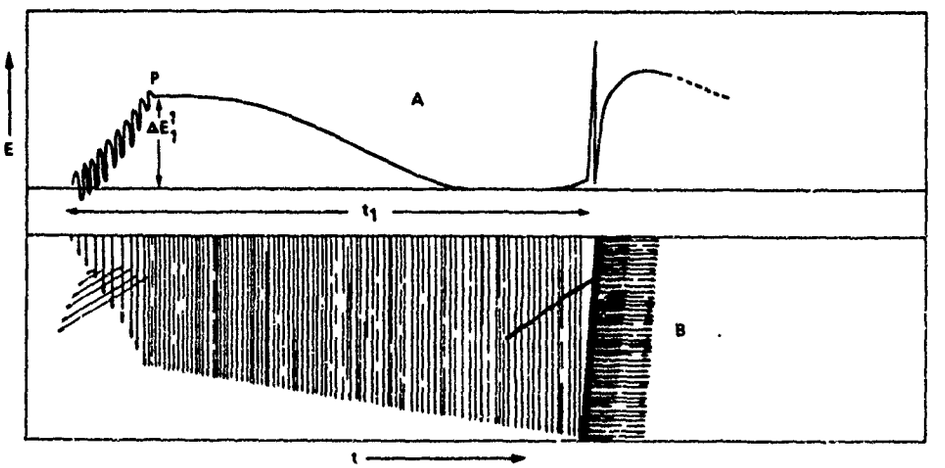

Fig. 28. Diagrammatic illustration, not to scale, of electric field variation in A and streak photograph in B of a 'type β' stepped leader. From *Schonland et al.* [1938a].

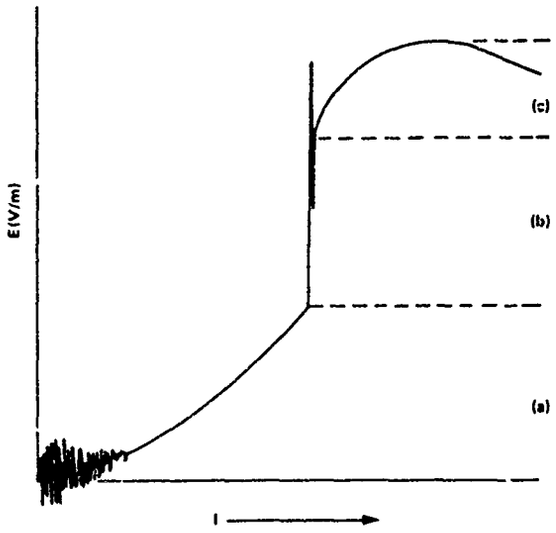

Fig 29. The 'typical' variation of electric field due to a single lightning stroke, as observed at a 'short' distance from the discharge. Perturbations at beginning were usually seen on first strokes. From *Chapman* [1939].

reproduced here as Figure 33. We checked the electric field records of 52 of our 79 flashes to see how many would fit the BJL' description. We found that only three (6%) had the exact shape and features presented by Clarence and Malan as 'typical.' We found eight more (15%) that almost fit except that the 'B' field change did not start with a discernible discontinuity in slope. We found four (8%) that had the three segments but the polarity of the 'B' field change was wrong for its distance. If we wish to interpret the 'B' field change as being caused by the lowering of negative charge along a vertical line, our results suggest that the charge associated with the 'B' field change is sometimes higher and sometimes lower than that at the origin of the leader. This contrasts with the conclusion of Clarence and Malan that the 'B' field change always resulted from a breakdown at the base of the cloud, below the level at which the leader begins. The largest number of our cases, 18 (35%), had only two sections. The 'B, I, L' description of Clarence and Malan allowed for the possibility that the 'I' section might have duration of zero, reducing the field change to 'B, L,' but they did not mention the possibility of a field change having a shape best described in their terminology as 'I, L.' In our data, the 35% having only two sections were better described in the latter way, generally having no sharp discontinuity in slope at their beginnings. The first section usually started gradually with little slope until the beginning of the second ('L') section where the slope increased.

In 25% of the cases, there was only one section and it was clearly an 'L' section. Also, 13% of the waveforms were too complex to interpret in terms of the 'B, I, L' description. We found that of the 15 cases (29%) that could possibly be interpreted as having 'B, I, L' form (with nonzero 'I' duration), 47% had the 'B' section beginning at the same time we had chosen independently as the beginning of the preliminary variations. In 53% of the cases we had chosen the start time for preliminary variations at least 10 ms earlier than the 'B,' and in 20% of the cases, 100 ms or more earlier. We also found that the start time of the 'preliminary variations' was uncertain by more than 20 ms in 7 (56%) of the cases. In all cases susceptible of the 'B, I, L' interpretation, we had independently previously chosen the section they would have labeled 'L' as the stepped leader by our decision procedure.

It appears that, although the 'B, I, L' description is not wrong, in that it applies in all cases if the possibilities of varying sign of B and the duration of the 'I' section being zero are allowed and literally in a fraction of the cases (6% in our data, 15% in the data of *Pierce* [1955]), we feel it unwise to use it since 60% of our waveforms had only one or two sections. The designation of *Schonland* [1956], which calls all prestroke field changes 'B' and the leader 'L,' seems more appropriate. It is probably reasonable to assume that what we have called 'preliminary variations' are essentially the same as what Schonland labeled 'B.'

A paper by *Kitagawa* [1957], devoted entirely to study of leader processes, verified the results of *Schonland et al.* [1935] and *Schonland et al.* [1938*a*], as reinterpreted later by *Malan and Schonland* [1951], in that 80% of electric field-change records of first-stroke leaders were of type β as defined by the occurrence of an 'inactive portion.' Kitagawa found that the type β field changes had longer durations (13–53) ms than type α (8–30 ms). He also cited remarks by Malan on unusually long (100–200 ms) leader field changes (which Malan named 'preliminary discharges') which may have included more than the stepped leader proper, perhaps even an intracloud discharge preceding the ordinary stepped leader, but probably a long horizontal section.

A subsequent paper from Japan, by *Ishikawa et al.* [1958], partly clarifies the situation. They classified stepped leader field changes in two categories, α and β type, according to whether

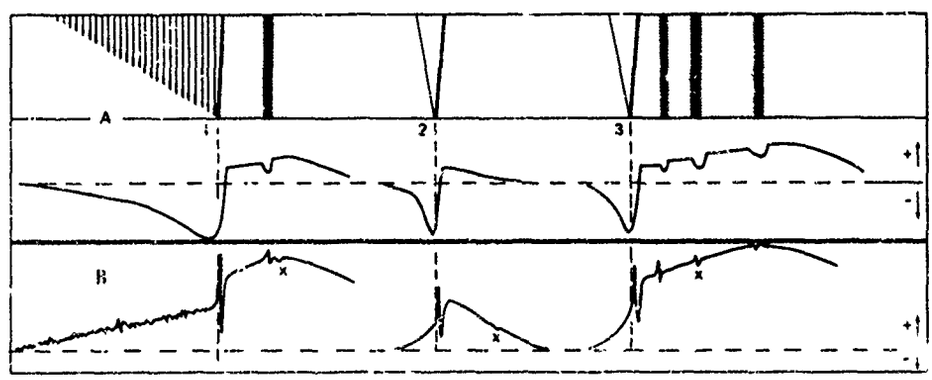

Fig 30. General illustration of streak photograph and electric field variation at a distance of 3–4 km (A) and electric field variation at 10–15 km (B) during a three-stroke lightning flash, based on correlated measurements of photographs and electric fields. From *Malan and Schonland* [1947].

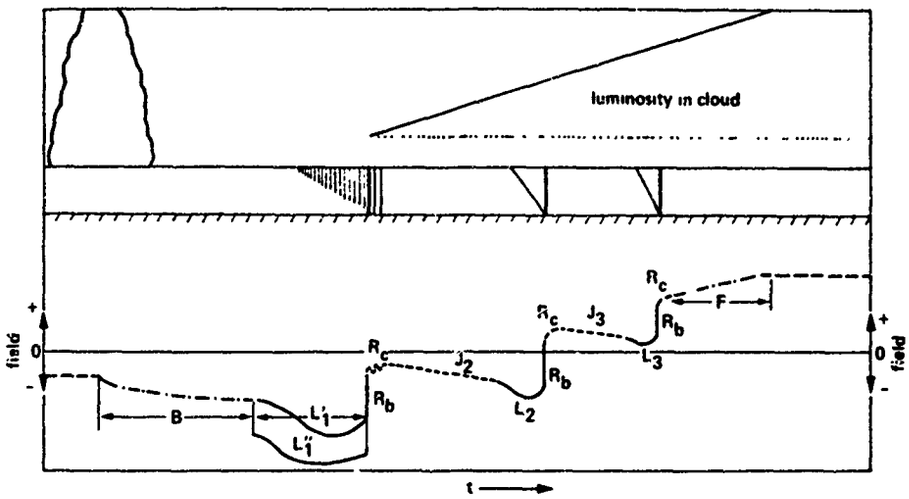

Fig. 31. Variations in electric field, at a distance of 3 km, and corresponding luminous effects. From *Schonland* [1956].

the pulses that start at the beginning of the field change continue throughout the duration up to the return stroke or stop midway through. By that criterion, 80% of their records were of the β type. Perhaps their most important conclusion, from our viewpoint, was that the initial portion of a stepped leader (characterized by pulsations) was the same for both types. They attributed a 'fold point' in many of their field-change records to the slowing of the leader as it encounters a presumed region of positive space charge near cloud base. They note that the 'fold point' occurs more often with their type β class of field-change records. They then reason that the space-charge accumulation may actually bring about the formation of type β leaders in some cases, if strong enough, and not in others, with a range of intermediate possibilities. Though their mechanism may or may not be plausible, the observed effects for which they postulate it as cause fit the hypotheses that there are not two types of stepped leader of fundamentally different natures, having completely different phenomenologies and physical mechanisms, but actually just one, with a wide range of possible variations in relative importance of various features.

In a comparison of cloud-to-ground and intracloud discharges, *Kitagawa and Brook* [1960] have made some interesting observations that are of some relevance. They found, after careful comparison of the initial portion of cloud discharges and first leader field changes of ground discharges, that the cloud discharge field change is of 2–5 times longer duration and has mean pulse repetition intervals of about 700 μs, an order of magnitude larger than the most frequent interval, 40–60 μs, of the stepped-leader pulses. They also found that the initial portions of cloud discharge field changes appeared in several groups separated by quiet intervals of about 0.3–10 ms. Within each group the pulse intervals were similar to those of the leader. They also noted exceptions. For example, 11 of 30 first leader field changes exceed 120 ms. It should be noted that they designate as 'first leader field change' the entire variation labeled 'B, I, L' by Clarence and Malan. These 11 had pulse intervals similar to those of the initial portion of cloud discharges. Likewise, there were cases of cloud discharges having trains of pulses like those of leader field changes, lasting usually no more than about 4 ms. Finally, they speculate as to why the two precesses differ so markedly. They claim that the differences are so clear that it is possible to determine in the first milliseconds (say 10) whether a flash will go to ground or not.

A paper by *Krider and Radda* [1975] presents observations

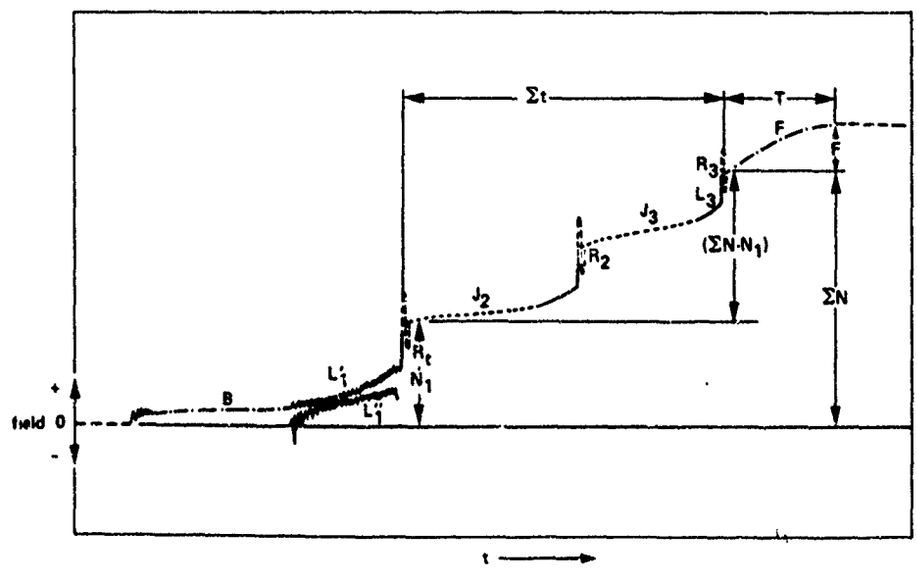

Fig. 32. Variations in electric field, at 15 km, of same flash as in Figure 32 From *Schonland* [1956]

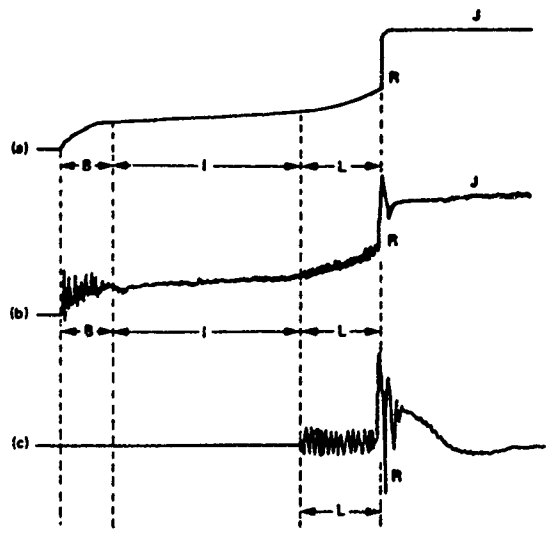

Fig. 33. Diagrams of 'typical' field changes of ground-flash first return strokes at 5 km (*a*), 50 km (*b*), and 500 km (*c*), not to scale. Durations are B, 2–10 ms; I, 0–400 ms; L, 4–30 ms. From *Clarence and Malan* [1957].

of pulses both near the beginning of the leader field change and just prior to the return stroke. The pulses that occurred several milliseconds before a return stroke were bipolar and symmetric and had a large fast-rising initial portion followed by a small, more slowly varying opposite overshoot. Pulse durations were usually 15–40 μs and repetition intervals apparently 75–150 μs. The pulses sometimes had additional narrow pulses superimposed on the initial rise. These are the pulses we have called 'characteristic pulses,' illustrated in Figure 2.

A later paper, by *Weidman and Krider* [1979], analyzed the pulses we have been calling 'characteristic' at the beginning of stepped leaders. They analyzed 150 sequences of pulses with initial positive polarity (same as ground return stroke) of which 77% were followed by a ground discharge, with a mean time between pulses and return stroke of about 53 μs $\pm$ 40 μs. In those cases not followed by return strokes, the pulses were quite similar to those that were. *Weidman and Krider* [1979] also found that 77% of the pulses with initial negative polarity were not followed by return strokes. The shapes of the negative pulses were very similar to those of the positive pulses, but had more variability. The mean time interval between positive pulses was 130 μs, whether or not they were followed by a return stroke. Between negative pulses the mean time interval was 780 μs. These figures are in reasonably good agreement with the results of *Kitagawa and Brook* [1960].

The recent extensive paper on charge structure of lightning discharges, by *Krehbiel et al.* [1979], discusses stepped leaders and the field changes of long duration that sometimes precede them. Their impression, in general agreement with that of *Proctor* [1976] based on a VHF source location technique, was that the preliminary activity preceding stepped leaders consisted of a succession of breakdown events, with considerable horizontal extent, one of which turned into a leader to ground. They comment that it is reasonable to argue that only horizontal development of discharge paths could be of such long duration as the observed preliminary field variations without reaching ground. This explanation probably applies to the anomalous case we presented in Figure 17. The difference between that case and other cases of long duration was that there was no obvious way to differentiate between preliminary, presumably horizontally oriented processes, and the beginning of the stepped leader. Eventually we hope to sort out these cases by comparing the broadband electric field variations with the delineation of discharge paths by location of VHF radiation sources. *Krehbiel et al.* [1979] found that the 'B, I, L' description of *Clarence and Malan* [1957] applied in that the breakdown and leader processes appeared to be vertically oriented, but the separation of the preliminary variation into B and I sections did not seem justified. Our results, reported here, based on analysis of single-station broadband electric field change records alone, independently led us to the same conclusion concerning the 'B, I, L' description.

Thomson [1980] also found it difficult to divide the preliminary part of ground discharges that occurred in Papua-New Guinea into the 'B, I, L' stages of *Clarence and Malan* [1957]. Thomson used the term 'prestroke' meaning 'pre-first-stroke' for the period from first evidence of field change up to the return stroke. (This means that 'prestroke' includes the stepped leader.) Thomson's distribution of prestroke field change duration showed 50% greater than about 200 ms, 97% greater than about 20 ms. His distribution of stepped leader duration showed 95% greater than about 4 ms, 50% greater than about 21 ms, and only about 4% greater than about 36 ms. Thomson refers to results of varying interpretation by *Harris and Salman* [1972] whose results agreed with those of *Clarence and Malan* [1957] and by *Takeuti et al.* [1960], who believed that 50% of their records could not be explained in terms of a preliminary discharge associated with an ensuing ground flash. They believed that a prestroke duration greater than 100 ms meant there was an intracloud discharge as well. Finally, Thomson found the mean prestroke duration of his 80 flashes was 240 ms with standard deviation 220 ms. These values are about twice as large as the overall mean and standard deviation of the start time of preliminary variation in our results given in Table 1. (Start time, by our definition, is comparable with prestroke duration by Thomson's.) Thomson's mean duration of 53 stepped leaders was 21 ms, with standard deviation of 8 ms. Our results in Table 3 show a mean stepped-leader duration of 27 ms, with standard deviation of 15 ms, for 79 events. Considering the quite different preliminary field-change variations of Florida and Papua-New Guinea lightning, it is perhaps remarkable that the stepped-leader durations are so similar.

CONCLUSION

In the introduction we raised six questions. The results of our attempts to address them are summarized below.

1. We were unable to determine whether there are any preliminary electric field variations that may precede first return strokes by tens or hundreds of milliseconds and which are also unambiguously related to or even precursors of the first return strokes of cloud-to-ground flashes.

2. Based on a highly subjective decision process, we attempted to label the beginning of preliminary electric field variations that were possibly related to the eventual return stroke and thus to derive estimates of their durations. These were plotted in Figure 4 and tabulated in Table 2. We were unable to formulate an objective means by which to distinguish 'related' preliminary variations from 'unrelated' ones.

3. We found that the best means to identify the beginning of a stepped-leader electric field change is probably the oc-

currence of 'characteristic' bipolar pulses in the broadband field record for a period of a few milliseconds at the beginning of the electrostatic field change. We also believe that limits on shape, duration, and ratio of stepped leader and return-stroke field changes, derived from a simple physical model, provide additional guidelines in ambiguous cases.

4. We attempted, in Figure 16, a categorization of stepped-leader field-change shapes in overlapping distance ranges.

5. We plotted the duration of stepped-leader electric field changes in Figures 19–21 and tabulated them in Table 3. We found no evidence for dependence of duration on distance or storm.

6. Our observations, supported by our review of the literature, show that the electric field variations preceding first return strokes are best characterized as having two sections: preliminary variations and stepped leader. Our view of the sequence of events leading up to the first return stroke of a ground flash includes the possibility of sufficiently wide range of variation in observables to explain, at least qualitatively, most of the exceptions, special cases, and unusual varieties of observations in the literature. It appears that the duration of preliminary variations may vary widely from storm to storm and with geographical region. The range of variability includes the possibility that in some environments there may be considerable intracloud discharge activity preceding ground flashes with less direct connection to the eventual first return stroke than is implicit in our analysis. It appears that at least in some cases, preliminary variations of long duration may be caused by extensive horizontal development of discharge paths prior to the formation of a stepped leader. In contrast, it appears that the durations of stepped leaders have much less variability. We believe, but do not claim to have proven incontrovertibly, that there is only one type of stepped leader. Variations in relative importance of particular features in field change records (such as the characteristic pulses at the beginning, the time between and size of pulses just prior to the return stroke, curvature, ratio of leader and return-stroke field changes, etc.) we believe result from combinations of real variability in the physical phenomena giving rise to the field-change features and such observational variabilities as distance to the discharges, bandwidth and dynamic range of recording systems, and limitation in length of record that can be examined at high time resolution. The historical use of such terms as 'type α' and 'type β' could be viewed as identifying extremes in the range of variability of the discharge processes rather than completely different physical processes, but we feel it prudent to discontinue use of the designations in order to emphasize the point of view that there is only one stepped-leader process.

Acknowledgments. We wish to acknowledge the following individuals, without whose dedication, skill and encouragement this study would have been more difficult, if not impossible: J. Gulick, W. Jafferis, D. M. Jordan, C. L. Lennon, Y. T. Lin, J. Nicholson, K. J. Rambo, and J. A. Tiller. We acknowledge gratefully the research funding that made possible the data acquisition and analysis and the preparation of this paper. Funds wholly or partially in support of this work were provided under the following grants and contracts: NSF, ATM7918172; NSF, ATM7902627; NSF, ATM7601454; NASA, NAS10-0378; NASA, NGR10-005-169; ONR, N00014-75-C-0143. Finally, we acknowledge our debt to the NASA Kennedy Space Center and the individuals who made the extra effort to see that TRIP 1976–1978 was successful.

REFERENCES

Appleton, E. V., and F. W. Chapman, On the nature of atmospherics, 4, *Proc. R. Soc. London, Ser. A, 158*, 1–22, 1937.

Brantley, R. D., J. A. Tiller, and M. A. Uman, Lightning properties in Florida thunderstorms from videotape records, *J. Geophys. Res., 80*, 3402–3406, 1975.

Chapman, F. W., Atmospheric disturbances due to thundercloud discharges, 1, *Proc. Phys. Soc., London, 51*, 876–894, 1939.

Clarence, N. D., and D. J. Malan, Preliminary discharge processes in lightning flashes to ground, *Q. J. R. Meteorol. Soc., 83*, 161–172, 1957.

Harris, D. J., and Y. E. Salman, The measurement of lightning characteristics in northern Nigeria, *J. Atmos. Terr. Phys., 34*, 775–786, 1972.

Hodges, D. B., A comparison of the rates of change of current in the step and return process of lightning flashes, *Proc. Phys. Soc., London, Ser. B, 67*, 582–584, 1954.

Ishikawa, H., M. Takagi, and T. Takeuti, On the leader waveforms of atmospherics near the origins, *Proc. Res. Inst. Atmos. Nagoya Univ., 5*, 1–11, 1958.

Jacobson, E. A., and E. P. Krider, Electrostatic field changes produced by Florida lightning, *J. Atmos. Sci., 33*, 103–117, 1976.

Kitagawa, N., On the electric field change due to the leader processes and some of their discharge mechanism, *Pap. Meteorol. Geophys., Tokyo, 7*, 400–414, 1957.

Kitagawa, N., and M. Brook, A comparison of intracloud and cloud-to-ground lightning discharges, *J. Geophys. Res., 67*, 637–647, 1960.

Krehbiel, P. R., M. Brook, and R. A. McCrory, An analysis of the charge structure of lightning discharges to ground, *J. Geophys. Res., 84*, 2432–2456, 1979.

Krider, E. P., and G. J. Radda, Radiation field waveforms produced by lightning stepped leaders, *J. Geophys. Res., 80*, 2653–2657, 1975.

Krider, E. P., R. C. Noggle, and M. A. Uman, A gated, wideband magnetic direction finder for lightning return strokes, *J. Appl. Meteorol., 15*, 301–306, 1976.

Krider, E. P., G. J. Radda, and R. C. Noggle, Regular radiation field pulses produced by intracloud lightning discharges, *J. Geophys. Res., 80*, 3801–3804, 1975.

Lennon, C. L., LDAR-A lightning detection and ranging system, Minutes of Frequency Management Group, Range Commanders Council, White Sands Missile Range, 1975.

Lin, Y. T., M. A. Uman, J. A. Tiller, R. D. Brantley, W. H. Beasley, E. P. Krider, and C. D. Weidman, Characterization of lightning return stroke electric and magnetic fields from simultaneous two-station measurements, *J. Geophys. Res., 84*, 6307–6314, 1979.

Livingston, J. M., and E. P. Krider, Electric fields produced by Florida thunderstorms, *J. Geophys. Res., 83*, 385–401, 1978.

Malan, D. J., and B. F. J. Schonland, Progressive lightning, 7, Directly correlated photographic and electrical studies of lightning from near thunderstorms, *Proc. R. Soc., London, Ser. A, 191*, 485–503, 1947.

Malan, D. J., and B. F. J. Schonland, The distribution of electricity in thunderclouds, *Proc. R. Soc. London, Ser. A, 209*, 158–177, 1951.

Pierce, E. T., Electrostatic field changes due to lightning discharges, *Q. J. R. Meteorol. Soc., 81*, 211–228, 1955.

Pierce, E. T., The Thunderstorm Research International Program (TRIP)—1976, *Bull. Am. Meteorol. Soc., 57*, 1214–1216, 1976.

Proctor, D. E., A radio study of lightning, Ph.D. thesis, Univ. of Witwaterscand, Johnnesburg, 1976.

Rustan, P. L., Properties of lightning derived from time series analysis of VHF radiation data, Ph.D. dissertation, Univ. of Florida, Gainesville, 1979.

Rustan, P. L., M. A. Uman, D. G. Childers, W. H. Beasley, and C. L. Lennon, Lightning source locations from VHF radiation data for a flash at Kennedy Space Center, *J. Geophys. Res., 85*, 4893–4903, 1980.

Schonland, B. F. J., Progressive lightning, 4, The discharge mechanism, *Proc. R. Soc., London, Ser. A. 164*, 132–150, 1938.

Schonald, B. F. J., The pilot streamer in lightning and the long spark, *Proc. R. Soc., London, Ser. A, 220*, 25–38, 1953.

Schonland, B. F. J., The lightning discharge, in *Handbuch der Physik*, vol. 22, edited by S. Flugge, pp 576–628, Springer, New York, 1956.

Schonland, B. F. J., D. J. Malan, and H. Collens, Progressive lightning, 2, *Proc. R. Soc., London, Ser. A, 152*, 595–625, 1935.

Schonland, B. F. J., D. B. Hodges, and H. Collens, Progressive lightning, 5, A comparison of photographic and electrical studies of the discharge, *Proc. R. Soc., London, Ser. A. 166*, 56–75, 1938*a*.

Schonland, B. F. J., D. J. Malan, and H. Collens, Progressive lightning, 6. *Proc. R. Soc., London, Ser. A, 168*, 455–469, 1938*b*.

Takeuti, T., H. Isikawa, and M. Takagi, On the cloud discharge preceding the first ground stroke, *Proc. Res. Inst. Atmos. Nagoya Univ., 7*, 1–6, 1960.

Thomson, E. M., Characteristics of Port Moresby ground flashes, *J. Geophys. Res., 85*, 1027–1036, 1980.

Uman, M. A., *Lightning*, McGraw-Hill, New York, 1969.

Weidman, C. D., and E. P. Krider, The radiation field wave forms produced by intracloud lightning discharge processes, *J. Geophys. Res., 84*, 3159–3164, 1979.

(Received May 18, 1981;
revised February 5, 1982;
accepted March 8, 1982.)

APPENDIX 3

A Comparison of Lightning Electromagnetic Fields with the Nuclear Electromagnetic Pulse in the Frequency Range 10^4-10^7 Hz

A Comparison of Lightning Electromagnetic Fields with the Nuclear Electromagnetic Pulse in the Frequency Range 10^4–10^7 Hz

MARTIN A. UMAN, SENIOR MEMBER, IEEE, MANECK J. MASTER, AND E. PHILIP KRIDER

Abstract—**The electromagnetic fields produced by both direct lightning strikes and nearby lightning are compared with the nuclear electromagnetic pulse (NEMP) from an exoatmospheric burst. Model calculations indicate that, in the frequency range from 10^4 to near 10^7 Hz, the Fourier amplitude spectra of the return stroke magnetic fields near ground 1 m from an average lightning strike will exceed that of the NEMP. Nearby first return strokes at a range of about 50 m, if they are severe, produce electric-field spectra near ground which exceed that of the NEMP below about 10^6 Hz, while the spectra of average nearby first return strokes exceed that of the NEMP below about 3×10^5 Hz. Implications of these results for aircraft in flight are discussed.**

Key Words—**Lightning, EMP, electromagnetic fields, amplitude spectra aircraft.**

Manuscript received March 29, 1982; revised August 2, 1982. This paper was funded primarily by the National Science Foundation (ATM-79-02627) and the Office of Naval Research (N00014-81-K-0177 and N00014-76-C-0206). Additional funding was provided by the Air Force Wright Aeronautical Laboratories, Wright Patterson Air Force Base, under Contract F33615-81-C-3410, and by SRI, International, under Subcontract C-10681, through Lightning Location and Protection, Inc.

M. A. Uman is with the Department of Electrical Engineering, University of Florida, Gainsville, FL 32611 (904) 392-0940, and also with Lightning Location and Protection, Inc., Tucson, AZ 85719.

M. J. Master is with Bell Laboratories, Holmdel, NJ 07733.

E. P. Krider is with the Institute of Atmospheric Physics, University of Arizona, Tucson, AZ 85721, and also with Lightning Location and Protection, Inc., Tucson, AZ 85719

I. INTRODUCTION

A SERIES of recent articles describe the threat to the United States command, control, and communications (C^3) network from a nuclear electromagnetic pulse (EMP or NEMP) generated by an exoatmospheric nuclear explosion. Broad [1]–[3] has critically examined the various technical and political problems surrounding NEMP; Lerner [4], [5] has discussed the damaging effects of NEMP on the C^3 network and

0018-9375/82/1100-0410$00.75

on nuclear power plants; and Raloff [6], [7] has considered the threat posed by NEMP and the implementation of defensive strategies. It has often been stated [4], [6], [8] that the effects of NEMP are comparable to, or greatly exceed, those of the most severe lightning. For example, Holden [8] states that "the EMP is a microsecond burst of electromagnetic energy, a hundred times more powerful than a lightning bolt." As far as we are aware, the claims that NEMP effects almost always exceed those of lightning are not quantitatively justified in the literature. On the other hand, a recent letter to the Editor of the IEEE SPECTRUM [9] cites references to the lightning literature to support the view that lightning effects can be equivalent to or exceed those of the NEMP.

The effects of NEMP from an exoatmospheric burst will be felt over a large geographical area, whereas the effects of a single lightning discharge are local. Nevertheless, the frequency of direct and nearby strikes to sensitive earthbound structures like nuclear power plants, to electric transmission and distribution systems, and to aircraft in flight is sufficiently high to warrant a careful assessment of the lightning hazard. Here we present frequency-domain comparisons of the electric and magnetic fields near ground due to model lightning return strokes with those of the NEMP from an exoatmospheric burst. The applicability of these results for altitudes at which, for example, aircraft operate, is presently a matter of speculation due to the paucity of airborne measurements, as we will discuss. We will show that, in the frequency range from 10^4 to near 10^7 Hz, the calculated Fourier amplitude spectra of the return stroke magnetic fields near ground 1 m from an average lightning strike will exceed that of the NEMP; and that electric-field spectra near ground of severe nearby first return strokes at 50 m exceed that of the NEMP below about 10^6 Hz and spectra of average nearby first return strokes are greater below about 3×10^5 Hz. To the extent that fields in the frequency ranges in which lightning spectra exceed that of NEMP represent a hazard by, for example, exciting resonances in a structure which couple damaging voltages and currents to electronics in the interior of that structure [10], [11], lightning effects can apparently be as severe as those due to the NEMP.

II. LIGHTNING

Recently, it has been reported that the electric and magnetic fields produced by all important lightning discharge processes contain significant variations on a submicrosecond time scale [12]-[18]. The existence of these field components, in turn, implies that the currents which produce them contain large submicrosecond variations [13], [15], [16], [19]. The few direct wide-band measurements of lightning currents during strikes to airplanes in flight show submicrosecond rise times for current pulses in the 100-A range [20], [21]. These pulses are probably associated with small cloud discharge processes.

Uman *et al.* [22] have calculated the distant electric and magnetic radiation fields produced at ground level by a fixed current waveshape propagating up a straight vertical channel

$$E_{rad}(D, t) = -\frac{\mu_0 v}{2\pi D} \cdot i(t - D/c)a_z, \qquad t \geq D/c \tag{1}$$

$$H_{rad}(D, t) = \frac{v}{2\pi c D} \cdot i(t - D/c)a_\phi, \qquad t \geq D/c \tag{2}$$

where $i(t)$, $t \geq 0$, is the current at time t, v is the velocity with which the current pulse propagates up the channel. D is the horizontal distance from the channel to the point at which the field is measured, c is the speed of light, μ_0 is the permeability of free space, z is the vertical coordinate, and ϕ is the azimuthal coordinate. The best available models for the current in the return stroke phase of a cloud-to-ground discharge [23], [24] (see [25], [26] for a general review of lightning discharge phenomena) have model currents which, in the time domain, produce electric and magnetic fields in good agreement with wide-band (dc to about 2 MHz) time-domain measurements made at ground level. For these models, (1) and (2) provide a good approximation to the relation between the initial return stroke radiation field and the initial return stroke current. Weidman and Krider [16] have measured the maximum rate-of-rise of the initial return stroke radiation field for first strokes and find a mean of about 30 V/m·μs normalized by an inverse range relation to a distance of 100 km. This mean value, when substituted in (1), with an assumed return stroke velocity of 10^8 m/s, leads to a calculated mean maximum rate-of-rise of the return stroke current of about 150 kA/μs, a value which is representative of the current just above ground. The maximum values of maximum rate-of-rise of field and current from 97 measured first strokes are about 2.5 times the mean [16].

Lightning return stroke current waveforms have been directly measured during strikes to instrumented towers in Switzerland [27], in Italy [28], and in South Africa [29]. Unfortunately, currents to tall towers do not necessarily provide a good estimate of the current encountered by small earthbound structures or of the current in the lightning channel above ground because of the effects of the relatively long upward-propagating leader which is initiated by the tower and because of the effects of the tower inductance, capacitance, and relatively large ground impedance characteristic of the mountaineous terrain where most measurements have been made. The upward-propagating discharge, for example, could cause a slower overall current rise time at the tower than a comparable strike to normal ground and could conceivably alter or mask the fast current components. This effect should be more pronounced for first return strokes than for subsequent strokes, since the latter are thought not to have long upward-propagating leaders. Berger *et al.* [27] found that the median peak current for first return strokes which lowered negative charge to a tower in Switzerland was 30 kA and that the median maximum rate-of-rise of the current was 12 kA/μs. The corresponding values at the 5-percent level were 80 kA and 32 kA/μs. For negative strokes subsequent to the first in multiple-stroke flashes, the median peak current was 12 kA, and the median maximum rate-of-rise was 40 kA/μs. Subsequent strokes at the 5-percent level had a peak current of 30 kA and a maximum rate-of-rise of 120 kA/μs. It is interesting to note that the subsequent stroke currents reported in [27] have shorter overall rise times and larger maximum rates-of-rise than first strokes. This result should be contrasted with the electric radiation field measurements made by Weidman and Krider [13], [16], who report no significant differences in the maximum rates-of-rise of first and subsequent stroke fields. The tower on which Berger *et al.* [27] made their measurements was on top of Mt. San Salvatore in Switzerland.

TABLE I A
CURRENT PARAMETERS FOR AN AVERAGE FIRST RETURN STROKE OBTAINED FROM REMOTE FIELD MEASUREMENTS IN ACCORDANCE WITH THE PROCEDURE OUTLINED IN [23], [24]

Current at ground

Time (μs)	Current (kA)
0.0	0.0
100.0	5.0
105.0	20.0
105.1	35.0
107.0	18.0
112.5	25.0
120.0	27.0
140.0	18.0
160.0	12.4
200.0	5.0
300.0	0.0

given by the following parameters

(1) Breakdown pulse current with velocity 1×10^8 m/s:

t(μs)	I_p(kA)
0.0	0.0
5.0	15.0
5.1	30.0
7.0	8.0
15.0	2.0
40.0	0.0

The pulse decays exponentially with height above the ground with a decay constant $\lambda_p = 2.0 \times 10^3$ m

(2) Uniform current $I_u = 5$ kA

time duration = 0.3 ms; turn-on time = 0.1 ms

(3) Corona current per unit length is $I_c = I_{co}\, e^{-z/\lambda}(e^{-\alpha t} - e^{-\beta t})$ A/m

where,

$I_{co} = 50.0$ A/m
$\lambda = 2.0 \times 10^3$ m
$\alpha = 1 \times 10^5\ s^{-1}$
$\beta = 3 \times 10^6\ s^{-1}$

TABLE I B
CURRENT PARAMETERS FOR AN AVERAGE FIRST RETURN STROKE OBTAINED FROM TOWER MEASUREMENTS [27]

Time (μs)	Current (kA)
0.0	0.0
3.0	3.2
5.0	7.0
6.5	14.0
7.8	21.0
8.3	28.0
8.6	32.0
9.0	34.0
10.0	35.0
40.0	28.0
80.0	21.0
250.0	0.0

TABLE II A
CURRENT PARAMETERS FOR AN AVERAGE SUBSEQUENT RETURN STROKE OBTAINED FROM REMOTE FIELD MEASUREMENTS [23], [24]

Current at ground

Time (μs)	Current (kA)
0.0	0.0
100.0	3.1
101.0	6.0
101.1	18.0
103.8	13.5
106.5	13.5
111.0	11.6
120.0	11.2
140.0	7.0
200.0	3.0
300.0	0.0

given by the following parameters

(1) Breakdown pulse current with velocity 1×10^8 m/s:

t(μs)	I_p(kA)
0.0	0.0
1.0	3.0
1.1	15.0
3.7	7.4
11.0	1.4
40.0	0.0

The pulse decays exponentially with height above the ground with a decay constant, $\lambda_p = 1.5 \times 10^3$ m

(2) Uniform current $I_u = 3$ kA

time duration = 0.3 ms; turn-on time = 0.1 ms

(3) Corona current per unit length is $I_c = I_{co}\, e^{-z/\lambda}(e^{-\alpha t} - e^{-\beta t})$ A/m

where,

$I_{co} = 21.0$ A/m
$\lambda = 1.5 \times 10^3$ m
$\alpha = 1 \times 10^5\ s^{-1}$
$\beta = 3 \times 10^6\ s^{-1}$

TABLE II B
CURRENT PARAMETERS FOR AN AVERAGE SUBSEQUENT RETURN STROKE OBTAINED FROM TOWER MEASUREMENTS [27]

Time (μs)	Current (kA)
0.00	0.0
0.60	7.2
0.74	14.4
1.4	18.0
4.0	13.8
8.0	11.7
20.0	10.8
80.0	7.2
250.0	0.0

On the other hand, the tower used in the South African study [29] was situated on a comparatively flat terrain. In [29], a maximum current rate-of-rise of 180 kA/μs was reported for a subsequent stroke, although the total sample size was only 11 flashes.

Berger *et al.* [27] have computed "mean lightning current waveshapes" for first and subsequent negative strokes. These were determined by first normalizing all the measured waveforms to a peak value of unity and then averaging the measured values at each time. If this "mean waveshape" is scaled up in current to produce a large-amplitude waveform, as we shall do to model a severe lightning, the rate-of-rise necessarily scales also. On the other hand, the reported tower measurements do not show a very strong correlation between the peak current and the rate-of-rise of current [27], [30].

There is general agreement that the mean peak current during strikes to normal objects on the ground is in the 20-40-kA range, and that peak currents of 175-225 kA are present in about 1 percent of the strikes [31].

To calculate return stroke fields for comparison with the NEMP, we will use first and subsequent return stroke current waveforms that are inferred from both the remote electromagnetic-field measurements and the tower measurements. Specification of currents for average first and subsequent strokes is given in Tables I and II. The peak current value for an average first stroke is chosen to be 35 kA, and for an average subsequent stroke, 18 kA. The currents derived from the electromagnetic-field measurements [23], [24], differ from the directly measured currents on Mt. San Salvatore [27] primarily in the relatively slow rate-of-rise of first stroke current in the tower measurements compared to that derived from the fields. Severe lightning currents are obtained by multiplying by a factor of *five* both the typical currents derived from electromagnetic fields [23], [24] and the "mean lightning current waveshapes" from tower measurements [27] given in Tables I and II. Although the peak value of the currents determined this way are representative of measured severe lightning [31], the rate-of-rise we use for severe lightning, five times the average value, may be excessive if the rate-of-change of current does not scale with the current. As noted previously, no strong correlation has been found between peak current and rate-of-change of current in the tower measurements [27], [30]. No data have been published on this correlation for the currents derived from the fields; and, as noted previously, the largest value of the maximum rate-of-rise of the electric radiation field for 97 first strokes was only about 2.5 times the mean [16].

III. NEMP

The characteristics of the NEMP are a function of whether the nuclear event is in or out of the atmosphere and the distance from it. A thorough survey of the mechanisms by which the NEMP is generated, the details of the coupling of the NEMP to a variety of systems, and the response of those systems is found in two volumes of collected papers [10], [11]. Reasonable approximations to the NEMP waveform at the surface of the earth or at aircraft altitude due to an exoatmospheric burst have been given in Lee [11]. For the present study, we choose the exoatmospheric burst NEMP waveform from Lee [11] which appears to be the choice of most NEMP researchers

$$E(t) = E_0[e^{-\alpha t} - e^{-\beta t}], \qquad t \geq 0 \tag{3}$$

$$H(t) = H_0[e^{-\alpha t} - e^{-\beta t}], \qquad t \geq 0 \tag{4}$$

with $E_0 = 5.2 \times 10^4$ V/m, $H_0 = 1.4 \times 10^2$ A/m, $\alpha = 4.0 \times 10^6$ s^{-1}, and $\beta = 5.0 \times 10^8$ s^{-1}.

IV. COMPARISONS

A. Direct Strike and NEMP

To compare the fields from lightning direct strikes with NEMP fields, we must choose an example object to be struck. Let us consider the fields at the surface of a hypothetical cylindrical metallic aircraft fuselage of radius r. We choose the aircraft as an example because of its considerable practical importance. If a lightning return stroke attaches directly to this aircraft and the current flows uniformly along the fuselage, the magnetic-field intensity at the surface will be about

$$H = \frac{I}{2\pi r} \tag{5}$$

where I is the lightning current and where the total field has been approximated as magnetostatic. Obviously, the field will be the same at a distance r from the axis of any structure much longer than r which uniformly carries the current, and hence, the results to be obtained are generally applicable. If the aircraft is struck by an average first return stroke with a peak current of about 35 kA, the peak magnetic field at the surface with an assumed radius of 1 m will be about 5.6×10^3 A/m. A 175-kA severe stroke will produce a peak field of about 2.8×10^4 A/m. If about half of the lightning field rises to peak in about 0.1 μs, as suggested by the electromagnetic-field measurements of Weidman and Krider [13], [16], then the maximum rate of change of the magnetic field from an average first stroke will be about 2.8×10^{10} A/m·s and from a severe stroke will be about 1.4×10^{11} A/m·s. The peak NEMP field, 2.8×10^2 A/m, can be obtained by multiplying (4) by a factor of 2, to take account of the reflection of the NEMP plane wave from the metallic surface of the aircraft. The maximum field rate-of-change for NEMP is 1.4×10^{11} A/m·s and exists for a time of the order of a nanosecond. The return stroke peak fields from normal lightning exceed those of the NEMP by a factor of about 20. The NEMP maximum rate-of-change exceeds that of normal lightning by a factor of about 5 and is about equal to that of severe lightning.

We now examine how the time-domain parameters derived above for lightning and NEMP are reflected in the Fourier amplitude spectra for the two events. Again we use the example of the fields on the surface of an aircraft, the calculated lightning fields, however, being essentially the same at comparable distance from any direct strike. For the computations involving currents derived from electric and magnetic fields, both the radiation and induction field terms in the general field equations have been included [23], [24], although (5), with the currents given in Tables IA and IIA, provides a good approximation to the end result. In calculations involving currents from tower measurements, the magnetic field is calculated directly from (5).

Figs. 1 and 2 show the Fourier amplitude spectra of the time-domain magnetic fields produced by currents given in Tables I and II for both average and severe return strokes derived from both tower and remote field measurements. The current waveforms are composed of straight-line segments between the points given in Tables I and II and are digitized at 0.005-μs intervals for the calculation of the Fourier amplitude spectra. The spectra inferred from the electromagnetic-field measurements are larger above 10^5 Hz than those derived from the tower data for first strokes, due to the relatively slow first-stroke current rate-of-rise measured on towers, but the two spectra are similar for subsequent strokes. For average return strokes, the spectral amplitudes for the first and subsequent stroke fields determined from remote electromagnetic measurements, and the subsequent-stroke measured tower current, are equal to the NEMP at a frequency near

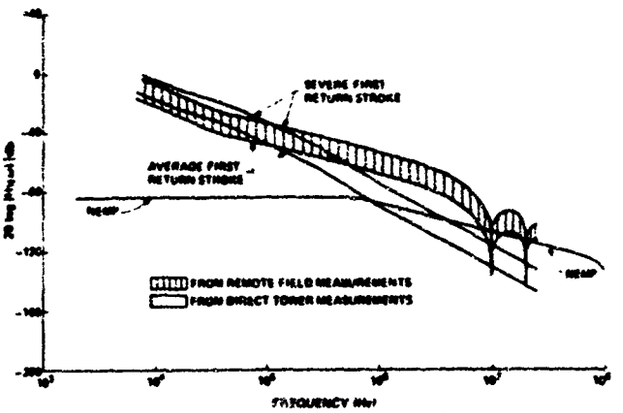

Fig. 1. Magnetic-field Fourier amplitude spectra for a direct strike by an average and a severe first return stroke from both tower and remote field measurements and for NEMP. The dips in the remote field data at 1×10^7 and 2×10^7 Hz are due to the large linear current transition taking place in 0.1 μs during the current rise to peak. Since real waveshapes do not have such linear transitions, the dips in the spectra are artificial.

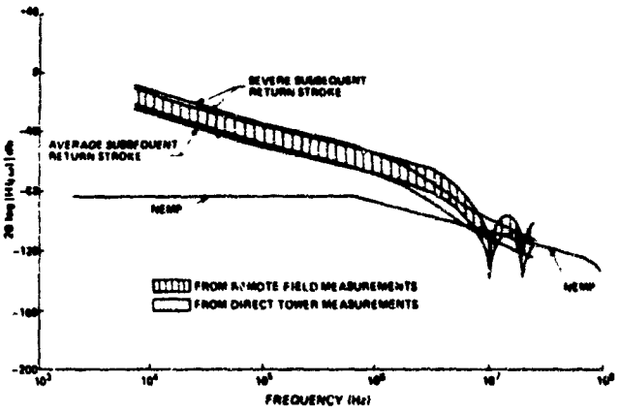

Fig. 2. Magnetic-field Fourier amplitude spectra for a direct strike by an average and a severe subsequent return stroke from both tower and remote field measurements and for NEMP. The dips in the remote field data at 1×10^7 and 2×10^7 Hz are due to the large linear current transition taking place in 0.1 μs during the current rise to peak. Since real waveshapes do not have such linear transitions, the dips in the spectra are artificial.

10^7 Hz and exceed the NEMP at frequencies below that value. For above-average return strokes, the lightning spectra exceed the NEMP spectra to frequencies above 10^7 Hz.

The preceding comparisons between lightning and NEMP fields are, strictly speaking, applicable only near ground. We use the example of an aircraft because of its practical importance, and, for that reason, a discussion of the fields above ground is in order. An aircraft in flight would probably not encounter the full return stroke current which would flow through a structure on the ground since the return stroke current will probably decrease with height [24]. In fact, Clifford and Kasemir [32] argue that most strikes to aircraft are not return strokes but are triggered by the aircraft and are some sort of in-cloud discharge with a rate-of-change of current an order of magnitude less than that of the average return strokes we are considering. Clifford and Kasemir [32] contend that aircraft are only occasionally involved with return strokes, although the total data from instrumented aircraft, on which this opinion is based, are meager. In any event, relatively large return stroke currents at ground level may well still produce currents at aircraft operational altitudes to cause fields equivalent to the NEMP at frequencies below about 10^7 Hz. More important is the observation that both the in-cloud discharge processes which precede stepped leaders in ground flashes and certain pulses in intracloud lightning discharges produce Fourier amplitude spectra measured near ground for distant discharges comparable to those of distant return strokes [17], implying that there are in-cloud events which produce close fields in the cloud equivalent to close return stroke fields near ground. These in-cloud processes can be expected to interact with aircraft. An accurate assessment of the probability of aircraft involvement with different types and phases of lightning awaits further research. Finally, it is worth noting that the NEMP wavefront is plane while the lightning field is circular and that lightning channel attachment to an aircraft may alter the behavior of traveling and reflected waves on the aircraft structure from the free field NEMP case, and hence there may be additional factors in the comparison which we have not considered.

B. Nearby Lightning and NEMP

For the direct lightning strike, we have compared the magnetic field at an aircraft surface with the NEMP. For a nearby flash, we will compare the electric fields. The fields are those which would exist in the absence of the aircraft. We will plot spectra only for the severe first return stroke at ground level. In Fig. 3, we show the NEMP spectrum calculated from the expression given in (3) along with three electric-field amplitude spectra for severe first return strokes which strike the ground 50 m from the observation point. The three lightning amplitude spectra are: 1) the average first stroke electric radiation field spectrum measured by Weidman *et al.* [17] for return strokes at about 50 km extrapolated to 50 m using an inverse distance relationship and multiplied by a factor of 5 to simulate a severe stroke; 2) the electric radiation field spectrum at 50 km calculated using the model of Master *et al.* [24] with the currents in Table IA multiplied by a factor of 5 and extrapolated to 50 m using an inverse distance relationship; and 3) the total electric-field spectrum at 50 m calculated using the model [24] with the currents in Table IA multiplied by a factor of 5.

The calculated and the measured radiation field spectra at 50 km extrapolated to 50 m are essentially identical. The amplitude spectrum computed for the total electric field of a 175-kA lightning at 50 m is equal to the extrapolated radiation field near 10^7 Hz and is greater for lower frequencies because the electrastatic and induction components of the total field add to the radiation component. The spectrum of the total electric field exceeds that of the NEMP below about 10^6 Hz. For an average nearby first return stroke, the total electrical field spectrum exceeds that of the NEMP below about 3×10^5 Hz.

The nearby discharge has been assumed to be at a distance of 50 m because this is about the range at which an earth-bound structure or an aircraft in flight would be expected to become involved in a typical direct strike. The closest distance at which the lightning return stroke fails to attach to a ground-

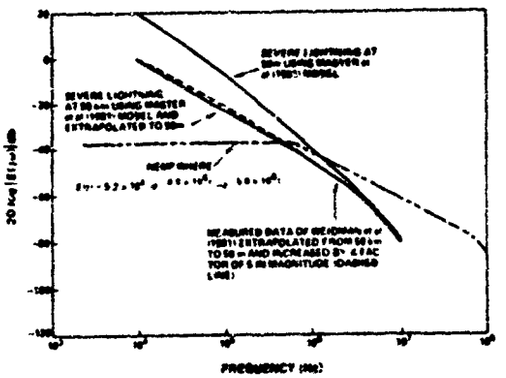

Fig. 3. Electric-field Fourier amplitude spectra for a severe first return stroke at 50 m and for NEMP. For the purpose of clarity, dips in the computed 50-km spectrum, similar to those shown in Figs. 1 and 2, have been omitted.

based structure may be derived from the "striking distance" concept developed by Gold [33].

Fig. 3 shows the vertical electric field at ground level. Master *et al.* [24] have computed the horizontal and vertical electric fields and the horizontal magnetic fields above ground level. The validity of these calculations, however, depends on the validity of the assumed currents above ground level. Field measurements above ground are needed before the adequacy of the calculated nearby return stroke-field environment above ground can be evaluated. Further, future calculations should include the effects of channel tortuosity which are not taken into account in the model [23], [24] used in this paper. Although nearby return stroke fields may well decrease with altitude to the point that they are unimportant compared to the NEMP, in-cloud processes, as noted earlier, can produce distant fields near ground with comparable Fourier amplitude spectra to return strokes [17], implying that nearby in-cloud processes at aircraft altitudes can produce a similar electromagnetic environment to that of nearby return strokes at ground level.

V. DISCUSSION AND CONCLUSIONS

In this paper, we have compared calculations of the electromagnetic environment in the frequency range 10^4-10^7 Hz produced near ground by direct and nearby lightning return strokes with those due to the NEMP produced by an exoatmospheric burst. In that frequency range, the calculated Fourier amplitude spectra of the magnetic fields 1 m from a direct lightning strike by an average return stroke are greater than that of the NEMP. The spectra of severe nearby first return strokes at about 50 m exceed that of the NEMP below about 10^6 Hz of average nearby first strokes below about 3×10^5 Hz. These results follow primarily from the time-domain return stroke currents given in Tables IA and IIA, which were determined by theory from measured time-domain electric and magnetic fields. The frequency spectra calculated from fields computed using these currents are in excellent agreement with measured frequency spectra up to 10^7 Hz for lightning at a distance of 50 km, as is evident from Fig. 3, providing confidence in the model currents.

Although many of the computations in this paper were performed for an idealized aircraft near ground, the basic results are applicable to any similar size ground-based system and, to the extent discussed, to aircraft at flight altitudes.

REFERENCES

[1] W. J. Broad, "Nuclear pulse (I): Awakening to the chaos factor," *Sci.*, vol. 212, pp. 1009–1012, 1981.

[2] W. J. Broad, "Nuclear pulse (II): Ensuring delivery of the doomsday signal," *Sci.*, vol. 212, pp. 1116–1120, 1981.

[3] W. J. Broad, "Nuclear pulse (III) Playing a wild card," *Sci.*, vol. 212, pp. 1248–1251, 1981.

[4] E. J. Lerner, "Electromagnetic pulses. Potential crippler," *IEEE Spectrum*, vol. 18, pp. 41–46, May 1981.

[5] E. J. Lerner, "EMPs and nuclear power," *IEEE Spectrum*, vol. 18, pp. 48–49, June 1981.

[6] J. Raloff, "EMP. A sleeping electronic dragon," *Sci. News*, vol. 119, pp. 300–302, 1981.

[7] J. Raloff, "EMP Defensive strategies," *Sci. News*, vol. 119, pp. 314–315, 1981.

[8] C. Holden, "Energy, security, and war," *Sci.*, vol. 211, p. 683, 1981.

[9] P. B. Corn and J. C. Corbin, "Letter to the editor," *IEEE Spectrum*, vol. 18, p. 20, Oct. 1981.

[10] Special Issue on *IEEE Trans. Electromagn. Compat.*, vol. EMC-20, Feb. 1978 (also published as *IEEE Trans. Antennas Propagat.*, vol. AP-26, Jan. 1978).

[11] K. H. S. Lee, Ed., "EMP interaction: Principles, techniques, and reference data," *EMP Interaction 2-1*, AFWL-TR-80-402, Dec. 1980.

[12] E. P. Krider, C. D. Weidman, and R. C. Noggle, "The electric fields produced by lightning stepped-leaders," *J. Geophys. Res.*, vol. 82, pp. 951–960, 1977.

[13] C. D. Weidman and E. P. Krider, "The fine structure of lightning return stroke waveforms," *J. Geophys. Res.*, vol. 83, pp. 6239–6247, 1978.

[14] C. D. Weidman and E. P. Krider, "Submicrosecond rise times in produced by intracloud lightning discharge processes," *J. Geophys. Res.*, vol. 84, pp. 3159–3164, 1979.

[15] C. D. Weidman and E. P. Krider, "Submicrosecond rise times in lightning radiation fields, in lightning technology," in *Proc. Tech. Symp. NASA Langley Research Center*, Apr. 1980, NASA CP2128, FAA-RD-80-30, 1980, pp. 29–38.

[16] C. D. Weidman and E. P. Krider, "Submicrosecond rise times in lightning return-stroke fields," *Geophys. Res. Lett.*, vol. 7, pp. 955–958, 1980.

[17] C. D. Weidman, E. P. Krider, and M. A. Uman, "Lightning amplitude spectra in the interval from 100 kHz to 20 MHz," *Geophys. Res. Lett.*, vol. 8, pp. 931–934, 1981.

[18] R. K. Baum, "Airborne lightning characterization in lightning technology," NASA Conf. Pub. 2128, FAA-RD-80-30, pp. 1–19, Apr. 1980.

[19] D. W. Clifford, E. P. Krider, and M. A. Uman, "A case of submicrosecond rise-time lightning current pulses for use in aircraft induced-coupling studies," presented at 1979 IEEE Int. Symp. EMC, San Diego, CA, Oct. 1979.

[20] F. L. Pitts and M. E. Thomas, "1980 direct strike lightning data," NASA Tech. Memo. 81946, Langley Research Center, Hampton, VA, Feb. 1981.

[21] F. L. Pitts and M. E. Thomas, "1981 direct strike lightning data," NASA Tech. Memo. 83273, Langley Research Center, Hampton, VA, Mar. 1982.

[22] M. A. Uman, D. K. McLain, and E. P. Krider, "The electromagnetic radiation from a finite antenna," *Amer. J. Phys.*, vol. 43, pp. 33–38, 1975.

[23] Y. T. Lin, M. A. Uman, and R. B. Standler, "Lightning return stroke models," *J. Geophys. Res.*, vol. 85, pp. 1571–1583, 1980.

[24] M. J. Master, M. A. Uman, Y. T. Lin, and R. B. Standler, "Calculations of lightning return stroke electric and magnetic fields above ground," *J. Geophys. Res.*, vol. 86, pp. 12127–12132, 1981.

[25] M. A. Uman, *Lightning*. New York, NY: McGraw-Hill, 1969.

[26] M. A. Uman and E. P. Krider, "A review of natural lightning: experimental data and modeling," *IEEE Trans. Electromagn. Compat.*, vol. EMC-24, pp. 79–112, 1982.

[27] K. Berger, R. B. Anderson, and H. Kroninger, "Parameters of lightning flashes," *Electra*, vol. 41, pp. 23–37, 1975.

[28] E. Garbagnati, E. Guidice, G. B. LoPiparo, and U. Magagnoli,

"Rilievi dell caratteristiche dei Fulmini in Italia Risultati ottenuti negli anni 1970–1973," *l'Elettrotechnica*, vol 62, pp 237–249, 1975.

[29] A J Eriksson, "Lightning and tall structures," *Trans South African Inst Elec Eng*, vol 69, pp 2–16, Aug 1978

[30] R B Anderson and A J. Eriksson, "Lightning parameters for engineering application," *Electra*, vol 69, pp 65–102, 1980

[31] F Popolansky, "Frequency distribution of amplitudes of lightning currents," *Electra*, vol. 22, pp 139–147, May 1972

[32] D W Clifford and H. W Kasemir, "Triggered lightning," *IEEE Trans Electromagn. Compat*, vol. EMC-24, pp 112–122, 1982

[33] R H. Golde, "Lightning conductor," in *Lightning, Vol. II. Lightning Protection* R H Golde, Ed New York, NY Academic Press, 1977, pp 545–576.

APPENDIX 4

Transient Electric and Magnetic Fields Associated with Establishing a Finite Electrostatic Dipole

Transient electric and magnetic fields associated with establishing a finite electrostatic dipole

M. J. Master[a] and M. A. Uman
Department of Electrical Engineering, University of Florida, Gainesville, Florida 32611

(Received 23 October 1981; accepted for publication 17 March 1982)

We obtain analytical solutions in the time domain for the electric and magnetic fields associated with establishing a finite electrostatic dipole. We assume that a simple source current distribution, a square pulse of current, produces the dipole, and solve for the fields produced by that source current distribution using Maxwell's equations. Salient features of the fields are discussed from a physical point of view. We outline a technique to determine in the time domain the electric and magnetic fields produced by any arbitrary time-varying current propagating along a straight antenna, given the calculated fields due to a short square pulse of current.

INTRODUCTION

Expressions in cylindrical coordinates for the two components of the electric field intensity due to a finite electrostatic dipole with charges $+Q$ at $z' = H$ and $-Q$ at $z' = 0$, as shown in Fig. 1, are easily derived using Coulomb's law[1-3]

$$E_r(r,\phi,z) = \frac{Q}{4\pi\epsilon_0}\left(\frac{r}{[r^2+(z-H)^2]^{3/2}} - \frac{r}{(r^2+z^2)^{3/2}}\right) \text{V/m}, \tag{1}$$

$$E_z(r,\phi,z) = \frac{Q}{4\pi\epsilon_0}\left(\frac{z-H}{[r^2+(z-H)^2]^{3/2}} - \frac{z}{(r^2+z^2)^{3/2}}\right) \text{V/m}, \tag{2}$$

where Q is the dipole charge in coulombs, ϵ_0 is the permittivity in farads per meter, and all lengths are in meters. Since in the electrostatic case there is no current flow, the magnetic field associated with the dipole is zero. In this paper we calculate the transient electric and magnetic fields produced in establishing such a finite electrostatic

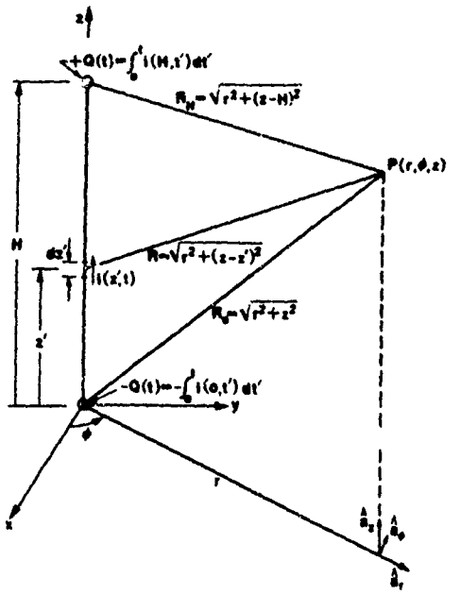

Fig. 1. Definition of geometrical factors used in the electric and magnetic field computations. For the electrostatic dipole, the charge at $z' = 0$ and $z' = H$ is constant at $-Q$ and $+Q$, respectively, and $i(z',t) = 0$.

dipole with a square pulse of current. An extension of this approach is described for a general source current distribution. Salient features of the calculated fields are discussed from a physical point of view. The time domain calculation leads to an analytical closed-form solution which allows much more physical insight than the more standard frequency domain approach.[4]

MODEL

We choose to establish the electrostatic dipole whose fields are given by Eqs. (1) and (2) by injecting, at $z' = 0$, a square pulse of current with magnitude I_0 and duration T, as shown in Fig. 2(a). The square pulse of current is composed of an initial step function at $z' = 0$ and $t = 0$, followed by another step function of equal magnitude but opposite sign at $z' = 0$ and later time T, as illustrat · · Fig. 3.

At any point on the antenna the current may be determined from the reasonable assumption that the current waveform propagates undistorted with a constant velocity v:

$$I(z',t) = I[t - (z'/v)]. \tag{3}$$

The top of the antenna is assumed to be terminated in its characteristic impedance so that no reflection is produced. The current waveform at the top of the channel, $z' = H$, is shown in Fig. 2(b). We adopt the standard approach in antenna theory: we assume a reasonable form for the current and derive the fields rather than deriving the current and the fields simultaneously. The actual current waveform, however, will be influenced to some extent by its own radiation. The velocity of the current waveform will likely be c or very near c, but, for increased generality, we have allowed an arbitrary velocity, $v \leqslant c$, as noted above.

Since the charge delivered to the top of the dipole is

$$\int_0^\infty i(H,t')dt'$$

and to the bottom of the dipole is

$$-\int_0^\infty i(0,t')dt',$$

it follows that the charge on the electrostatic dipole is

$$Q = \pm I_0 T, \tag{4}$$

CALCULATIONS

We need to determine only the electromagnetic fields due to the positive step function of current in Fig. 3(a). The fields due to a square wave of current at any height can then be obtained by superposition of appropriately time-delayed and inverted fields. At any time t, the electric and magnetic fields at an arbitrary point $P(r,\phi,z)$ are due to the integrated effect of the fields radiated from various small dipoles along the antenna at different earlier times. The field expressions in cylindrical coordinates for an infinitesimal dipole of length dz', at $z = z'$, carrying current $i(z',t)$, as shown in Fig. 1, may be obtained by substituting $(z - z')$ for z in Eqs. (A9), (A21), and (A22), derived in Appendix A:

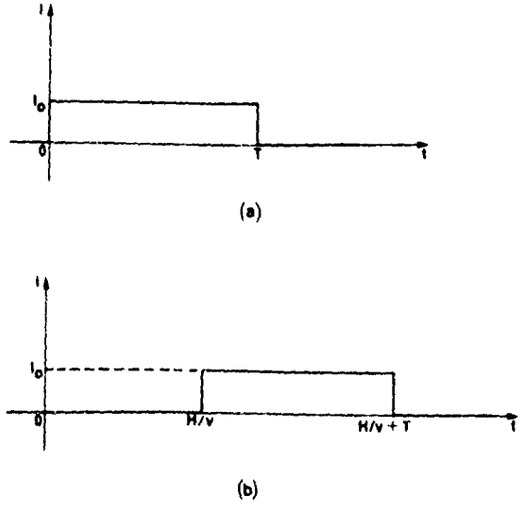

Fig 2. Assumed current as a function of time (a) at $z' = 0$ and (b) at $z' = H$

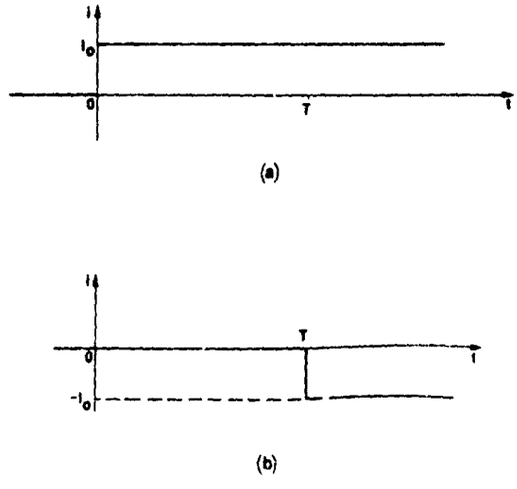

Fig 3 Current at $z' = 0$ decomposed into two components

$$dB_\phi(r,\phi,z,t)=\frac{\mu_0 dz'}{4\pi}\left(\frac{r}{R^3}i(z',t-R/c)+\frac{r}{cR^2}\frac{\partial i(z',t-R/c)}{\partial t}\right); \quad (5)$$

$$dE_r(r,\phi,z,t)=\frac{dz'}{4\pi\epsilon_0}\left(\frac{3r(z-z')}{R^5}\int_0^t i(z',\tau-R/c)d\tau+[3r(z-z')/cR^4]i(z',t-R/c)+\frac{r(z-z')}{c^2R^3}\frac{\partial i(z',t-R/c)}{\partial t}\right); \quad (6)$$

and

$$dE_z(r,\phi,z,t)=\frac{dz'}{4\pi\epsilon_0}\left(\frac{2(z-z')^2-r^2}{R^5}\times\int_0^t i(z',\tau-R/c)d\tau+\frac{2(z-z')^2-r^2}{cR^4}i(z',t-R/c)-\frac{r^2}{c^2R^3}\frac{\partial i(z',t-R/c)}{\partial t}\right). \quad (7)$$

The first terms on the right-hand side of Eqs. (6) and (7) are the so-called electrostatic field; the middle terms are the so-called induction or intermediate field; and the last terms are the radiation or far-zone field. In Eq. (5) the first term is the induction field and the second the radiation field.

The current shown in Fig. 3(a), injected at $z'=0$, may be defined as follows:

$$i(0,t)=0 \quad t<0$$
$$=I_0 \quad t>0, \quad (8)$$

where we have assumed that the current is turned on at $t=0^+$.

From the definition of the current in Eq. (8) we can write down its derivative and its integral,

$$\frac{\partial i(0,t)}{\partial t}=0 \quad t<0$$
$$=I_0\delta(0) \quad t=0 \quad (9)$$
$$=0 \quad t>0,$$

where $\delta(0)$ represents the unit impulse at $t=0$, and

$$\int_0^t i(0,\tau)d\tau=0 \quad t<0$$
$$=I_0 t \quad t>0. \quad (10)$$

Equations (8) through (10) generalized for z' between 0 and H can be substituted in Eqs. (5) through (7) to determine the fields. For all times $t<R/c$, the current, its derivative, and its integral are all zero, and hence the fields given by Eq. (5) through (7) are also zero. At $t=R/c$, the contributions from the electrostatic and induction terms are zero. However, the current derivative is infinite at this point and results in a "turn-on field." The field values at $t=R/c$ will be determined in the next paragraph. For values of time $t>R/c$, the current derivative is zero so that the radiation field is zero. However, there are finite contributions due to both the electrostatic and the induction terms. Hence, Eq. (5) becomes

$$dB_\phi(r,\phi,z,t)=\frac{\mu_0 I_0 r}{4\pi R^3}dz' \quad t>R/c. \quad (11)$$

To find the radial electric field for $t>R/c$, we set the radiation field to zero in Eq. (6):

$$dE_r(r,\phi,z,t)=\frac{dz'}{4\pi\epsilon_0}\left(\frac{3r(z-z')}{R^5}\int_{R/c}^t I_0 d\tau+\frac{3r(z-z')}{cR^4}I_0\right)$$
$$=\frac{dz'}{4\pi\epsilon_0}\left[\frac{3r(z-z')}{R^5}I_0\left(t-\frac{R}{c}\right)+\frac{3r(z-z')}{cR^4}I_0\right].$$

Thus

$$dE_r(r,\phi,z,t)=I_0 t\frac{3r(z-z')}{4\pi\epsilon_0 R^5}dz' \quad t>R/c. \quad (12)$$

Note that for the electrostatic term above the limits of integration are from R/c to t since the retarded current is zero for times $t<R/c$. A similar analysis for the vertical electric field yields

$$dE_z(r,\phi,z,t)=I_0 t\frac{2(z-z')^2-r^2}{4\pi\epsilon_0 R^5}dz' \quad t>R/c. \quad (13)$$

To determine the turn-on fields which occur at $t=R/c$, let us assume that the current goes from zero to the value I_0 in a short time ΔT. In the limit $\Delta T\to 0$ the current is shown in Fig. 3(a) and defined in Eq. (8). During ΔT, the current wave front moves a distance $\Delta z'$ where

$$\Delta z'=v\Delta T. \quad (14)$$

The turn-on magnetic field due to the current in the length $\Delta z'$ is found from Eq. (5):

$$B_\phi(r,\phi,z,t)=(\mu_0/4\pi)\Delta z'(r/cR^2)(I_0/\Delta T),$$

since the induction field contribution to the turn-on field is zero in the limit $\Delta T, \Delta z'\to 0$. In that limit, the turn-on magnetic field becomes

$$B_\phi(r,\phi,z,t)=\mu_0 I_0 vr/4\pi cR^2 \quad t=R/c. \quad (15)$$

A similar analysis for the electric field components give the following turn-on fields:

$$E_r(r,\phi,z,t)=I_0 vr(z-z')/4\pi\epsilon_0 c^2 R^3 \quad t=R/c, \quad (16)$$

$$E_z(r,\phi,z,t)=-I_0 vr^2/4\pi\epsilon_0 c^2 R^3 \quad t=R/c. \quad (17)$$

To find the total fields at $P(r,\phi,z)$ we need to integrate the individual contributions of the various dipoles along the finite length of the antenna. There is no field at point P until time $t=R_0/c$ where R_0 is defined in Fig. 1. At $t=R_0/c$ only the turn-on terms are nonzero and the magnetic and electric fields are computed from Eq. (15)–(17) with $R=R_0$ and $z'=0$. For $t>R_0/c$ we perform the integration over the antenna. We first assume that

$$R_0/c<t<H/v+R_H/c, \quad (18)$$

where R_H is defined in Fig. 1 so that the turn-on term is always present in the field at point $P(r,\phi,z)$. For this case, the magnetic flux density is found from Eqs. (11) and (15):

$$B_\phi(r,\phi,z,t)=\frac{\mu_0 I_0 r}{4\pi}\int_0^{z'_{max}}\frac{dz'}{[r^2+(z-z')^2]^{3/2}}+(\mu_0 I_0 vr/4\pi cR^2)_{z'=z'_{max}},$$

where z'_{max} is computed from the equation,

$$(z'_{max}/v)+[r^2+(z-z'_{max})^2]^{1/2}/c=t. \quad (19)$$

Note that, if $v=c$, Eq. (19) simplifies considerably. Integrating the first term in the magnetic field expression, we obtain

$$B_\phi(r,\phi,z,t) = \frac{\mu_0 I_0}{4\pi r}\left(\frac{z}{(r^2+z^2)^{1/2}} - \frac{z-z'_{\max}}{[r^2+(z-z'_{\max})^2]^{1/2}} + \frac{vr^2}{c[r^2+(z-z'_{\max})^2]}\right), \tag{20}$$

where the last term represents the turn-on field.

Similarly, using Eqs. (12), (13), (16), and (17), we obtain the expressions for the electric field components:

$$E_r(r,\phi,z,t) = \frac{I_0 t}{4\pi\epsilon_0}\left(\frac{r}{[r^2+(z-z'_{\max})^2]^{3/2}} - \frac{r}{(r^2+z^2)^{3/2}}\right) + \frac{I_0 v r}{4\pi\epsilon_0 c^2}\left(\frac{z-z'_{\max}}{[r^2+(z-z'_{\max})^2]^{3/2}}\right); \tag{21}$$

$$E_z(r,\phi,z,t) = \frac{I_0 t}{4\pi\epsilon_0}\left(\frac{z-z'_{\max}}{[r^2+(z-z'_{\max})^2]^{3/2}} - \frac{z}{(r^2+z^2)^{3/2}}\right) - \frac{I_0 v r^2}{4\pi\epsilon_0 c^2[r^2+(z-z'_{\max})^2]^{3/2}}. \tag{22}$$

The turn-on terms are zero once the fields from the top of the antenna have reached $P(r,\phi,z)$; and the values of $z'_{\max}$ is H, the height of the channel. Thus for all times t, such that

$$H/v + R_H/c < t < \infty, \tag{23}$$

Eqs. (20)–(22) become

$$B_\phi(r,\phi,z,t) = \frac{\mu_0 I_0}{4\pi r}\left(\frac{r}{(r^2+z^2)^{1/2}} - \frac{z-H}{[r^2+(z-H)^2]^{1/2}}\right); \tag{24}$$

$$E_r(r,\phi,z,t) = \frac{I_0 t}{4\pi\epsilon_0}\left(\frac{r}{[r^2+(z-H)^2]^{3/2}} - \frac{r}{(r^2+z^2)^{3/2}}\right); \tag{25}$$

and

$$E_z(r,\phi,z,t) = \frac{I_0 t}{4\pi\epsilon_0}\left(\frac{z-H}{[r^2+(z-H)^2]^{3/2}} - \frac{z}{(r^2+z^2)^{3/2}}\right). \tag{26}$$

Equations (15)–(17), (20)–(22), and (24)–(26) comprise a complete description of the electromagnetic fields due to the positive component of current shown in Fig. 3(a). The field expressions for the negative current component shown in Fig. 3(b) are obtained by advancing all times by T, i.e., substituting $t = t + T$, and using $I = -I_0$ in the equations derived for the positive step. We leave this exercise for the reader. The electromagnetic fields due to the positive and negative current components may then be summed to obtain the fields due to the square current pulse of duration T.

These are two separate cases to consider, a "long" and a "short" pulse. When the pulse is relatively short, i.e.,

$$R_0/c + T < R_H/c + H/v, \tag{27}$$

there are times when turn-on and turn-off (turn on of the negative current component) terms are simultaneously present in the field expressions. The analytical solution for the electromagnetic fields due to a short pulse is given in Appendix B. A long pulse propagating up the antenna is defined by the relation

$$R_H/c + H/v < R_0/c + T. \tag{28}$$

Equation (28) ensures that the fields generated by the positive component of current at $z' = H$ have reached the field point before any fields generated by the negative component of current. The calculation of the electromagnetic fields produced by such a long pulse is left as an exercise for the reader.

The electric and magnetic field waveforms for the case of a short pulse are shown in Figs. 4(a) and (b). These waveforms are derived for the following conditions: $H = 10$ m, $T = 10$ ns, and $I_0 = 2$ A, using $v = c/3 = 1.0\times10^8$ m/s in (a) and $v = c = 3.0\times10^8$ m/s in (b). The fields are computed at an altitude $z = 5$ m and at ranges of 1, 10, and 100 m. As we shall discuss later, these lengths, times, and currents may be scaled to obtain the electric and magnetic fields shown in Figs. 4(a) and 4(b) for different sets of input parameters. The lengths, time, and currents used for the specific example were chosen to motivate comparison with an experiment which could be performed on a football field.

The analytical solutions for both the long and the short pulse cases have been translated into a simple computer program. The program input consists of the specification of the field point, the antenna height, the pulse width and amplitude. A listing of the Fortran code is available from the authors.

DISCUSSION

We now discuss some of the more interesting features of the electric and magnetic field waveforms shown in Fig. 4.

(a) After the current has stopped flowing and after the appropriate propagation delay, the magnetic field is zero at all field points as is evident from Eq. (5). As a result of the two equidistant equal and opposite charges, the horizontal component of the electric field at $z = H/2$ is also zero, as is evident from Eqs. (1) and (6). The vertical component of the electric field at $z = H/2$ is constant at

$$E_z(r,\phi,H/2,t) = -(Q/4\pi\epsilon_0)\{H/[r^2+(H/2)^2]^{3/2}\}, \tag{29}$$

which follows from Eqs. (2) and (7).

(b) At a distance of 100 m, the electric and magnetic fields are essentially due to the radiation component. Initially, magnetic and the vertical electric fields have exactly the same shape as the current pulse. When this current pulse reaches the top of the antenna and "turns off," it produces a "mirror image" in these field waveforms: that is, it produces fields which have exactly the same shape as the current pulse but are of opposite polarity. This effect has been previously discussed.[5]

(c) We discuss now the structure of the waveforms at close distances (about 1 m) as shown in Fig. 4. The magnetic field attains its peak value at a time when the current pulse is at approximately at the same altitude as the field point, that is, at the time of closest approach to the field point. The magnetic field peak is essentially due to the induction component of the total magnetic field. The electric fields at this range are primarily due to the electrostatic component

of the total electric fields. We have assumed that the positive component of the antenna current begins at $t = 0$, and the negative component at $t = T$. Since the current is uniform except at the discontinuous front, charge can only be accumulated at the front. In particular, at some time $t\,(t > T)$, a charge $Q_+ = I_0 t$ is accumulated at the front, an equal and opposite charge accumulation taking place at $z' = 0$. At that instant, the negative current component has a charge $Q_- = I_0(t - T)$ accumulated at its front, with an equal and opposite accumulaton taking place at $z' = 0$. Thus at $z' = 0$ there is a fixed charge equal to $-I_0 T$. As the pulse propagates up the channel, the positive and negative charges at the respective current fronts also travel up the channel producing electrostatic fields at close range, a good approximation to which are found using Coulomb's law. The field from each charge is therefore inversely proportional to the square of the distance from the charge to the field point. The horizontal and vertical components of these electric fields are determined by the angle from the charge to the field point.

We first explain the shape of the horizontal component of the electric field. The field from the positive charge is always in the positive radial direction and the field from the negative charge is always in the negative radial direction as the pulse propagates up the antenna from 0 to H. As long as the pulse is below the field point, the positive charge is closer to the field point and hence makes a larger contribution to the horizontal electric field as compared with that of the negative charge. The positive contribution reaches its peak as the positive charge reaches the height of the field point. As the charges continue to propagate up the channel, the negative charge reaches the height of the field point and the horizontal electric field has a pronounced negative peak. The time separation between the positive and the negative peaks is T, the width of the pulse. The transition from the positive to the negative peak occurs continuously, the field being zero at approximately the time when the charges are equidistant from the field point. With the current pulse now completely above the field point the field contribution from the closer negative charge dominates until the pulse reaches the top of the channel and turns off, leaving a charge $Q = +I_0 T$, which together with the charge $-I_0 T$ at $z' = 0$, yields a net zero horizontal electric field for all further time.

We discuss now the shape of the vertical component of the electric field. As the pulse moves up the channel, the

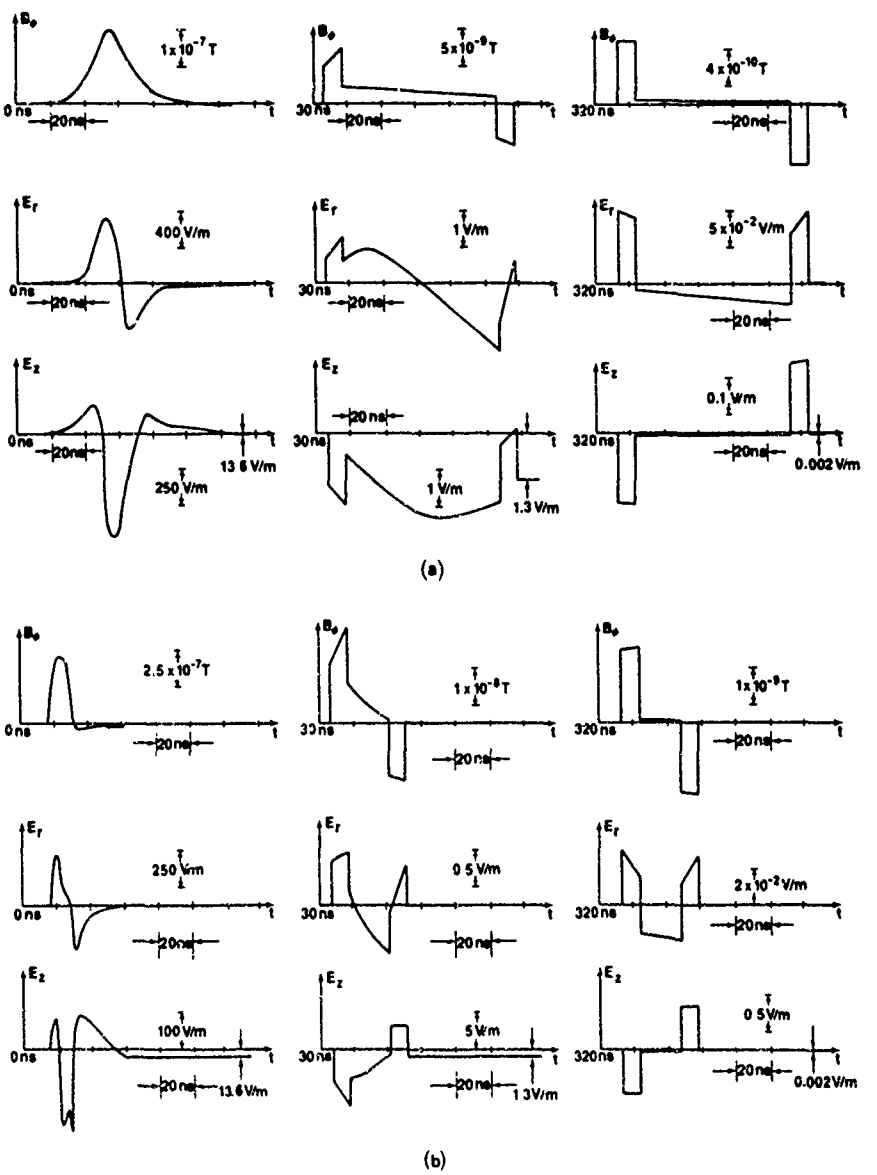

Fig. 4. Calculated magnetic flux density, horizontal electric field intensity, and vertical electric field intensity produced by a current pulse of width 10 ns and magnitude 2 A in vertical antenna of 10 m height at distances of 1 m (left), 10 m (center), and 100 m (right) from the antenna and at a height of $z = 5$ m. The waveforms shown in (a) are for $v = c/3$ and in (b) for $v = c$

positive charge is initially closer to the field point than the negative charge and hence the net field is in the positive z direction. However, as the positive charge moves by the altitude of the field point, it produces a field reversal in the vertical component of electric field. For a short time (approximately equal to the pulse width) the contributions to the vertical electric field due to the positive and the negative charges are both in the negative z direction and hence there is a sharp dip in the field which reaches its negative maximum at about the time when the positive and the negative charges are symmetrical with respect to the field point. As the pulse continues its upward propagation beyond this point, the negative vertical electric field decreases and passes through zero. The field increases in the positive z direction when the negative charge is a little above the field point. As the current pulse continues upward, the increasing distance from the field point results in a reduction in the net positive field. When the pulse reaches the top of the channel and is turned off, it leaves a charge $Q_+ = I_0T$ at the top of the channel, which together with the charge of $Q_- = -I_0T$ at $z' = 0$, produces a net negative vertical electric field. Thus, to produce this final negative field, another field zero occurs as the current pulse reaches the top of the antenna.

The radiation field, which represents a significant fraction of the total fields at distances beyond the close range and discussed in (b) above, is still present at close ranges, but is relatively small, and is completely masked by the large electrostatic component of the total electric field.

(d) At intermediate distances (about 10 m), the electrostatic, induction, and the radiation components all contribute to the total electric fields; the induction and the radiation components both contribute to the magnetic field. The radiation peaks due to the current "turn on" and "turn off," both at $z' = 0$, and at $z' = H$, are readily indentified in the field waveforms.

(e) Comparing the waveforms obtained in Fig. 4(a) for $v = c/3$ and in Fig. 4(b) for $v = c$, we observe that the difference in the velocity of the propagating pulses does not appreciably alter the overall shape of the fields but does change amplitudes and time scales. At 1-m range we note that there is added structure on the waveforms for $v = c$. Also for $v = c$, the peak magnitude of the magnetic field is larger, whereas the peak horizontal and vertical electric fields have decreased compared to the case with $v = c/3$. The radiation fields at 100-m range for $v = c$ have peak amplitudes three times larger than those for $v = c/3$, because the radiation fields are directly proportional to v as shown by Uman *et al.*[5], as is evident from Eqs. (15) through (17). For the intermediate distance, i.e., 10 m, the waveforms for the two velocities are similar, but again the radiation peaks are three times larger for the case $v = c$.

(f) The transient vertical electric fields at all ranges generated by the charging current considered here are larger in peak amplitude than the final static field values. The final static field is only a function of the charge transferred to the ends of the antenna, I_0T. All field components scale with I_0. However, T can be made large enough so that final field values exceed the transient fields at all ranges.

(g) If length, time, and current used in the problem described here are multiplied by a factor f, the same waveforms shown in Figs. 4(a) and (b) for the electric and magnetic fields are obtained for the new distance and time scales. For example, for $f = 500$, $H = 5$ km, $I_0 = 1$ kA, and $T = 5\ \mu$s, the fields at $D = 500$ m, 5 km, and 50 km are the same as those shown with time and distance scales on the figures increased by a factor of 500. Note that since length and time are both scaled by the same factor, velocity is maintained constant.

(h) We have derived an analytical solution for the electric and magnetic fields generated by a pulse of current propagating up an antenna. If the width of this pulse is made arbitrarily small, the resultant fields may be used to determine the fields from any arbitrary time-varying current propagating up the same antenna. By the Superposition Principle the solution for the case of an arbitrary current may be written as an appropriate summation of the solutions due to the component pulse currents. This result stems directly from the linearity property embodied in Maxwell's equations and is analogous to the concept of using the pulse response of a discrete linear system to obtain its response due to any arbitrary excitation.[6] Let us assume that the field solution due to a short current pulse $I_p(t)$ of unit amplitude and width T is given by $F_p(t)$. Any arbitrary current $I(t)$ can be written as

$$I(t) = \sum_{k=0}^{N-1} [I(kT)I_p(t - kT)], \tag{30}$$

where we assume that the total interval of interest is from 0 to NT. The field solution $F(t)$ due to the current $I(t)$ is found from the convolution summation[6]

$$F(t) = \sum_{k=0}^{N-1} [I(kT)F_p(t - kT)]. \tag{31}$$

This summation can be easily carried out on a computer. In general, this time-domain approach is computationally more efficient than the standard frequency domain analysis[4] and allows for considerably more physical insight.

ACKNOWLEDGMENTS

The work reported here was funded in part by the Department of Energy (DE-AC02-81RA50570), the National Science Foundation (ATM-79-02627), the National Aeronautics and Space Administration, Kennedy Space Center (NGR-10-005-169), and the Office of Naval Research (N00014-81-K-0177). We also wish to thank Markus Zahn, Massachusetts Institute of Technology, for his critical review and valuable comments.

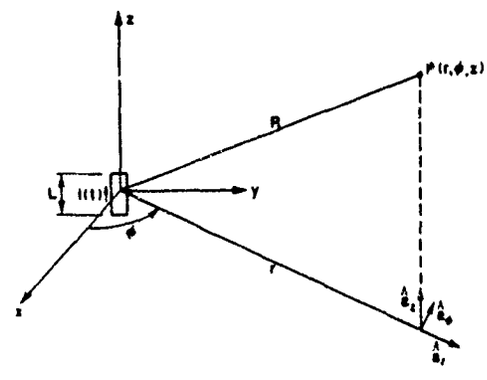

Fig 5 Definition of geometrical factors used in the derivation of the electric and magnetic fields at any arbitrary point due to a current carrying dipole at the origin.

APPENDIX A

The electric field intensity $\mathbf{E}(\mathbf{R},t)$ and the magnetic flux density $\mathbf{B}(\mathbf{R},t)$ at any arbitrary point $\mathbf{R}$ in space due to an arbitrary current $i(\mathbf{R}',t)$ in a small isolated dipole of length L may be derived in the time domain from Maxwell's equations in terms of the vector potential $\mathbf{A}(\mathbf{R},t)$[1]:

$$\mathbf{B}(\mathbf{R},t) = \nabla \times \mathbf{A}(\mathbf{R},t), \tag{A1}$$

$$\mathbf{E}(\mathbf{R},t) = -\frac{\partial \mathbf{A}(\mathbf{R},t)}{\partial t} + c^2 \int_{-\infty}^{t} \nabla[\nabla \cdot \mathbf{A}(\mathbf{R},t)]\, dt \tag{A2}$$

where

$$\mathbf{A}(\mathbf{R},t) = \frac{\mu_0 L}{4\pi}\left[i\left(\mathbf{R}', t - \frac{|\mathbf{R}-\mathbf{R}'|}{c}\right)\right] \Big/ (|\mathbf{R}-\mathbf{R}'|), \tag{A3}$$

and we have used the usual notation of representing field points by unprimed coordinates and source points by primed coordinates.

Equations (A1)–(A3) will now be applied to the case of a small dipole located at the origin of the coordinate system shown in Fig. 5. Since the problem under consideration has cylindrical symmetry, we shall compute the electric and magnetic fields in a cylindrical coordinate system. Uman *et al.*[5] have solved the identical problem using spherical coordinates. Consider the point $P(r,\phi,z)$ in Fig. 5 at which we wish to determine the fields. Using $\mathbf{R}' = 0$ in Eq. (A3), we obtain

$$\mathbf{A}(\mathbf{R},t) = \left(\frac{\mu_0}{4\pi}\frac{i(0,t-R/c)}{R}L\right)\mathbf{a}_z = A_z(\mathbf{R},t)\mathbf{a}_z. \tag{A4}$$

From Eq. (A1) we find

$$\begin{aligned}\mathbf{B}(r,\phi,z,t) &= \nabla \times \mathbf{A} \\ &= \mathbf{a}_\phi\left(-\frac{\partial A_z}{\partial r}\right) \\ &= -\frac{\mu_0 L}{4\pi}\frac{\partial}{\partial r}\left(\frac{i(t-R/c)}{R}\right)\mathbf{a}_\phi.\end{aligned} \tag{A5}$$

Since

$$r^2 = x^2 + y^2 \quad \text{and} \quad R^2 = r^2 + z^2, \tag{A6}$$

it follows that

$$\frac{\partial}{\partial r}\left[i\left(t-\frac{R}{c}\right)\right] = -\frac{r}{cR}i'\left(t-\frac{R}{c}\right)$$

and

$$\frac{\partial}{\partial t}\left[i\left(t-\frac{R}{c}\right)\right] = i'\left(t-\frac{R}{c}\right),$$

where primes denote derivatives with respect to the whole argument, $t - R/c$. Hence, we find the following relation between the time derivative and the radial space derivative

$$\frac{\partial}{\partial r}\left[i\left(t-\frac{R}{c}\right)\right] = -\frac{r}{cR}\frac{\partial}{\partial t}\left[i\left(t-\frac{R}{c}\right)\right]. \tag{A7}$$

We will also need the following relation in the derivative to follow:

$$\frac{\partial}{\partial r}\left(\frac{1}{R}\right) = -\frac{r}{R^3}. \tag{A8}$$

We can expand Eq. (A5) as follows:

$$\begin{aligned}\mathbf{B}(r,\phi,z,t) = -\frac{\mu_0 L}{4\pi}\Bigg[&\frac{1}{R}\frac{\partial i(t-R/c)}{\partial r} \\ &+ i\left(t-\frac{R}{c}\right)\frac{\partial}{\partial r}\left(\frac{1}{R}\right)\Bigg]\mathbf{a}_\phi.\end{aligned}$$

Substituting Eqs. (A7) and (A8) into the above equation, we find

$$\begin{aligned}\mathbf{B}(r,\phi,z,t) = \frac{\mu_0 L}{4\pi}\Bigg[&\frac{r}{cR^2}\frac{\partial i(t-R/c)}{\partial t} \\ &+ \frac{r}{R^3}i\left(t-\frac{R}{c}\right)\Bigg]\mathbf{a}_\phi,\end{aligned} \tag{A9}$$

the desired relation for the magnetic flux density.

We now determine the electric field from Eq. (A2). We begin by finding

$$\begin{aligned}\nabla \cdot \mathbf{A} = \frac{\partial A_z}{\partial z} &= \frac{\mu_0 L}{4\pi}\frac{\partial}{\partial z}\left(\frac{i(t-R/c)}{R}\right) \\ &= \frac{\mu_0 L}{4\pi}\left[\frac{1}{R}\frac{\partial i(t-R/c)}{\partial z} - \frac{z}{R^3}i\left(t-\frac{R}{c}\right)\right].\end{aligned} \tag{A10}$$

Since there is no ϕ variation, the gradient operator becomes

$$\nabla = \mathbf{a}_r\frac{\partial}{\partial r} + \mathbf{a}_z\frac{\partial}{\partial z}.$$

Thus the integrand in Eq. (A2) is

$$\begin{aligned}\nabla(\nabla \cdot \mathbf{A}) = \frac{\mu_0 L}{4\pi}\Bigg[&\frac{\partial}{\partial r}\left(\frac{1}{R}\frac{\partial i(t-R/c)}{\partial z}\right) \\ &- \frac{\partial}{\partial r}\left(\frac{z}{R^3}i(t-R/c)\right)\Bigg]\mathbf{a}_r \\ &+ \frac{\mu_0 L}{4\pi}\Bigg[\frac{\partial}{\partial z}\left(\frac{1}{R}\frac{\partial i(t-R/c)}{\partial z}\right) \\ &- \frac{\partial}{\partial z}\left(\frac{z}{R^3}i(t-R/c)\right)\Bigg]\mathbf{a}_z.\end{aligned} \tag{A11}$$

Expanding Eq. (A11), we find

$$\begin{aligned}\frac{\nabla(\nabla \cdot \mathbf{A})}{\mu_0 L/4\pi} = \Bigg[&\frac{1}{R}\frac{\partial^2 i(t-R/c)}{\partial r \partial z} + \left(-\frac{r}{R^3}\right)\frac{\partial i(t-R/c)}{\partial z} \\ &- z\left(-\frac{3r}{R^5}\right)i\left(t-\frac{R}{c}\right) \\ &- -\frac{z}{R^3}\frac{\partial i(t-R/c)}{\partial r}\Bigg]\mathbf{a}_r \\ &+ \Bigg[\frac{1}{R}\frac{\partial^2 i(t-R/c)}{\partial z^2} + \left(-\frac{z}{R^3}\right)\frac{\partial i(t-R/c)}{\partial z} \\ &- \frac{1}{R^3}i(t-R/c) - z\left(-\frac{3z}{R^5}\right)i\left(t-\frac{R}{c}\right) \\ &- \frac{z}{R^3}\frac{\partial i(t-R/c)}{\partial z}\Bigg]\mathbf{a}_z.\end{aligned} \tag{A12}$$

In a derivation similar to that leading to Eq. (A7), it can be shown that

$$\frac{\partial}{\partial z}\left[i\left(t-\frac{R}{c}\right)\right] = -\frac{z}{cR}\frac{\partial i(t-R/c)}{\partial t} \tag{A13}$$

and that

$$\frac{\partial^2 i(t-R/c)}{\partial z^2} = \frac{\partial}{\partial z}\left(-\frac{z}{cR}\frac{\partial i(t-R/c)}{\partial t}\right)$$
$$= -\left[\frac{1}{cR}\frac{\partial i(t-R/c)}{\partial t} + \frac{z}{c}\left(\frac{-z}{R^3}\right)\right.$$
$$\left.\times\frac{\partial i(t-R/c)}{\partial t} + \frac{z}{cR}\frac{\partial^2 i(t-R/c)}{\partial z\partial t}\right]$$
$$= -\frac{1}{cR}\frac{\partial i(t-R/c)}{\partial t} + \frac{z^2}{cR^3}\frac{\partial i(t-R/c)}{\partial t} + \frac{z^2}{c^2R^2}\frac{\partial^2 i(t-R/c)}{\partial t^2}. \quad \text{(A14)}$$

Similarly, it may be shown that

$$\frac{\partial^2 i(t-R/c)}{\partial r\partial z} = \frac{zr}{cR^3}\frac{\partial i(t-R/c)}{\partial t} + \frac{zr}{c^2R^2}\frac{\partial^2 i(t-R/c)}{\partial t^2} \quad \text{(A15)}$$

Substituting Eqs. (A7), and (A13)–(15) into Eq. (A12), we arrive at

$$\frac{\nabla(\nabla\cdot\mathbf{A})}{\mu_0 L/4\pi} = \left[\frac{1}{R}\left(\frac{zr}{cR^3}\frac{\partial i(t-R/c)}{\partial t} + \frac{zr}{c^2R^2}\frac{\partial^2 i(t-R/c)}{\partial t^2}\right) + \frac{r}{R^3}\left(-\frac{z}{cR}\frac{\partial i(t-R/c)}{\partial t}\right) + \frac{3zr}{R^5}i\left(t-\frac{R}{c}\right) - \frac{z}{R^3}\left(-\frac{r}{cR}\frac{\partial i(t-R/c)}{\partial t}\right)\right]\mathbf{a}_r$$
$$+\left\{\frac{1}{R}\left[\left(-\frac{1}{cR}+\frac{z^2}{cR^2}\right)\frac{\partial i(t-R/c)}{\partial t} + \frac{z^2}{c^2R^2}\frac{\partial^2 i(t-R/c)}{\partial t^2}\right] - \frac{z}{R^3}\left(-\frac{z}{cR}\frac{\partial i(t-R/c)}{\partial t}\right) - \frac{1}{R^3}i\left(t-\frac{R}{c}\right) + \frac{3z^2}{R^5}i\left(t-\frac{R}{c}\right) - \frac{z}{R^3}\left(-\frac{z}{cR}\frac{\partial i(t-R/c)}{\partial t}\right)\right\}\mathbf{a}_z$$
$$= \left[\frac{3rz}{R^5}i\left(t-\frac{R}{c}\right) + \frac{3rz}{cR^4}\frac{\partial i(t-R/c)}{\partial t} + \frac{rz}{c^2R^3}\frac{\partial^2 i(t-R/c)}{\partial t^2}\right]\mathbf{a}_r$$
$$+\left[\left(\frac{3z^2}{R^5}-\frac{1}{R^3}\right)i\left(t-\frac{R}{c}\right) + \left(\frac{3z^2}{cR^4}-\frac{1}{cR^2}\right)\frac{\partial i(t-R/c)}{\partial t} + \frac{z^2}{c^2R^3}\frac{\partial^2 i(t-R/c)}{\partial t^2}\right]\mathbf{a}_z. \quad \text{(A16)}$$

Hence we can write the second term on the right of Eq. (A2) as

$$c^2\int_{-\infty}^{t}\nabla(\nabla\cdot\mathbf{A})dt = \frac{L}{4\pi\epsilon_0}\left\{\left[\frac{3rz}{R^5}\int_0^t i\left(\tau-\frac{R}{c}\right)d\tau + \frac{3rz}{cR^4}i\left(t-\frac{R}{c}\right) + \frac{rz}{c^2R^3}\frac{\partial i(t-R/c)}{\partial t}\right]\mathbf{a}_r + \left[\left(\frac{3z^2}{R^5}-\frac{1}{R^3}\right)\int_0^t i\left(\tau-\frac{R}{c}\right)d\tau + \left(\frac{3z^2}{cR^4}-\frac{1}{cR^2}\right)i\left(t-\frac{R}{c}\right) + \frac{z^2}{c^2R^3}\frac{\partial i(t-R/c)}{\partial t}\right]\right\}\mathbf{a}_z, \quad \text{(A17)}$$

where we have used the relation

$$c^2 = 1/\mu_0\epsilon_0. \quad \text{(A18)}$$

From Eq. (A4), we have

$$-\frac{\partial\mathbf{A}}{\partial t} = -\frac{L}{4\pi\epsilon_0 c^2}\left(\frac{1}{R}\frac{\partial i(t-R/c)}{\partial t}\right)\mathbf{a}_z \quad \text{(A19)}$$

and thus we are in a position to write down the complete expression for E from Eq. (A2). If we write

$$\mathbf{E} = E_r\mathbf{a}_r + E_z\mathbf{a}_z, \quad \text{(A20)}$$

the components in Eq. (A20) may be obtained by substituting Eqs. (A17) and (A19) into Eq. (A2):

$$E_r(r,\phi,z,t) = \frac{L}{4\pi\epsilon_0}\left[\frac{3rz}{R^5}\int_0^t i\left(\tau-\frac{R}{c}\right)d\tau + \frac{3rz}{cR^4}i\left(t-\frac{R}{c}\right) + \frac{rz}{c^2R^3}\frac{\partial i(t-R/c)}{\partial t}\right] \quad \text{(A21)}$$

and

$$E_z(r,z,\phi,t) = \frac{L}{4\pi\epsilon_0}\left[\frac{2z^2-r^2}{R^5}\int_0^t i\left(\tau-\frac{R}{c}\right)d\tau + \frac{2z^2-r^2}{cR^4}i\left(t-\frac{R}{c}\right) - \frac{r^2}{c^2R^3}\frac{\partial i(t-R/c)}{\partial t}\right]. \quad \text{(A22)}$$

The three equations (A9), (A21), and (A22) represent the field solution due to a small dipole at the origin. If the dipole lies along the z axis at an arbitrary source coordinate z', the field may be obtained by substituting $(z-z')$ for z in Eqs. (A9), (A21), and (A22).

APPENDIX B

In this Appendix we write down the solution for the magnetic and electric fields at any point for the case of a short pulse,

$$R_0/c + T < R_H/c + H/v. \quad \text{(B1)}$$

The equations given here are obtained from Eqs. (15)–(17), (20)–(22), and (24)–(26) derived in the text, and their counterparts for the negative current pulse. For brevity, we present the equations in the compact form below.

$$B_\phi(r,\phi,z,t) = \frac{\mu_0 I}{4\pi r}\left(\frac{\alpha(z-z_\alpha)}{[r^2+(z-z_\alpha)^2]^{1/2}} - \frac{\beta(z-z_\beta)}{[r^2+(z-z_\beta)^2]^{1/2}} + \frac{\gamma v r^2}{c[r^2+(z-z_\gamma)^2]} - \frac{\delta v r^2}{c[r^2+(z-z_\delta)^2]}\right), \tag{B2}$$

where the coefficients α, z_α, etc., at any time t may be selected from the matrix row below:

	α	z_α	β	z_β	γ	z_γ	δ	z_δ
$t<R_0/c$	0	0	0	0	0	0	0	0
$t=R_0/c$	0	0	0	0	1	0	0	0
$R_0/c<t<T+R_0/c$	1	0	1	$z'_{p_{max}}$	1	$z'_{p_{max}}$	0	0
$t=T+R_0/c$	1	0	1	$z'_{p_{max}}$	1	$z'_{p_{max}}$	1	0
$T+R_0/c<t\leq H/v+R_H/c$	1	$z'_{n_{max}}$	1	$z'_{p_{max}}$	1	$z'_{p_{max}}$	1	$z'_{n_{max}}$
$H/v+R_H/c<t\leq T+H/v+R_H/c$	1	$z'_{n_{max}}$	1	H	0	0	1	$z'_{n_{max}}$
$T+H/v+R_H/c<t<\infty$	0	0	0	0	0	0	0	0

$$E_r(r,\phi,z,t) = \frac{I_0}{4\pi\epsilon_0}\left(\frac{\alpha r}{[r^2+(z-z_\alpha)^2]^{3/2}} - \frac{\beta r}{[r^2+(z-z_\beta)^2]^{3/2}} - \frac{\theta r T}{(r^2+z^2)^{3/2}}\right) + \frac{I_0 v r}{4\pi\epsilon_0 c^2}\left(\frac{\gamma(z-z_\gamma)}{[r^2+(z-z_\gamma)^2]^{3/2}} - \frac{\delta(z-z_\delta)}{[r^2+(z-z_\delta)^2]^{3/2}}\right), \tag{B3}$$

$$E_z(r,\phi,z,t) = \frac{I_0}{4\pi\epsilon_0}\left(\frac{\alpha t(z-z_\alpha)}{[r^2+(z-z_\alpha)^2]^{3/2}} - \frac{\beta(z-z_\beta)}{[r^2+(z-z_\beta)^2]^{3/2}} - \frac{\theta z t}{(r^2+z^2)^{3/2}}\right) - \frac{I_0 v r}{4\pi\epsilon_0}\left(\frac{\gamma r}{[r^2+(z-z_\gamma)^2]^{3/2}} - \frac{\delta r}{[r^2+(z-z_\delta{}^2]^{2/2}}\right), \tag{B4}$$

where the coefficients are defined below:

	α	z_α	β	z_β	γ	z_γ	δ	z_δ	θ
$t<R_0/c$	0	0	0	0	0	0	0	0	0
$t=R_0/c$	0	0	0	0	1	0	0	0	0
$R_0/c<t<T+R_0/c$	1	$z'_{p_{max}}$	t	0	1	$z'_{p_{max}}$	0	0	0
$t=T+R_0/c$	1	$z'_{p_{max}}$	t	0	1	$z'_{p_{max}}$	1	0	0
$T+R_0/c<t\leq H/v+R_H/c$	1	$z'_{p_{max}}$	$t-T$	$z'_{n_{max}}$	1	$z'_{p_{max}}$	1	$z'_{n_{max}}$	1
$H/v+R_H/c<t\leq T+H/v+R_H/c$	1	H	$t-T$	$z'_{n_{max}}$	0	0	1	$z'_{n_{max}}$	1
$T+H/v+R_H/c<t<\infty$	1	H	t	0	0	0	0	0	0

The values for $z'_{p_{max}}$ and $z'_{n_{max}}$ in the matrices above are determined from Eq. (19) for the positive and negative pulses, respectively.

[a] Present address. Bell Laboratories, Holmdel, NJ 07733.

[1] J. A. Stratton, *Electromagnetic Theory* (McGraw-Hill, New York, 1941), pp. 175–176

[2] L. M. Magid, *Electromagnetic Fields, Energy and Waves* (Wiley, New York, 1972), pp. 159–162.

[3] M. Zahn, *Electromagnetic Field Theory: A Problem Solving Approach* (Wiley, New York, 1979), p 231

[4] H. J. Schmitt, C. W. Harrison, Jr., and C. S. Williams, Jr. Trans. IEEE AP-14, p. 120–127 (March 1966).

[5] M. A. Uman, D. K. McKain, and E P. Krider, Am J Phys 43, 33–38 (1975).

[6] K Ogata, *Modern Control Engineering* (Prentice-Hall, New York, 1976), pp. 218–210

APPENDIX 5

Variation in Light Intensity With Height and Time From Subsequent Lightning Return Strokes

JOURNAL OF GEOPHYSICAL RESEARCH, VOL. 88, NO. C11, PAGES 6555–6562, AUGUST 20, 1983

Variation in Light Intensity With Height and Time From Subsequent Lightning Return Strokes

DOUGLAS M. JORDAN AND MARTIN A. UMAN

Department of Electrical Engineering, University of Florida

Relative light intensity has been measured photographically as a function of height and time for seven subsequent return strokes in two lightning flashes at ranges of 7.8 and 8.7 km. The film used was Kodak 5474 Shellburst, which has a roughly constant spectral response between 300 and 670 nm. The time resolution was about 1.0 μs, and the spatial resolution was about 4 m. The observed light signals consisted of a fast rise to peak, followed by a slower decrease to a relatively constant value. The amplitude of the initial light peak decreases exponentially with height with a decay constant of about 0.6 to 0.8 km. The 20% to 80% rise time of the initial light signal is between 1 and 4 μs near ground and increases by an additional 1 to 2 μs by the time the return stroke reaches the cloud base, a height between 1 and 2 km. The light intensity 30 μs after the initial peak is relatively constant with height and has an amplitude that is 15% to 30% of the initial peak near the ground and 50% to 100% of the initial peak at cloud base. The logarithm of the peak light intensity near the ground is roughly proportional to the initial peak electric field intensity, and this in turn implies that the current decrease with height may be much slower than the light decrease. The absolute light intensity has been estimated by integrating the photographic signals from individual channel segments to simulate the calibrated all-sky photoelectric data of Guo and Krider (1982). Using this method, we find that the mean peak radiance near the ground is 8.3×10^5 W/m, with a total range from 1.4×10^5 to 3.8×10^6 W/m.

INTRODUCTION

There is very little information in the lightning literature regarding the light produced by subsequent return strokes as a function of height and time. *Schonland et al.* [1935, p. 618] have described Boys camera data which indicate that "Unbranched subsequent strokes show an effect of the same character (as the first stroke), for the intensity of the bright luminosity decreases in general from the base upwards. No case has yet been observed in which the trunk luminosity was greatest at the cloud end of the discharge." *Schonland* [1956, p. 594] later reported that "the luminosity of the streamer tends to decrease as it travels upwards but the effect is not very marked." *Boyle and Orville* [1976] show curves of light vs. time derived from streak photography for two heights on one subsequent stroke channel. Here we present the first detailed measurements of the relative light intensity as a function of height and time for subsequent return strokes. (We use the word "intensity" as it is commonly used in the lightning and other literature, i.e., as the amount of light reaching an emulsion, rather than as it is defined scientifically, i.e., the flux per unit solid angle emitted by a point source.) The data were obtained by using the technique of streak photography.

The characteristics of the return-stroke light, to the extent that these characteristics relate to the return-stroke current, contain important information for deriving and testing models of return-stroke currents. For example, a preliminary analysis of the data presented in this paper has enabled *Master et al.* [1981] to modify the model of *Lin et al.* [1980], which relates the channel current to measured electric and magnetic fields, to take into account the variation of peak current with height.

Paper number 3C0602.
0148-0227/83/003C-0602$05.00

THE EXPERIMENT

The data to be presented were recorded during the summer of 1979 at a site in Wimauma, Florida, southeast of Tampa. To support the streak photographic measurements, there were videotapes from a five-station television network covering an area of 400 km², still photographs, time-to-thunder records, and electric field measurements. The electric fields from close lightning were recorded with equipment having a 3-db frequency response that extended from 0.3 Hz to 1.5 MHz [*Lin et al.*, 1979]. Simultaneously, the fields about 50 km from the primary observation site were recorded by University of Arizona researchers [*Weidman and Krider*, 1980].

Return strokes were streak photographed by using a Beckman and Whitley model 351 streaking camera in a fashion very similar to that described by *Idone and Orville* [1982]. The streaking camera shutters were triggered by the light from the first stroke of the flash, were opened in about 7 ms, and remained open for 0.5 s. Thus the camera could be operated in daylight, but only subsequent strokes were recorded. The 0.5-s exposure time was chosen so as to capture as many strokes in the flash as possible without excessive film exposure as a result of background light. Typically, two or three flashes, corresponding to a 1- to 2-s total exposure time, could be recorded in daylight under storm conditions. The film velocity obtained with the Beckman and Whitley drum rotating at speeds of 50 to 70 rps (revolutions per second) was approximately 0.04 mm/μs, and this with the spatial resolution of the digitization process discussed in the next paragraph provided a time resolution of about 0.5 μs on the film. Kodak 5474 Shellburst film was used because of its antihalation properties and because of the mechanical strength associated with the "grey base" option. Kodak 5474 Shellburst has an ASA rating of approximately 125 and a spectral response that is roughly constant from 300 to 670 nm [*Eastman Kodak Company*, 1974].

The film images were analyzed with a Photomation MKII

TABLE 1. A Listing of the Strokes Analyzed

Time	Distance	Stroke Number	Stroke Identifier
220651, UT July 27, 1979	7.8 km		
		2	2
		3	3
		5	5
		6	6
		7	7
224645, UT July 27, 1979	8.7 km		
		2	B
		3	C

microdensitometer manufactured by Optronics International. The spatial resolution of the digitization on the photographic emulsion was 25.0 μ. The images were aligned by hand in the holder of the densitometer, a digitization was performed, and the resultant data were transferred to nine-track digital tape.

The data for seven subsequent strokes from two flashes are summarized in Table 1. Number or letter identifiers are given for each stroke in the flash according to the stroke order, and these identifiers are used in the subsequent figures and elsewhere.

To obtain relative light intensity on a calibrated scale, three factors need to be determined: (1) the distance to the strokes; (2) the object size, given both the stroke distance and image size; and (3) the relative light intensity, given the measured film density.

1. The 22:06:51 UT flash on July 27, 1979 (whose strokes are identified as 2, 3, 5, 6, 7), was located at a distance of 7.8 km by time to thunder. This flash also appeared on one of the television cameras. According to the electric field records, the flash had a total of 13 strokes, of which six occurred within the 0.5-s exposure time of the streak camera, and five strokes produced sufficient film density to be analyzable. The 22:46:45 UT July 27, 1979, flash (whose two subsequent strokes are identified as B and C) struck near a power substation, causing an accurately timed circuit-breaker lockout and burning through an overhead wire. The distance to the broken wire was known and was confirmed by time to thunder and by the television network. The flash had three strokes and was at a distance of 8.7 km. A photographic still image was also obtained for this flash.

2. The relation between object and image size was determined by measuring an image on the streak camera that was obtained while the camera drum was stationary. The image was digitized and was displayed on a plotter such that the number of samples between two objects of high contrast with the background could be determined. The objects used were two power poles 16.8 m apart at a distance of 153 m.

3. A strip of film was exposed for 0.5 s, using a panchromatic source through a standard neutral density stepped wedge. Then both the stepped-wedge density and the developed-film density were digitized on the densitometer, and from these data the film calibration was determined. A plot showing the resultant relative light intensity vs. film density is shown in Figure 1. A supporting film calibration performed with a time-varying source is discussed in the paragraph after next.

A potential source of error in measuring the time variation of light intensity comes when one assumes that the width of the image channel is negligibly small. The problem has two aspects: that of the actual size of the channel and that of the size of a thin bright source imaged on the film. The actual channel diameter is probably in the range 1 to 10 cm, as indicated from recent photographic measurements [e.g., *Evans and Walker*, 1963; *Orville et al.*, 1974] and most other physical evidence (e.g., fulgarities, scars on trees, etc., see *Uman* [1971]), although *Connor* [1968] and *Connor and Barasch* [1968] have reported on unusual lightning channels that apparently are tens of meters in diameter. To calibrate the optical system and film for possible image broadening resulting from halation and other effects characteristic of thin but bright sources, an experimental determination of the effect of source intensity on image width, similar to that discussed by Evans and Walker, was performed. This calibration consisted of imaging a 0.2-mm slit at a distance of 1-m onto the film, the slit being illuminated from the rear by a single falsh of 3-μs duration from a General Radio 1531-A Strobatac xenon lamp. The spectrum of the xenon lamp has a number of peaks in the 300- to 500-nm range, falls to one-half value at about 600 nm, to one-tenth value at 1000 nm, and has several small subsidiary peaks in the 800- to 1000-nm (infrared) range. The same Kodak stepped-density wedge that was used in the film linearity calibration was placed behind the slit. In the absence of image broadening, the 0.2-mm slit should have had a width on the film of 0.01 mm or 10 μ. The images obtained at two light intensities with a microdensitometer sample size of 25.0 μ are shown in Figure 2. The two light intensity peaks are representative of all observed strokes, except the single and brightest—identified as C. The image full widths at half of peak value are equivalent to a time of about 1 μs if the streak camera were

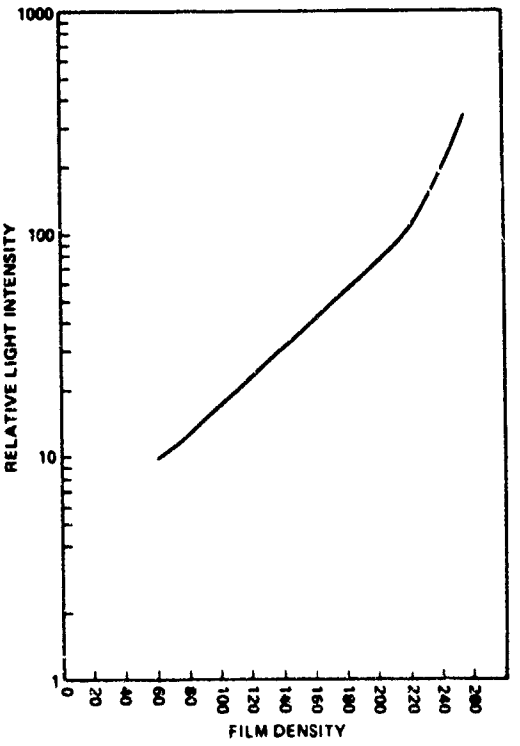

Fig. 1 Relative light intensity vs. film density determined by exposing a film strip through a step wedge and comparing the resultant film density with a direct microdensitometer reading of the step wedge. The microdensitometer was calibrated in units of diffuse density.

running at normal speed. The 0.2-mm slit that was used for this calibration corresponds to a channel diameter of 2.0 m at 10 km. As noted above, most available physical evidence indicates that the channel width is almost two orders of magnitude less than 2.0 m. Therefore the spatial distribution of the image of even a relatively large-diameter channel would cause less than 1-μs error in the time-resolved relative light intensity.

In a final calibration experiment, the 0.2-mm slit was illuminated by the strobe and was imaged on moving film in order to test the time response of the film and optical system. The film velocity was 70 rps, corresponding to a linear film velocity of 0.06 mm/μs, and this gave a time between 25.0 μ samples of 0.42 μs. Figure 3 shows the light intensity of the xenon source measured with a linear photodetector superimposed on the relative light intensity obtained from the film using the calibration in Figure 1. The light intensity is comparable to that of the observed strokes. The film adequately reproduces a 20%–80% rise to peak of about 1.0 μs, as well as the overall xenon lamp pulse shape measured by the photodetector, thus lending strong support to the densitometer calibration and indicating that reciprocity failure is not a problem. On the basis of the data in Figures 1, 2, and 3 we conclude that the system used had the capability of measuring return-stroke relative light intensity on a time scale of 1.0 μs or less.

Finally, we list several other potential sources of error. One of the most critical parameters is the velocity of the film in the streak camera. The velocity determines the time scale of the relative light intensity measurement and is determined from the signal generated by a magnetic pickup mounted adjacent to the camera drum. In the present experiment the film velocity was measured with an error of less than 1%.

The two-dimensional height of the channel is computed from the range to the discharge, and both the range and channel height errors are estimated to be on the order of 10%, not significant for the purposes of the present study. The effect of a nonvertical or tortuous channel can cause additional errors in both height and length of isolated channel segments. For the strokes studied the vertical sections resolved by the microdensitometer scans were about 4 m.

Atmospheric scattering, if significant, could lengthen the measured-light rise times, and therefore the actual rise times may be shorter than measured.

The final possible errors are due to the microdensitometer. One of these is due to errors in the mechanical positioning of the film strip on the densitometer. This "tilt" angle was measured to be less than 5° and does not introduce a significant error in the relative light intensity data. The second error introduced by the microdensitometer is that of density noise. This noise is always about ±4 density units

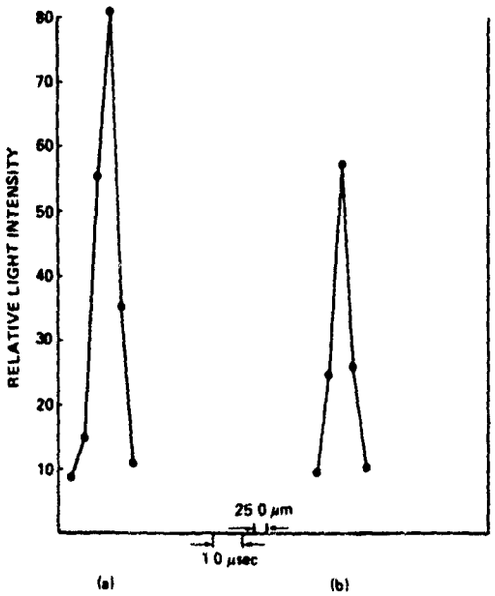

Fig. 2. Spatial distribution of the still image of a 0.2-mm slit 1 m from the camera lens. Distributions are shown for two intensities: (*a*) and (*b*). The slit was illuminated by the xenon flash pulse shown in Figure 3. If the film had been moving with a linear velocity of 0.06 mm/μs, the width of the spatial distribution would contribute less than 1.0 μs to the rise time as the time scale shown indicates. The light intensity scale is in the same units as that shown in Figure 1.

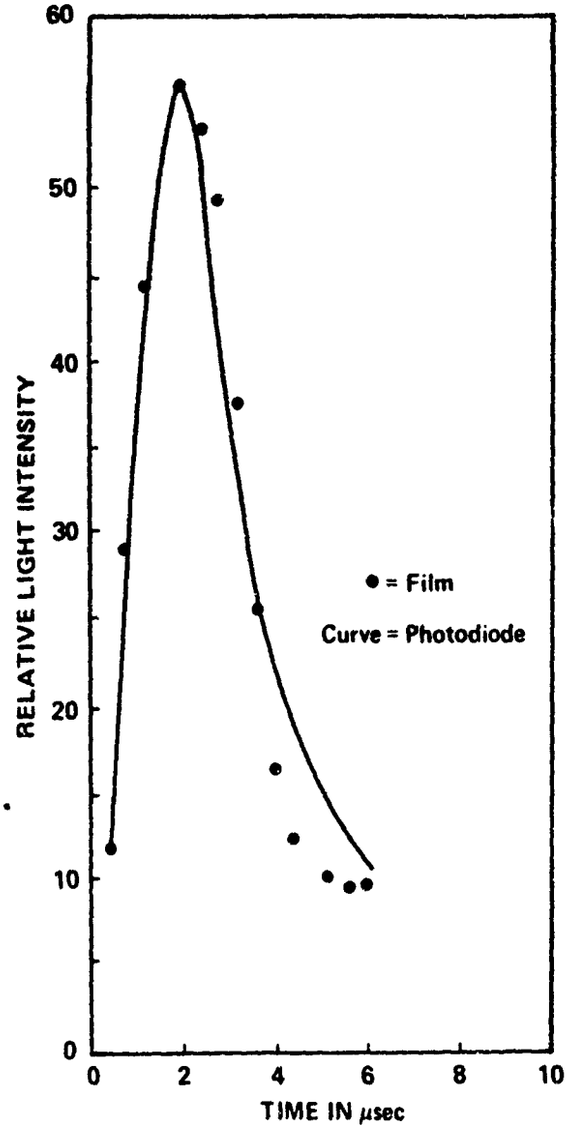

Fig. 3. Time-resolved image of a 0.2-mm slit 1 m from the streak camera lens illuminated by a xenon source as measured by a photodetector (solid line) and from film (crosses). Photodetector data were normalized to the peak light intensity from film, and the peak values of photodetector and film data were aligned to occur at the same time. Relative light intensity is in the same units as shown in Figure 1.

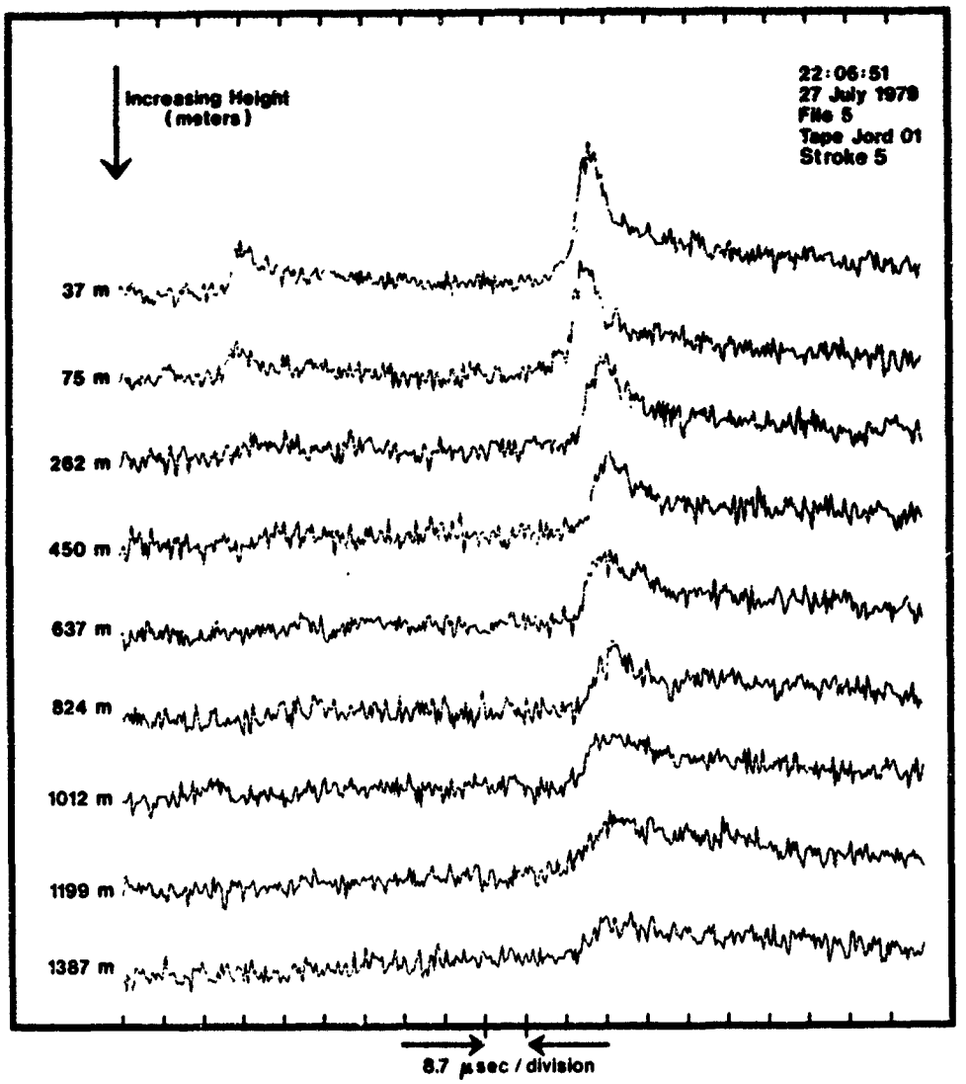

Fig. 4. Film density vs. height and time for stroke 5. Note that in these plots the bottom of the channel is at the top of the plot.

and causes some measurement uncertainty In the light intensity plots the microdensitometer noise was either increased or reduced relative to the peak signal, depending upon the average background density. The resultant light intensity noise was averaged by eye in making the measurements discussed next.

DATA

In Figure 4 we show, as an example of the data, the film density profiles at various heights for stroke 5. Density is plotted instead of relative light intensity to give the reader a view of the raw data, including the noise mentioned in the preceding paragraph. In Figure 5 we show the corresponding relative light intensity profile for a 4-m channel section near the ground of stroke 5 correlated with close and distant electric fields. The light vs. time curves are consistent with the wave shapes observed by *Boyle and Orville* [1976]. On data of the type shown in Figure 5 we have made the following measurements: (1) the magnitude of the initial peak light value, (2) the time it takes the relative light intensity to increase from 20% to 80% of the initial peak value, (3) the value of the relative light intensity 30 μs after the initial peak, and (4) the initial peak value of the electric field intensity.

From these measurements we plot the following: peak light vs. height (Figure 6), light rise time vs. height (Figure 7), light 30 μs after peak value vs. height (Figure 8), the ratio of peak light to 30 μs value vs. height (Figure 9), the logarithm of peak light near the ground vs. peak initial electric field (Figure 10), and total light as would be viewed by an all-sky detector vs. time (Figure 11;)

DISCUSSION

The straight-line least square fits in Figure 6 show that the initial peak of the light radiation by a subsequent return stroke decays exponentially with height. The height decay constant is about 0.6 km for B and C and about 0.8 km for 2, 3, 5, and 6. The difference in the decay constant for the two flashes may be due, in part, to differing channel geometries. One additional stroke from a flash recorded in Gainesville in 1980 showed a similar decrease with height, but the film density value was too low to allow adequate analysis, and hence we have not included it in this paper. The implication of the decrease in initial peak light with height is that the

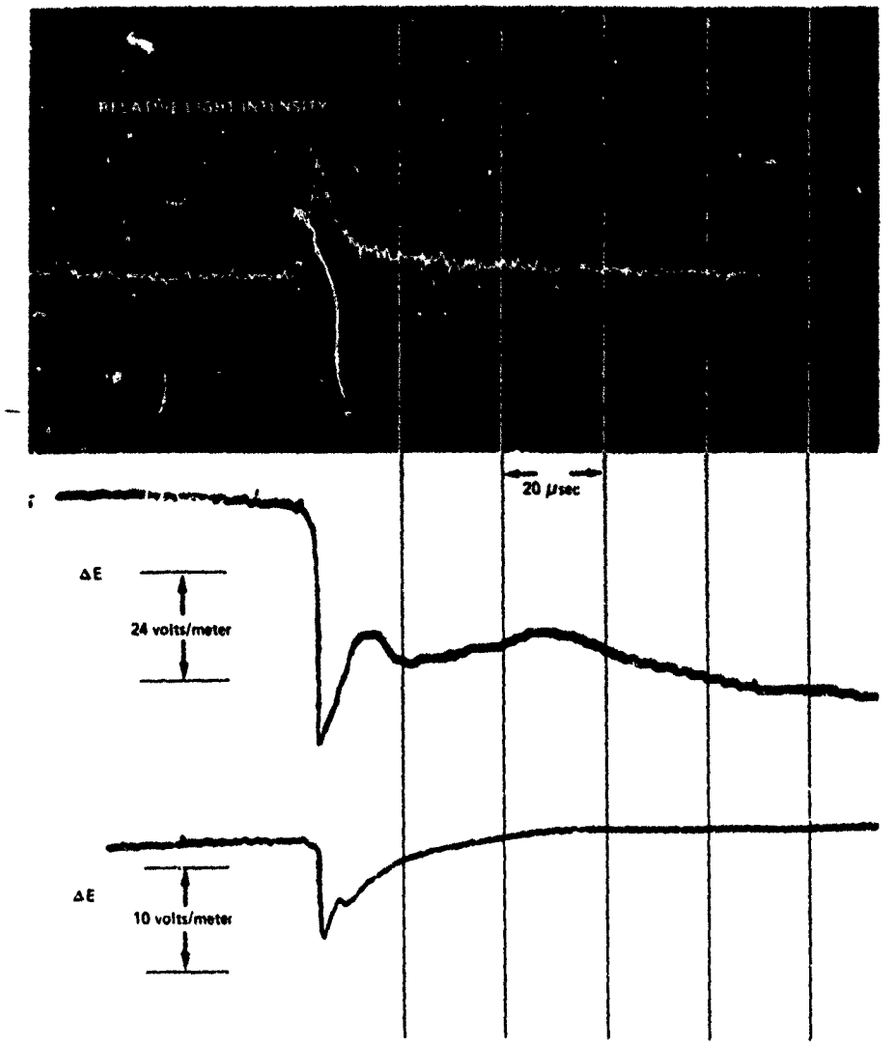

Fig. 5. Relative light intensity for 4 m of channel near ground correlated with electric field waveforms for stroke 5. The top trace is the relative light intensity. The middle trace is the electric field waveform taken at the University of Florida research site at a distance of 7.8 km from the flash. The bottom trace is the waveform from a University of Arizona research site at a distance of approximately 50 km.

initial current peak must also decrease, a result which we will discuss further in the paragraph after next. The results of Figure 6 are not consistent with the most recent view of *Schonland* [1956], who indicated that the luminosity of the subsequent return stroke does not have a marked decrease with height, but they are, more or less, in agreement with the earlier claim of *Schonland et al.* [1935, p. 618] that "the bright luminosity decreases in general from the base up."

As shown in Figure 7, the initial light rise time increases with height, indicating a loss of higher-frequency components in the light signal, and probably current, with altitude. The observation of a roughly uniform light intensity as a function of height 30 μs after the initial peak shown in Figure 8 can be interpreted to indicate both that a uniform current flows in the channel at and after this time and that there are no substantial differences in the atmospheric scattering with height. Figure 9 shows that the 30-μs light value is 15% to 30% of the peak light near the ground but, as the peak decreases with height, becomes 50% to 100% at cloud base. The 30-μs light value is obviously correlated with the peak value since the vertical spread in the data of Figure 9 is much less than the spread in either Figure 6 or Figure 8.

The above observations imply that the subsequent return stroke consists of an initial impulsive current which decays with height and that this is followed by a current that is roughly constant with height. In the return stroke model of *Lin et al.* [1980], the initial electric radiation field is proportional to the initial current near ground which subsequently propagates up the channel. The range of subsequent stroke peak currents derived by using the model of Lin et al. [1980], the field values from Figure 10, and a return stroke velocity of 1×10^8 m/s [*Idone and Orville*, 1982] is 9 kA to 34 kA, with a mean of 17 kA—values in good agreement with the subsequent stroke tower measurements of *Berger et al.* [1975].

From Figure 10, the logarithm of the light intensity peak extrapolated to the bottom of the channel by using Figure 6 is shown to be roughly proportional to the initial electric field peak. The correlation coefficient is 0.98, which for 5 degrees of freedom implies a significant correlation at the 0.1% level.

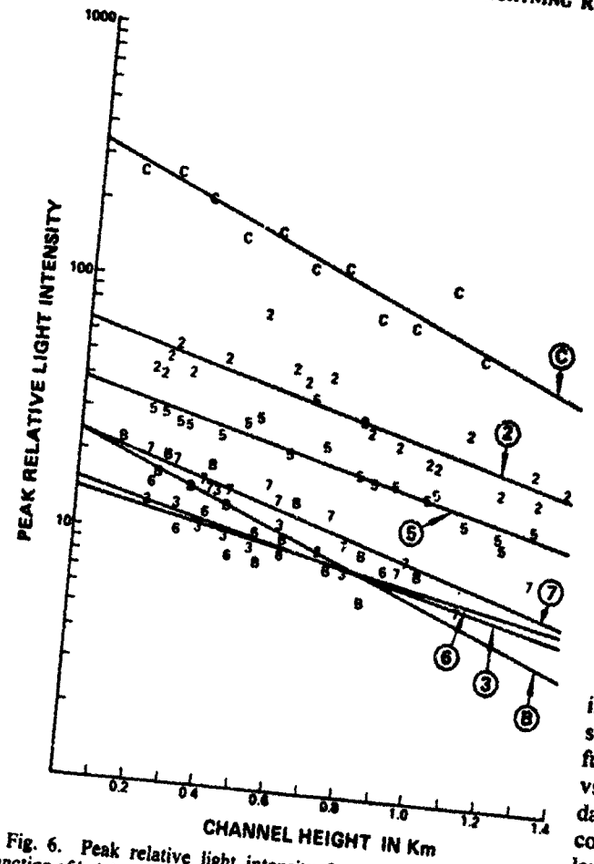

Fig. 6. Peak relative light intensity for 4 m of channel as a function of height along the channel. See Table 1 for identification of stroke symbols.

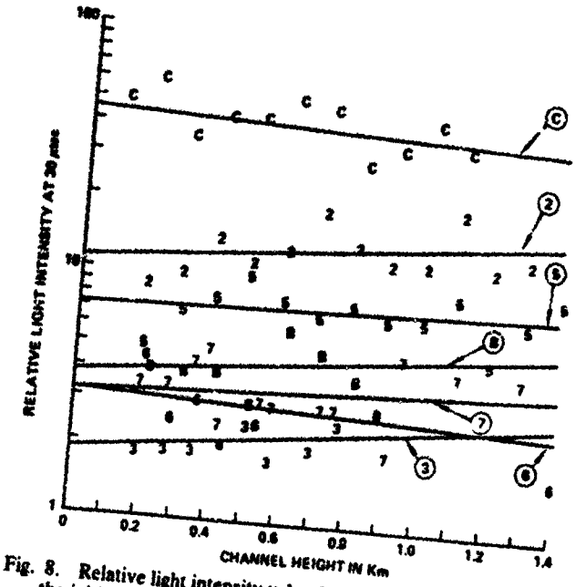

Fig. 8. Relative light intensity value for 4 m of channel 30 μs after the initial peak. See Table 1 for identification of symbols.

An equally good straight-line fit can be obtained by plotting the logarithm of the light against the square of the initial electric field peak. The correlation coefficient in this case is 0.99. Since we cannot tell whether the logarithm of the light is proportional to the field, the square of the field, or any similar function of the field, we choose to plot the simplest function of the field in Figure 10. We also plotted linear light vs. electric field and obtained a poorer straight-line fit to the data than for the logarithm of the light. However, the correlation coefficient of 0.85 is still significant at the 1% level. Since the initial peak electric field is proportional, by the model of *Lin et al.* [1980], to the initial current peak near the ground, we suggest that the peak relative light intensity $L_p(z)$, a distance z above ground may be found by extrapolating the peak value found at ground level, $L_p(z = 0) = A \exp(kI_p(z = 0))$, where A and k are constants, to currents above ground. Thus, the peak return-stroke current apparently decreases more slowly with height than the peak light decreases. *Master et al.* [1981] assumed that the decrease in light and current with height were about the same in order to

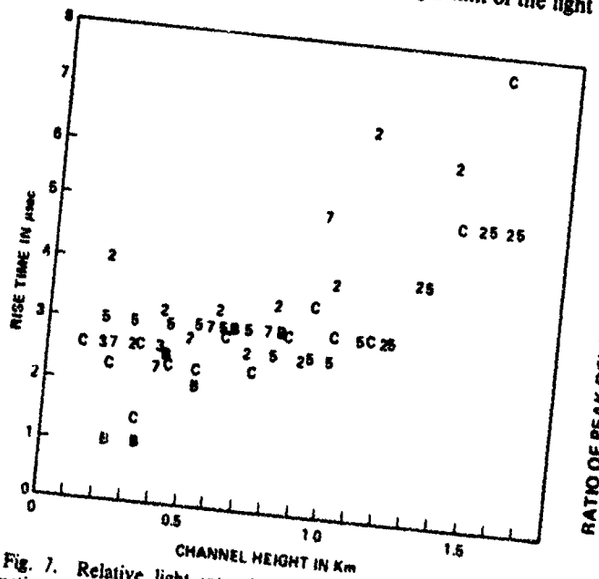

Fig. 7. Relative light intensity rise time, 20% to 80%, as a function of height along the channel. See Table 1 for identification of stroke symbols.

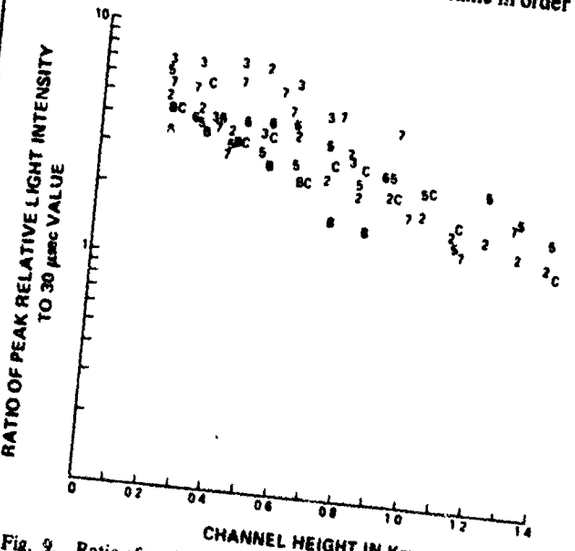

Fig. 9. Ratio of peak relative light intensity to the light intensity value 30 μs after the peak vs. height. See Table 1 for identification of symbols.

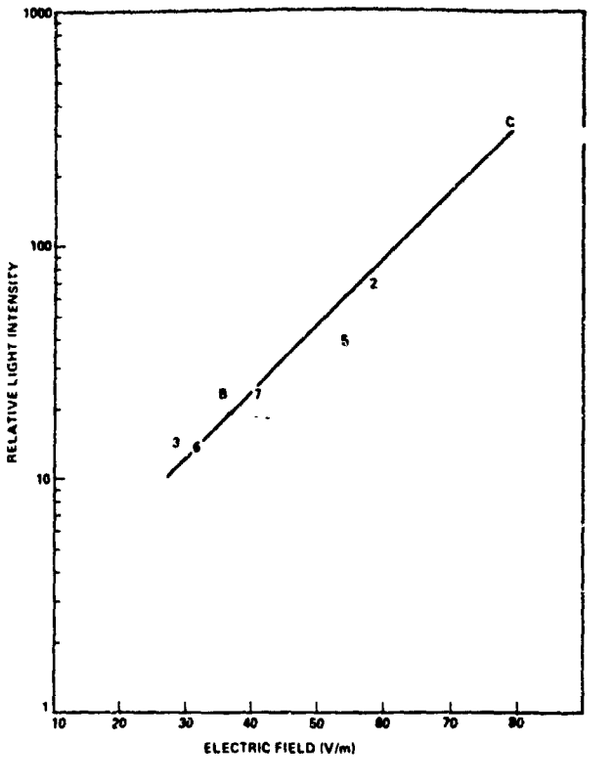

Fig. 10. Peak relative light intensity for 4 m of channel on a logarithmic scale vs peak electric field. Relative light intensity peaks are extrapolated to the bottom of the channel from the data in Figure 6. Electric field measurements were made at 7.8 km for 2, 3, 5, 6, and 7 and at 8.7 km for B and C. No adjustments in the data have been made for the different distances.

calculate the return-stroke electric and magnetic fields to be expected above ground level. They also calculated the fields for a current which did not decrease with height. Apparently, the proper assumption is between these two extremes.

The return-stroke model of *Lin et al.* (1980) predicts a current after the initial peak that decreases in an upward direction because of the decrease of charge per unit length stored on the leader's corona envelope and the use of current sources to simulate the discharge of this corona envelope. Since the light after the peak is relatively uniform with height, it appears that the model needs further refinement in treating the corona charge and current.

Guo and Krider [1982] have measured the total optical power vs. time from return strokes by using an all-sky photoelectric system. We can use their data for subsequent strokes to obtain a rough calibration of our photographic results, although the spectral responses of the film and the photoelectric systems are not identical. We simulated the all-sky data of Guo and Krider by adding the light from succeeding channel heights and assuming a return-stroke velocity of 1×10^8 m/s [*Idone and Orville*, 1982]. Curves obtained are shown in Figure 11, where the scale on the left of the figure is in relative light intensity units. The absolute scale in watts on the right of Figure 11 is determined by assuming that our largest and smallest simulated all-sky output correspond to the largest and smallest values, respectively, measured by Guo and Krider. In the present case this is a reasonable approach, since both sets of data span about 1 order of magnitude, and the resultant mean light intensities, 2.7×10^5 W/m from our data and 2.5×10^5 W/m from Guo and Krider, are very similar. The calibration factor for our data found in this way is 4.6×10^4 W/m per relative light intensity unit. This power should be considered to be in the spectral bandwidth of the photoelectric detector used by Guo and Krider roughly from 400 to about 1100 nm. It follows from Figure 6, which gives the relative light intensity for 4-m sections of channel, that the peak light intensities near ground vary between 1.4×10^5 and 3.8×10^6 W/m, with a mean of 8.3×10^5 W/m. The peak values are 1.8 to 3.8 times the average values obtained from the all-sky simulation, with a mean value of 2.5.

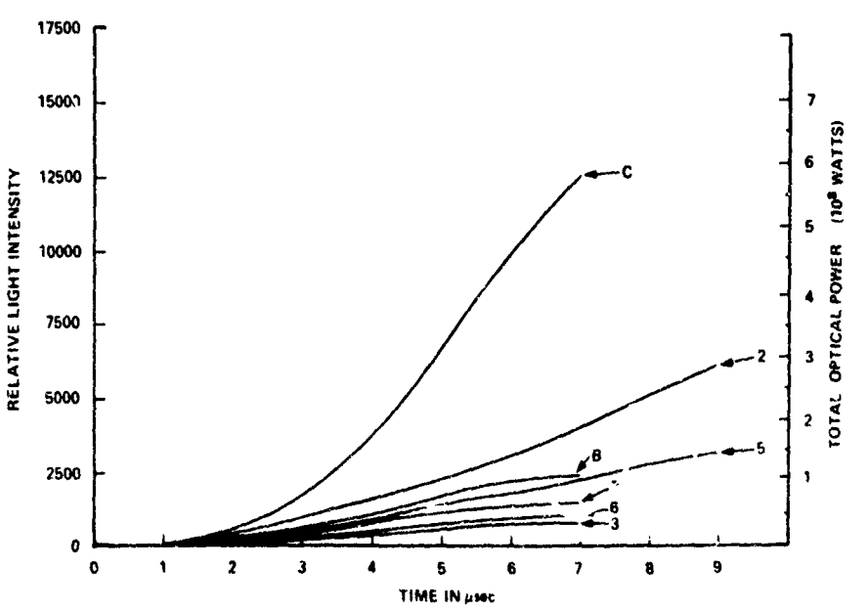

Fig. 11. Relative light intensity as would be viewed by an all-sky detector. Curves are derived by integrating relative light intensity from successively higher channel sections delayed by the appropriate time to simulate a return stroke velocity of 1×10^8 m/s. On the left ordinate is the relative light intensity derived from integrating the measured data. On the right ordinate is fitted the absolute intensity scale from *Guo and Krider* [1983].

Guo and Krider [1982] have shown that the experimental ratio of the radiance per unit length of channel to either the electric field or the square of the electric field for each stroke in five selected flashes shows less variability than does the average radiance itself. These results are consistent with ours, shown in Figure 10, considering the factor of 2 variability between the average and peak radiance.

Acknowledgment. The research reported in this paper was supported in part by NSF grant ATM-79-02627, NASA grant NGR-10-005-169, ONR contract N0014-81-K-0177, and DOE contract DE-AC02-81RA50570. We wish to express our appreciation to Mat Darveniza and William Beasley of the University of Florida and to personnel of both the Tampa Electric Company and Florida Power Corporation for making the overall experiment possible; to the NASA Kennedy Space Center Data Analysis Facility for making available the microdensitometer on which the film was analyzed; to E. Philip Krider and Charles D. Weidman of the University of Arizona for helpful discussions and for providing electric field data such as those shown in Figure 5; and to Richard E. Orville, both for helpful discussions and for providing us with essential equipment.

REFERENCES

Berger, K., R. B. Anderson, and H. Kroninger, Parameters of lightning flashes, *Electra*, *80*, 23–37, 1975.

Boyle, J. S., and R. E. Orville, Return stroke velocity measurements in multistroke lightning flashes, *J. Geophys. Res.*, *81*, 4461–4466, 1976.

Connor, T. R., Stroke and space-resolved slit spectra of lightning, *Rep. LA-3754* (addendum), Los Alamos Sci. Lab., Los Alamos, N. Mex., 1968.

Connor, T. R., and G. E. Barasch, The 1965 ARPA-AEC Joint Lightning Study at Los Alamos, vol. 3, Comparison of the lightning spectrum as measured by all-sky and narrow-field detectors: Propagation of light from lightning to all-sky detectors, *Rep. A-3756*, Los Alamos Sci. Lab., Los Alamos, N. Mex., 1968.

Eastman Kodak Company, *Kodak Pam. P-55*, Rochester, N.Y., 1974.

Evans, W. H., and R. L. Walker, High-speed photographs of lightning at close range, *J. Geophys. Res.*, *68*, 4455–4459, 1963.

Guo, C., and E. P. Krider, The optical and radiation field signatures produced by lightning return strokes, *J. Geophys. Res.*, *87*, 8913–8922, 1982.

Idone, V. P., and R. E. Orville, Lightning return stroke velocities in the Thunderstorm Research International Program (TRIP), *J. Geophys. Res.*, *87*, 4903, 1982.

Lin, Y. T., M. A. Uman, J. A. Tiller, R. D. Brantley, E. P. Krider, and C. D. Weidman, Characterization of lightning return stroke electric and magnetic fields from simultaneous two-station measurements, *J. Geophys. Res.*, *84*, 6307–6314 1979.

Lin, Y. T., M. A. Uman, and R. B. Standler, Lightning return stroke models, *J. Geophys. Res.*, *85*, 1571–1583, 1980.

Master, M. J., M. A. Uman, Y. T. Lin, and R. B. Standler, Calculations of lightning return stroke electric and magnetic fields above ground, *J. Geophys. Res.*, *86*, 12, 127, 1981.

Orville, R. E., J. H. Helsdon Jr., and W. H. Evans, Quantitative analysis of a lightning return stroke for diameter and luminosity changes as a function of space and time, *J. Geophys. Res.*, *79*, 4059–4067, 1974.

Schonland, B. F. J., The lightning discharge, *Handb. Phys.*, *22*, 576–628, 1956.

Schonland, B. F. J., D. J. Malan, and H. Collens, Progressive lightning, Pt. 2, *Proc. R. Soc. (London)*, *A152*, 595–625, 1935.

Uman, M. A., Understanding lightning, report, BEK Industries, Pittsburgh, Pa., 1971.

Weidman, C. D., and E. P. Krider, Submicrosecond rise times in lightning return stroke fields, *Geophys. Res. Lett.*, *7*, 955–958, 1980.

D. M. Jordan and M. A. Uman, Department of Electrical Engineering, University of Florida, Gainesville, FL 32611.

(Received December 30, 1982;
revised April 13, 1983;
accepted April 15, 1983.)